



Advances in Optics and Photonics

Fiber-based phase-sensitive optical amplifiers and their applications

PETER A. ANDREKSON  AND MAGNUS KARLSSON

Photonics Laboratory, Department of Microtechnology and Nanoscience, Chalmers University of Technology, SE-412 96 Gothenburg, Sweden

*Corresponding author: peter.andrekson@chalmers.se

Received November 6, 2019; revised February 10, 2020; accepted February 10, 2020; published April 30, 2020 (Doc. ID 382548)

Optical parametric amplifiers rely on second-order susceptibility (three-wave mixing) or third-order susceptibility (four-wave mixing) in a nonlinear process where the energy of incoming photons is not changed (elastic scattering). In the latter case, two pump photons are converted to a signal and to an idler photon. Under certain conditions, related to the phase evolution of the waves involved, this conversion can be very efficient, resulting in large amplification of an input signal. As the nonlinear process can be very fast, all-optical applications aside from pure amplification are also possible. If the amplifier is implemented in an optical input-phase-sensitive manner, it is possible to amplify a signal wave without excess noise, i.e., with a noise figure of 0 dB. In this paper, we will provide the fundamental concepts and theory of such amplifiers, with a focus on their implementation in highly nonlinear optical fibers relying on four-wave mixing. We will discuss the distinctions between phase-insensitive and phase-sensitive operation and include several experimental results to illustrate their capability. Different applications of parametric amplifiers are also discussed, including their use in optical communication links. © 2020 Optical Society of America

<https://doi.org/10.1364/AOP.382548>

1. Introduction	369
1.1. List of Acronyms	369
1.2. Introductory Remarks	370
1.3. Basic Aspects of Amplifiers and Their Use in Optical Transmission Links	371
2. Brief History of Parametric Amplifiers	373
2.1. Early Days of Nonlinear Optics	373
2.2. Optical Amplification and Squeezing	374
2.3. Fiber-Optic Parametric Amplifiers	375
3. Fundamental Aspects of Parametric Amplifiers	376
3.1. Parametric Pendulum	376
3.2. Nonlinearities in $\chi^{(2)}$ and $\chi^{(3)}$ Materials	378
3.2a. Second-Order Nonlinearities	379

3.2b. Third-Order Nonlinearities—The Nonlinear Schrödinger Equation	380
3.2c. Four-Wave Mixing	381
3.2d. Parametric Amplification: Phase-Insensitive Gain	383
3.2e. Phase-Sensitive Amplification	383
3.3. Quantum Mechanical Interpretations and 1/2/4 Mode Operation	384
4. Noise in Parametric Amplifiers	387
4.1. Amplifier Noise Basics	387
4.2. Noise in the Two-Mode Parametric Amplifier	389
4.2a. Quantum Noise	389
4.2b. Additional Noise Sources	391
4.3. Link Noise Figures and Distributed Amplification	391
5. Implementation Considerations	393
5.1. General Aspects of Parametric Amplifiers	393
5.2. Gain Spectrum Characteristics	394
5.3. Dealing with Detrimental Stimulated Brillouin Scattering	398
5.4. Saturation Properties and Nonlinear Penalties	399
5.5. Phase-Sensitive Operation of Parametric Amplifiers	400
5.5a. Optical Pump Recovery Using Injection Locking	402
5.5b. Dispersion Management in PSA Links	403
5.5c. Polarization Management in PSAs	404
5.5d. Capacity Considerations	405
5.5e. Parametric Amplification in Multimode Fibers	406
5.5f. Four-Mode PSAs	407
6. Transmission Fiber Nonlinearity Mitigation	408
7. Experimental Transmission Results Using Phase-Sensitive Amplifiers	409
7.1. System Results Using Highly Nonlinear Fiber-Based PSAs	410
7.2. System Results Using LiNbO ₃ -Based PSAs	411
8. Other Applications of Fiber-Optic Parametric Amplifiers	412
8.1. Amplitude and Phase Regeneration	412
8.2. All-Optical Sampling	415
9. Future Outlook Including Other Nonlinear Platforms	416
10. Conclusion	417
Funding	417
Acknowledgment	417
References	417

Fiber-based phase-sensitive optical amplifiers and their applications

PETER A. ANDREKSON AND MAGNUS KARLSSON

1. INTRODUCTION

1.1. List of Acronyms

ASE	Amplified spontaneous emission
BER	Bit error rate
CW	Continuous wave
XPM	Cross-phase modulation
DWDM	Dense wavelength division multiplexing
DSP	Digital signal processing
DFG	Difference-frequency generation
DCM	Dispersion compensating module
DRA	Distributed Raman amplification
EDFA	Erbium-doped fiber amplifier
FOPA	Fiber-optic parametric amplifier
FWM	Four-wave mixing
FSO	Free-space optical
GVD	Group-velocity dispersion
HLNF	Highly nonlinear fiber
NF	Noise figure
NLSE	Nonlinear Schrödinger equation
OIL	Optical injection locking
OSNR	Optical signal-to-noise ratio
PPLN	Periodically poled lithium niobate
PIA	Phase insensitive amplifier/amplification
PLL	Phase-locked loop
PSA	Phase sensitive amplifier/amplification
PZT	Piezoelectric transducer
PC	Polarization controller
PMD	Polarization-mode dispersion
PSD	Power spectral density
QPSK	Quadrature phase shift keying
QPM	Quasi phase matching
RF	Radio frequency
SHG	Second-harmonic generation
SPM	Self-phase modulation
SNR	Signal-to-noise ratio
SMF	Single-mode fiber
SDM	Spatial-division multiplexing
SSMF	Standard single-mode fiber
SOP	State of polarization
SBS	Stimulated Brillouin scattering
SRS	Stimulated Raman scattering
SFG	Sum-frequency generation
WDM	Wavelength division multiplexing

1.2. Introductory Remarks

Optical amplifiers are key enablers in numerous scientific and engineering fields such as optical communication, imaging, sensing, and spectroscopy. The internet revolution would not have been possible without optical amplifiers being used in virtually all long-haul optical fiber transmission links reaching ranges from 100 km to interoceanic distances. The invention of the erbium-doped fiber amplifier (EDFA) in 1987 [1] paved the way due to its outstanding properties including being broadband, highly efficient, and polarization independent, and having small coupling loss and low noise. In addition, its transition energy fortuitously coincides with the low-loss spectral window of conventional optical fibers, allowing the simultaneous amplification of hundreds of waves at different wavelengths carrying interdependent data, thus eliminating expensive per-channel amplification or signal regeneration. Whenever one sends an email, makes an internet search, or interacts in social media, it is certain that these data have passed through numerous optical amplifiers.

There are many types of amplifiers, and they can be broadly classified in different ways. All have their inherent benefits and drawbacks, so the proper choice depends on the application in mind. Some are based on rare-Earth-ion-doped optical fibers (such as the EDFA), and some are based on semiconductors, the latter normally being electrically pumped, while others are usually optically pumped by an external laser. Most rely on population inversion resulting in stimulated transitions between energy levels in the host material. Optical amplifiers are commonly operated as lumped elements (i.e., amplification taking place at one specific point in a system), while some can also suitably be implemented in a distributed fashion, e.g., amplification takes place along a transmission fiber itself. Optical amplification can also rely on stimulated scattering resulting from nonlinearities in a fiber. Examples include stimulated Raman scattering (SRS) and stimulated Brillouin scattering (SBS). The second- ($\chi^{(2)}$) or third-order ($\chi^{(3)}$, the Kerr effect) nonlinear susceptibility of a medium (such as LiNbO_3 or silica fiber, respectively) can also be used to create parametric amplification through the effect of three-wave or four-wave mixing (FWM), respectively. Here the optical pump wavelength defines a virtual energy transition state determining the spectral region of the gain. Some amplifiers have a slow spontaneous transition between the upper and lower energy state (which is the case in an EDFA, typically milliseconds), making them particularly power efficient, while others have a very fast transition (femtoseconds), allowing these to offer functionalities other than amplification, such as ultrafast all-optical switching and signal wavelength conversion. Finally, some amplifiers are bidirectional (i.e., amplifying light in both directions) such as the EDFA, while others are unidirectional (such as parametric amplifiers, and those based on SBS), which may be of practical importance in some cases.

During the past 20 years, there has been an increased interest in parametric amplifiers and their prospects in various applications. Their basic features are now well understood, and many of the implementation challenges have been solved, while others still do remain. In addition, several experimental demonstrations have been made showing some of their unique capabilities. Thus, these amplifiers now have the promise of wider use in different applications and attracting a broader range of users. This tutorial is therefore an attempt to condense the most important aspects of parametric amplifiers and their applications into a single paper addressing both fundamental and practical aspects. It is, however, not intended to be a comprehensive review of all the progress made over the years as there are other sources for that [2–5].

In this tutorial, we will focus mostly on parametric amplifiers relying on the nonlinearity of conventional silica fibers (albeit tailored for this application) and their application in optical communication systems operating in the low-loss attenuation

window around 1550 nm. However, much of the discussion here is generic and can, in principle, be applied using nonlinear platforms other than fibers as well as other wavelength ranges for a range of other applications. We will distinguish between phase-insensitive amplification (PIA) and phase-sensitive amplification (PSA), the difference among the two simply being that the gain in the latter is dependent on the absolute optical phase of the incoming signal wave, while it is not in the former. The EDFA is thus an example of the former. In addition, parametric amplifiers can, in principle, amplify light across a very broad spectrum as they do not rely on stimulated emission of light at a specific energy dictated by the amplification medium transition cross sections. In contrast, the spectral features of parametric amplifiers are dictated by dispersion properties of the medium used and by the pump wavelength. Therefore, the basic principles of these amplifiers can be translated to entirely new wavelength ranges including visible to mid-infrared, thereby having the potential to open up new application areas.

This paper is organized as follows. The remaining part of this section introduces some basic and general aspects of optical amplifiers and their use in fiber-optic transmission links. Section 2 provides a summary of the history of optical parametric amplifiers. In Section 3, the basics of $\chi^{(2)}$ -based and in particular $\chi^{(3)}$ -based parametric amplification is discussed including many of the various regimes of operation that are possible. It will also describe the specific case when an optical fiber is used as the medium for amplification. Section 4 focusses on the noise properties, while Section 5 presents practical implementation considerations. In Section 6, we discuss the ability to mitigate transmission-fiber-induced nonlinear impairments, self-phase modulation (SPM), and cross-phase modulation (XPM), in PSA-based optical transmission links. Section 7 overviews actual experimental transmission study examples, while Section 8 illustrates some other specific applications of parametric amplifiers. Finally, before concluding in Section 10, we discuss future prospects including the use of platforms other than optical fibers serving as the gain medium in Section 9.

1.3. Basic Aspects of Amplifiers and Their Use in Optical Transmission Links

In lightwave transmission systems, optical amplifiers are used primarily in three ways: (1) as a booster at the transmitter to provide the optimal launch power, (2) as an in-line amplifier to periodically compensate for the inherent transmission fiber loss, and (3) as a preamplifier in the receiver to improve the receiver sensitivity in an otherwise electronic-noise-limited receiver. Figure 1 shows a typical attenuation spectrum for optical fibers used in transmission systems indicating a low-loss window of several hundred nanometers depending on acceptable attenuation. Currently used EDFAs are suitable for amplification in the C-band (1525–1565 nm) and L-band (1565–1605 nm), thus representing only about 20% of the full potential of the transmission fiber. Therefore, there is ongoing research on other type of amplifiers covering a larger spectral region, including, e.g., semiconductor optical amplifiers [6] and parametric amplifiers being discussed here.

Aside from the ability to amplify light with sufficient gain across the desired optical frequency range, the noise properties of amplifiers are of essential importance in most applications. The noise figure (NF) is simply defined as the signal-to-noise ratio (SNR) degradation caused by the amplifier, as observed with an ideal optical detector (100% quantum efficiency) in the electrical domain before and after the amplification. Two important assumptions are made in order for this definition to be valid: (1) The input optical wave is noise limited only by shot noise, and (2) the amplifier is operating in a linear regime, i.e., there is no degradation of the signal waveform upon amplification. This is different from operating in saturation (i.e., when the amplifier gain is dependent on the power of the input signal); an EDFA experiencing saturation will normally not distort the signal waveform, a result of the very long excited state

lifetime in erbium, and can thus be considered a linear amplifier in this context, while for other types of amplifiers, this may not be the case.

Fundamentally, since the photon energy ($h\nu$) is much larger than the thermal energy (kT) at room temperature, the lowest possible NF of optical amplifiers operating at high gain ($\gg 10$) is 2 (3 dB). This is in contrast to radio-frequency (RF) amplifiers, which when operated at room temperature will be dominated by thermal noise both at the input and the output, and quantum noise can be ignored, thus resulting in $NF = 1$ (0 dB) being possible. A more general expression for this quantum limit applicable also at low optical gain is discussed in Section 4, $NF = 2(1 - 1/G) + 1/G$, thus ranging from 1 to 2 (0 to 3 dB) as the gain (G) is increased from 1 to infinity. In reality, a typical commercial EDFA has $NF \cong 5$ dB and a gain of 30 dB.

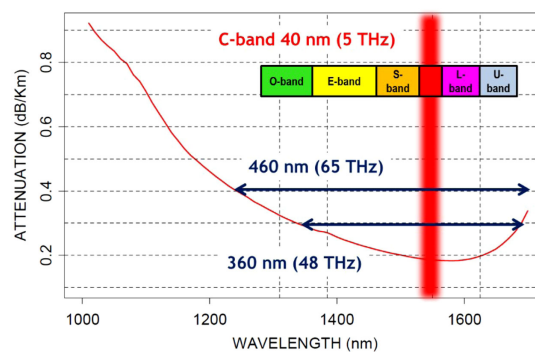
However, if an optical parametric amplifier is implemented in a phase-sensitive mode, it can under certain conditions operate without generating excess noise, i.e., providing a quantum-limited $NF = 0$ dB both at low and high gains, which is a unique property. The fundamental reason for noiseless amplification is that in the phase-sensitive regime, all the noise inputs of the amplifier also carry useful signal inputs, whereas in the PIA regime, there is an equivalent noise input without a signal. This is not in opposition to the Heisenberg uncertainty principle, since while the noise is reduced in one quadrature, it is increased in the other (as will be discussed in Subsection 4.2).

When considering an optical transmission link (see Fig. 2), it is convenient to introduce a NF for the whole link, thus describing the overall SNR degradation in the link. Let us consider a link with m spans of periodic, lumped amplification with gain equal to the span loss (L) at the conventional quantum limit ($NF = 3$ dB). In this case, the link NF can be expressed as (see Subsection 4.3 for details)

$$NF_{\text{lumped}} \approx 1 + 2mG \left(1 - \frac{1}{G}\right) \approx 2mG, \quad (1)$$

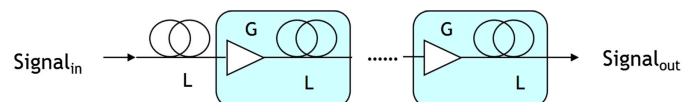
where the last approximation is made for many spans and $G \gg 1$.

Figure 1



Typical attenuation spectrum for a state-of-the-art silica fiber. The different amplification bands have been indicated.

Figure 2



Fiber optic communication link with in-line optical amplifiers.

This clearly illustrates the importance of span loss for the overall link noise performance. If we instead consider a case with an ideal distributed amplification (again with an inherent $NF = 3$ dB for the amplification process) with no signal power variation along the span, the resulting link NF is

$$NF_{\text{distributed}} \approx 1 + 2m \ln(G), \quad (2)$$

which illustrates the fundamental benefit of distributed amplification in terms of SNR degradation. The relative improvement compared to the case of lumped amplification after many spans is $G/\ln(G)$, showing that distributed amplification is particularly useful with long (or high loss) spans. As an example, using 200 km spans with a fiber having 0.2 dB/km loss, the link NFs in the above cases are 56 dB and 26 dB, respectively, a huge 30 dB advantage for the distributed case in this idealized scenario. In reality, the difference is significantly smaller, partly due to the fact that there will always be some amount of undesired signal variation along the spans. Nevertheless, this approach is used in many cases, e.g., when in-line amplification is undesired. The preferred approach is to use the SRS effect mentioned earlier, creating Raman gain in the transmission fiber itself by appropriately pumping it with one or several lasers in a counter- and/or copropagation fashion along with the signal [7].

Here, however, we have ignored optical nonlinearities. These are essential for parametric amplification as will be discussed later, but also need to be considered in optical fiber transmission systems where they will cause signal impairments. In fact, noise and nonlinearities are the two fundamental aspects that will ultimately limit the maximum throughput in any optical fiber communication link over long distances of fiber.

Equations (1) and (2) can be modified if ideal PSAs (and replacing the input signal in Fig. 2 with a signal and an idler wave each containing half the power of the signal in the figure) with 0 dB NF are used instead, by simply replacing $2m$ with m , resulting in an additional link NF improvement [8]. Thus, the best possible link performance in terms of maintaining the highest SNR is distributed amplification with PSAs.

Optical amplifiers can also be used in free-space optical (FSO) transmission links. In such links, nonlinearities can be ignored, and diffraction loss will often be the main limiting factor for the power budget, particularly for long-reach links. Thus, in this case, noise will be a particularly critical aspect when designing such links. The link NF (dB) in this case is simply equal to the loss (dB) between the transmitter and receiver plus the NF (dB) of the optical preamplifier (if being used as part of the receiver).

2. BRIEF HISTORY OF PARAMETRIC AMPLIFIERS

This section briefly reviews parametric amplifiers and, in particular, fiber optical parametric amplifiers.

2.1. Early Days of Nonlinear Optics

A parametric amplifier amplifies a signal via a medium in which some parameter is changed by an external “pump.” Originally, parametric amplifiers were considered for electrical transmission lines, e.g., by Cullen [9], who analyzed oscillating electric fields in a transmission line with varying capacitances. An analog effect can be observed for a mechanical pendulum, which can be pumped by periodically changing a parameter such as the pendulum length. This is well exemplified by a children’s swing, where the swinging child produces the pumping via periodically changing its center of mass (and thus effectively the length of the pendulum) *twice*

every swing period [10]. Thus, the parametric pump in this case has a frequency twice the swinging frequency.

Most often, however, we refer to parametric amplifiers in nonlinear systems, where the parameter responsible for pumping depends on the amplitude of the signal that is being amplified, or an external pump that drives the oscillation. In electronics, nonlinear capacitors are the typical example [9,11], whereas in nonlinear optics, the nonlinear susceptibility is responsible for coupling the signal with the pump.

Nonlinear optics started as a research field with the development of the laser [12], which enabled coherent, intense, and collimated light. Franken [13] demonstrated the first instance of optical nonlinearity, by showing second-harmonic generation (SHG) in 1961. Although harmonics are the simplest example of parametric mixing, other mechanisms such as sum- and difference- frequency mixing can be realized in second-order nonlinear media, and the theory for this was laid out in the extensive paper by Armstrong *et al.* [14], and also independently proposed by Akhmanov and Khoklov [15].

In second-order nonlinear media, two waves are mixed to generate a third, and the processes of sum/difference-frequency and SHG is then often called *three-wave mixing*. Similarly, wave mixing in third-order nonlinear media is called FWM. As will be explained in Subsection 3.2, the third-order nonlinearity is dominating in amorphous glasses such as silica fibers, and since fiber parametric amplifiers are central to this work, we will focus the review on these devices. However, since third-order nonlinearities, in general, are weaker than second order, they were demonstrated somewhat later [16,17], and it took until 1974 before FWM was demonstrated in a multimode fiber by Stolen *et al.* [18]. In single-mode fiber (SMF), FWM was demonstrated by Hill *et al.* in 1978 [19], although in the visible regime.

As will be shown in Subsection 3.2c, low dispersion facilitates FWM, and therefore the work on FWM in SMFs took off in the first half of the 1980s when lasers in the 1.3 μm regime became available [20–22]. These works demonstrated the three-wave configuration (a pump close to the zero-dispersion wavelength surrounded by signal and idler waves) that we today use most in parametric devices.

2.2. Optical Amplification and Squeezing

Optical amplifiers are a key ingredient in lasers, so the history of optical amplifiers follows that of lasers closely. Restricting ourselves to fiber amplifiers, some early work was done by Snitzer *et al.* in the 60s, [23,24], where glass rods doped with rare-Earth ions (Nd, Yb, Er) were demonstrated, as an early precursor to today's fiber amplifiers. However, as an alternative to amplifiers based on active fibers (i.e., fibers with specific dopants providing gain at specific frequencies), optical nonlinearities can also provide gain [15]. The earliest example was probably the Raman gain investigated already in the mid-70s by Stolen *et al.* in fused (amorphous) silica fibers [18,25,26]. In this context also, Brillouin gain [27] should be mentioned although the narrow bandwidth (10–100 of MHz) makes Brillouin amplification less useful in fiber communications. The mid-80s saw renewed interest in fiber amplifiers, because the fiber attenuation in telecom links was a critical hurdle to overcome. A key breakthrough was then the EDFA [1,28] that came to revolutionize the area of fiber communications, and related active-fiber amplifiers also became key drivers in laser welding and machining. The impact of the EDFA in (optical) telecommunications is hard to overstate, since it enabled both longer distances and increased bandwidths for the data carried by fibers [29].

Optical amplification is, in a quantum mechanical description, based on the process of *stimulated emission*, which emits photons in the same quantum mechanical state (often called *mode*) as an incoming photon—thus giving amplification. However, at the same time, *spontaneous emission*, i.e., the emission of a photon with the same energy but with otherwise random properties, has a nonzero probability. Spontaneously emitted photons are therefore the key source of noise in optical amplifiers and, concomitantly, the key limiting noise source in optical links where optical amplifiers are used. Therefore, the theory of quantum mechanical noise in amplification and photodetection are key elements in the understanding of optical amplifiers and long-haul optical links.

The important paper by Caves [30] laid out the facts around this, and established the noise properties of optical amplifiers, e.g., that PIAs always must add equivalent input noise relative to the shot noise limit—the so-called 3 dB NF limit of optical amplifiers. However, this limit can be somewhat circumvented by PSAs, where the two quadratures of the optical field are subject to different gains. In the mid 80s, Yamamoto *et al.* [31,32] also discussed the related fundamental quantum mechanical limits of photodetection and amplification for such systems, but it is noteworthy that the basic knowledge about the amplifier limitations to information capacity was known by Gordon already in the 60s [33]. Soon these results found their way into analyses of the noise limitations of transmission systems with optical amplifiers [34].

The unequal-quadrature gain provided by PSAs gives rise to so called *squeezed* photon states, where the uncertainty in the two quadratures are unequal [35,36]. It was proposed in these papers that a parametric amplifier could be used to synthesize such squeezed states, which would have uncertainties below the shot noise limit in one quadrature, at the expense of higher uncertainty in the other quadrature. As a result, a vivid research on parametric amplifiers and squeezing in the mid-80s was conducted, and in 1985, Slusher demonstrated the first squeezed state by use of a parametric amplification in Na-atoms [37]. In the following years, PSA [38] and squeezing [39] was observed also by using FWM in fibers, even if the observed gain was very small. It was also proposed [40,41] and later experimentally verified [42] that squeezing could be realized in a nonlinear phase-sensitive interferometer. Marhic *et al.* [43] took this idea a step further and demonstrated the first phase-sensitive parametric gain in a fiber Sagnac interferometer using 300 m of polarization-maintaining fiber.

Amplifier NFs below 3 dB were experimentally observed for the first time by Levenson *et al.* in a 1993 experiment using the second-order nonlinearity in KTP [44]. A set of experimental results by Imajuku *et al.* in the late 90s reported interferometric-fiber-based PSA up to 20 dB [45], which later was implemented and evaluated in various transmission link settings [46–49]. The first observation of a sub-3-dB NF in fiber-based amplifiers was reported in 1999 using nonlinear Sagnac loops by Levandovsky *et al.* [50,51] and independently also by Imajuku *et al.* [52,53].

2.3. Fiber-Optic Parametric Amplifiers

Fiber-optic parametric amplifiers (FOPAs), based on FWM in a guided wave (rather than interferometric structure), were not successfully realized until the late 90s and early 2000s. Even if EDFAs were available to provide high pump power, there were two practical problems. One was the SBS that prevented the launch of a strong continuous wave (CW) pump in the fiber, thus effectively limiting the possible pump power. The second was the nonlinearity of the fiber, which was so weak that kilometers of fiber were needed, and so long fibers suffer from imperfections such as varying zero-dispersion along the fiber length that will affect the FWM [54]. The latter problem was addressed by the development of single-mode highly nonlinear fibers

(HNLFs) whose mode field enabled low-loss splicing to standard single-mode fibers (SSMFs), while yet having a nonlinearity around 10 times higher. This was realized by a combination of GeO₂-doping of the core, a reduced core radius, and a W-shaped refractive index profile. An overview of these fibers and the trade-offs involved in their design can be found in Ref. [55]. The 1999 experiment by Imajuku *et al.* [52] discussed above was one early example of HNLFs being applied to nonlinear fiber-based amplifiers.

In 2001, Hansryd *et al.* [56,57] used HNLFs to develop the first fiber-based parametric amplifier with CW pumping and significant gain, now based on FWM. The SBS was suppressed by phase modulating the pump, thereby increasing the Brillouin threshold with 10–20 dB, virtually eliminating that problem. The HNLFF is typically designed with very low dispersion in the 1550 nm region, to facilitate phase matching (cf. Subsection 3.2c.), which makes it an almost ideal platform for the exploration of parametric devices. The smaller core radius contributes to shift the dispersion zero from 1300 nm (which is given by the material dispersion of silica) to longer wavelengths [58]. The HNLFF was thus the platform of choice in much of the parametric device research in the first and second decades of the 2000s. Parametric (phase-insensitive) amplifiers with very high gain [59] and large bandwidth [60–63] were then demonstrated, and the fundamental noise properties of these amplifiers were investigated as well [64–66].

Underlying much of this work was theoretical work on the understanding of FOPAs. For example, the impact of dispersion on the gain spectrum was studied by Marhic *et al.* [67,68]. By using a pair of pumps, a flat gain spectrum can be accomplished, as explored theoretically [69] and experimentally [70]. The quantum mechanical theory for parametric amplifiers was studied in a series of papers by McKinstrie *et al.* [71–73].

PSA operation started to pick up interest around 2005 by Vasilyev [8] and McKinstrie [73,74]. Experimentally, pioneering PSA work was done in the context of regeneration in a series of papers by Crussore *et al.* [75–77] and reviewed in Ref. [78]. Simultaneous phase and amplitude regeneration was shown in Refs. [79,80].

An important contribution to the studies of PSAs was the so-called copier-PSA setup, introduced by Tang *et al.* [81,82] that will be discussed more in Subsection 3.2e. Its key parts were a first parametric stage to “copy” the signal to a conjugate idler wave, and then as a second stage, another parametric amplifier became phase-sensitive due to the presence of all waves. Its phase and amplitude transfer characteristics were studied in more detail in Refs. [83–85] and in a series of experiments with coherent quadrature phase shift keying (QPSK) data by Tong *et al.* [86,87]. More recent developments including full transmission link experiments will be discussed later in this paper.

3. FUNDAMENTAL ASPECTS OF PARAMETRIC AMPLIFIERS

In this section, we will discuss the basic properties of optical parametric amplifiers. Since the optical wave phenomena we will discuss are generic, we will start by a simple mechanical oscillator example, and then move on to optics.

3.1. Parametric Pendulum

A parametric amplifier amplifies an oscillation by changing a *parameter* governing the properties of the oscillation. The simplest mechanical example is the children’s swing, i.e., a mechanical pendulum, where a child standing on the swing “pumps” the swing by periodically moving up and down. By periodically rising and squatting,

the pumping takes place via a change of the effective pendulum length, which is the parameter responsible for the interaction between the pumping motion and the swinging motion. If this periodic pumping is done with proper frequency and phase, the swing amplitude will increase, and the child thus *parametrically amplifies* the swing. We use an analysis inspired by [10,88]. Let us denote the mass with m and the swing angle relative to vertical with ϕ . The length of the swing is some function of time $L(t)$, so that the swing angular velocity is $v = L\phi'(t)$ and the angular momentum p is

$$p = mvL = mL^2\phi'(t). \quad (3)$$

The change in angular momentum is given by the torque around the rotation axis, which is given by $-mgL \sin(\phi)$, where g is the acceleration from gravity. Thus, we have

$$p'(t) = -mgL \sin(\phi) \approx -mgL\phi, \quad (4)$$

where the approximation of small angles is not necessary but suffices for this simple case study. By differentiating Eq. (3) and eliminating $p'(t)$, using Eq. (4), one can obtain the familiar equation of motion as a second-order equation for $\phi(t)$. However, that approach includes the derivative of L , which is not suitable for the simple case that we will study when L is piecewise constant, as elaborated in Ref. [88]. Instead, we use a matrix approach, and write the equations of motion as

$$\frac{d}{dt} \begin{pmatrix} \phi \\ p \end{pmatrix} = \begin{pmatrix} 0 & \frac{1}{mL^2(t)} \\ -mgL(t) & 0 \end{pmatrix} \begin{pmatrix} \phi \\ p \end{pmatrix} = M(L) \begin{pmatrix} \phi \\ p \end{pmatrix}, \quad (5)$$

where we introduced the matrix M , which is a function of L . If L is constant, the solution to these equations are given by

$$\begin{pmatrix} \phi(t) \\ p(t) \end{pmatrix} = T(t, L) \begin{pmatrix} \phi(0) \\ p(0) \end{pmatrix}, \quad (6)$$

where the transfer matrix $T(t, L) = \exp(Mt) = I \cos(\omega t) + M \sin(\omega t)/\omega$, the unity matrix is denoted I , and $\omega = \sqrt{g/L}$ is the frequency of oscillation. We can now model changing, and piecewise constant, pendulum lengths by multiplying sequences of the matrix T . For example, as kids quickly learn, by squatting (increasing L) on the downward motion and rising up (decreasing L) during the upward motion, they can amplify the swing. For one period of swinging, this is modeled by the T -matrix product $T_{\text{per}} = T_2 T_1 T_2 T_1$, where each matrix is evaluated at $\omega t = \pi/2$, and $T_{1,2} = M(L_{1,2})\sqrt{L_{1,2}/g}$. Evaluating the matrix products gives the transfer matrix for one period as

$$T_{\text{per}} = \begin{pmatrix} \left(\frac{L_1}{L_2}\right)^3 & 0 \\ 0 & \left(\frac{L_2}{L_1}\right)^3 \end{pmatrix}. \quad (7)$$

This means that the swing angle ϕ is amplified a factor $(L_1/L_2)^3$ every swing period. In Fig. 3, we plot $\phi(t)/\phi(0)$ in blue from a numerical solution of Eq. (5) when $L(t)$ changes between $L_1 = 1 + 0.05$ and $L_2 = 1 - 0.05$ at every quarter period (shown in purple). For simplicity, we have put $m = g = 1$, which makes the swing period approximately 2π . Figures 3(a) and 3(b) show the swing with two different initial conditions, and the red line shows (for reference) the undamped swing, i.e., the solution for $L(t) = 1$. In Fig. 3(a), the longer pendulum length (squatting child) occurs in the downward motion, and in Fig. 3(b), the shorter length (upright child) occurs in

the downward motion. The dashed yellow line shows the resulting parametric gain $(L_1/L_2)^{\pm 3t/(2\pi)}$ in the two cases. This reflects the phase-sensitive property of the parametrically amplified swing: given the same pump, one quadrature (the cosine-mode in our case) is amplified while the other quadrature (the sine-mode) is deamplified.

The above is a linear physics example. In a *nonlinear* parametric amplifier, the pumping is proportional to the signal itself or the powers of it, e.g., ϕ^2 or ϕ^3 , which we will refer to as second- or third-order nonlinearities. If ϕ comprises a single wave at frequency ω , the parametric interaction will lead to multiples of this frequency, which is called *harmonic generation*. If it comprises two or more frequencies, mixing components such a sum-frequency generation (SFG) or difference-frequency generation (DFG) will arise. The above case with the mechanical pendulum would then correspond to *parametric downconversion*, where the power of the pump with twice the signal frequency is converted to (or from) the signal wave.

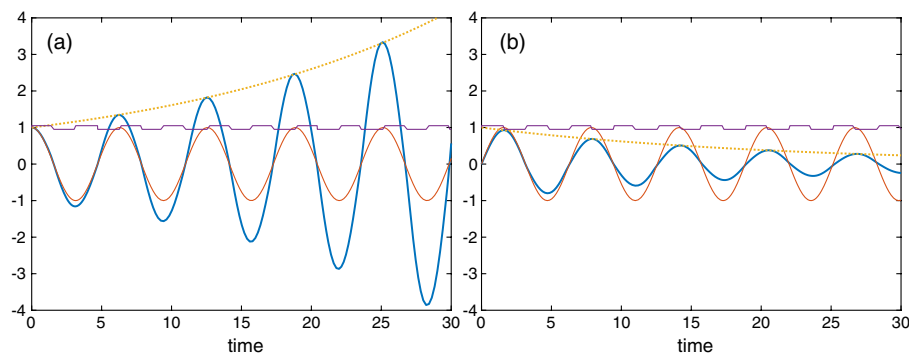
A context where this is particularly prevalent is in optics and more specifically, *nonlinear optics*. There the medium of wave propagation is nonlinear, and as a result the wave equations governing the optical waves will comprise nonlinear terms that will generate new frequencies via parametric mixing.

3.2. Nonlinearities in $\chi^{(2)}$ and $\chi^{(3)}$ Materials

Nonlinear optical materials are modeled electromagnetically via the polarization field vector \vec{P} , which is related to the electric field vector \vec{E} via the susceptibility χ . To allow for arbitrary functional dependencies, it is customary to write \vec{P} as a Taylor expansion of \vec{E} as $\vec{P} = \sum_{k=1} \chi^{(k)} (\vec{E})^k$, where the order k of the nonlinearity is modeled via the k th order susceptibility $\chi^{(k)}$. To connect with the previous section, the polarization vector will cause parametric interaction in the wave equation for the electric field, which can be derived from Maxwell's equations (under some simplifying assumptions) as

$$\nabla^2 \vec{E} - \frac{1}{c^2} \frac{\partial \vec{E}}{\partial t^2} = \frac{1}{c^2} \frac{\partial \vec{P}}{\partial t^2}. \quad (8)$$

Figure 3



Oscillations of a parametrically pumped swing in (a) amplified and (b) deamplified mode. The purple lines show an oscillating but piecewise constant pendulum length $L(t)$, which is the same in (a) and (b). The blue lines show the corresponding solution $\phi(t)/\phi(0)$ to Eq. (5) with different initial conditions so that in (a), L is longer during the downward motion and shorter in the upward motion, and for (b), the opposite holds. The yellow dashed lines show the parametric amplification/damping $(L_1/L_2)^{\pm 3t/(2\pi)}$ in the two cases. The red lines show for reference the unamplified solutions for the constant length $L(t) = 1$, which is simply $\cos(t)$ in (a) and $\sin(t)$ in (b).

Various material properties are then modeled via the susceptibility, e.g., inhomogeneity if χ is spatially dependent, dispersion if χ depends on frequency, anisotropy if χ is a matrix relating the components of \vec{P} to the components of \vec{E} .

In linear optics, $\vec{P} = \chi^{(1)}(t, \vec{r}) * \vec{E}$, and $\chi^{(1)}$ is in the most general case a spatially dependent matrix response function that should be convolved with the electric field.

In nonlinear optics, one must model χ as a *tensor*, a generalized array, relating each component of n electric field vectors to each of the three polarization field components. For an n th-order nonlinearity, the most general $\chi^{(n)}$ tensor contains 3^{n+1} components, which may obviously be quite complicated [89,90]. For this tutorial, however, we will restrict ourselves to scalar waves for simplicity, and we will discuss mainly the frequency content of these waves.

Obviously the second-order nonlinearity is the lowest order, and it should be the first one to manifest in most media as the optical power is increased. However, there is a caveat. Consider a medium with *inversion symmetry*, i.e., if you change sign of all coordinates, including the electric field direction, nothing should change, and the governing equations must be the same. However, if you change $\vec{E} \rightarrow -\vec{E}$ in Eq. (8) also, the right-hand side must change to negative in such media. Thus, for second (and all even nonlinearities), the minus signs cancel out, and the right-hand side (the polarization field) will not change sign. The conclusion from this exercise is very powerful: *media with inversion symmetry cannot contain even-order nonlinearities*. In fact, for such media, the lowest order nonlinearity is the third order.

What media has inversion symmetry, then? Clearly gases and liquids with randomly placed and oriented molecules will (macroscopically, on average) have inversion symmetry and also *amorphous* solids, i.e., solids with no dominating crystal structure but randomly placed and oriented molecules. Fused silica (normal window glass), which makes up telecom fibers, belongs to this class of solids and has $\chi^{(2)} = 0$. However, most crystalline glasses (e.g., KTP, LiNbO₃, crystalline silicon, and other semiconductors) do not, and will exhibit a second-order nonlinearity, $\chi^{(2)}$.

3.2a. Second-Order Nonlinearities

Consider a monochromatic wave oscillating as $E \sim \cos(\omega t)$, and propagating in a $\chi^{(2)}$ material. The source term, the polarization field in Eq. (8), will be proportional to $\cos^2(\omega t) = (1 + \cos(2\omega t))/2$, and thus comprise a constant (nonoscillating) part and a second-harmonic part. The constant part is called *optical rectification*, and usually of is limited interest, but it will indeed correspond to a static electric field directed transversally over the propagating wave.

The presence of a second-harmonic means that a wave at the double frequency will be generated, and the efficiency of this process will depend on many things, e.g., the attenuation in the medium at the second-harmonic frequency, as well as its propagation constant. If the propagation constant of the generating wave is $\beta = 2\pi/\lambda$, with λ being the wavelength in the medium, that of the resulting second harmonic will be 2β . However, the medium has a frequency-dependent dispersion relation $\beta(\omega)$ that forces any wave at the second harmonic to oscillate with wavenumber $\beta(2\omega)$, and if this is not equal to $2\beta(\omega)$, the process is *not* phase matched, and the generation of a strong second harmonic will be precluded. Therefore, phase matching, and whether the parametric process is strong or not, will in our context be determined by the linear dispersion relation for the ingoing waves (sometimes, which will then be stated explicitly, extended with nonlinear contributions to the linear dispersion relations). We can define a *phase mismatch*, $\Delta\beta$, for the second-harmonic process as

$$\Delta\beta = 2\beta(\omega) - \beta(2\omega). \quad (9)$$

Only when $\Delta\beta$ is small, (in relation to the inverse interaction length in the nonlinear medium), efficient harmonic generation is possible. One might think that it must be possible to at least find one frequency for which the relation [Eq. (9)] holds, but it is actually quite difficult in most nonlinear media, especially in waveguides. If one seeks an efficient SHG, a common trick is then to add a periodicity (of order $\Delta\beta$) in the waveguide to make up for the phase mismatch. This is sometimes called *quasi-phase matching* (QPM), originally proposed in Ref. [14]. This technique is commonly used in frequency-doubling crystals of LiNbO_3 , which can be used to generate green ($\lambda \approx 532$) light from NdYAG laser light ($\lambda = 1064$ nm).

3.2b. Third-Order Nonlinearities—The Nonlinear Schrödinger Equation

The third-order nonlinearity manifests in most cases as a power-dependent refractive index, the so-called *Kerr-effect*, and most Kerr-nonlinear effects can be physically interpreted from this power-dependent index. If the index increases with optical power, the media is said to be *focusing*, since an intense beam can induce its own waveguide, and thus suppress diffraction [91]. In most glass crystals, this effect is very weak, and kilo- to megawatts of power are required to induce such self-focusing over the length of the material (typically centimeter distances for bulk crystals).

The most popular platform for the study of third-order nonlinear effects is without doubt the single-mode optical fiber. Already in 1973, Hasegawa and Tappert [92] proposed the nonlinear Schrödinger equation (NLSE) as a good model for short-pulse propagation in SMFs, i.e.,

$$i \frac{\partial u}{\partial z} + \beta \left(\omega_0 - i \frac{\partial}{\partial t} \right) u + \gamma |u|^2 u = 0, \quad (10)$$

where $u(z, t)$ is the wave amplitude normalized so that $|u|^2$ is the optical signal power, z is the propagation distance along the fiber, and t is the time coordinate for the signal. The nonlinear coefficient is γ , and $\beta(\omega)$ denotes the dispersion relation, which contains contributions from both the material and the waveguide (mode profile) properties of the fiber. The dispersion relation can be Taylor expanded around the optical carrier frequency ω_0 , and the different orders in this series will correspond to derivatives in the time domain. The notation $\beta(\omega_0 - i\partial/\partial t)$ should thus be interpreted as an operator defined by the Taylor expansion of β around ω_0 where each term gives a derivative order. If one limits the Taylor expansion order to 2, and transforms the time and space coordinates to a comoving reference frame, the standard NLSE is obtained [90] as

$$i \frac{\partial u}{\partial z} - \beta_2 \frac{\partial^2 u}{\partial t^2} + \gamma |u|^2 u = 0, \quad (11)$$

where β_2 denotes the dispersion coefficient, which is negative (positive) in the anomalous (normal) dispersion regime. SSMFs have anomalous dispersion for wavelengths above 1310 nm, and in the 1550 nm region, which is most commonly used in transmission, $\beta_2 = -20$ ps²/km, and $\gamma = 1.3$ (W km)⁻¹. There are two properties that make fibers such a nice playground for nonlinear optics, and it is their low loss [< 0.2 (dB/km) typically] and their long propagation distances. In transmission systems over hundreds of kilometers, the Kerr-nonlinearity is well-known to be significant and distort the data. Thanks to the low losses, fibers enable kilometers of propagation distances with limited attenuation so that nonlinear effects can manifest, which is a curse in data communication but a blessing in nonlinear optics research.

3.2c. Four-Wave Mixing

The study of parametric gain involves the study of how different frequencies interact in a nonlinear medium, and to study this one, typically makes an ansatz for the interacting waves. For this purpose, we will study the interaction of three waves; a pump that is symmetrically surrounded by a signal wave and an idler wave, i.e., $u = u_p \exp(i\omega_p t) + u_s \exp(i\omega_s t) + u_i \exp(i\omega_i t)$, where $2\omega_p = \omega_s + \omega_i$. For simplicity, we assume CWs, which make the wave amplitudes $u_{p,s,i}(z)$ functions of z only. After inserting this ansatz in the NLSE, we will see that a number of mixing frequencies is generated by the nonlinear term $|u|^2 u$, i.e., $\omega_a + \omega_b - \omega_c$, where indices a, b, c may denote any of the pump, signal, or idler wave. For three input waves, 27 terms arise, but many of them are degenerate, i.e., will oscillate at the same frequency. For example, if $a = b = c$, we have terms $\sim |u_p|^2 u_p$ and refer to this interaction as SPM. For $a \neq b = c$ or $b \neq a = c$, e.g., terms $\sim |u_s|^2 u_p$ arise, which are referred to as XPM. These effects will not cause any power transfer between the waves. On the other hand, the remaining terms, e.g., $\sim u_p^2 u_s^*$, will cause power transfer between frequencies, and they are usually called FWM terms.

After inserting the ansatz into the NLSE and limiting ourselves to the terms oscillating at $\omega_p, \omega_s, \omega_i$, we obtain the coupled set of equations,

$$\frac{du_p}{dz} = iu_p(\gamma(2P - |u_p|^2) + \beta_p) + i\gamma 2u_p^* u_s u_i, \quad (12)$$

$$\frac{du_s}{dz} = iu_s(\gamma(2P - |u_s|^2) + \beta_s) + i\gamma u_p^2 u_i^*, \quad (13)$$

$$\frac{du_i}{dz} = iu_i(\gamma(2P - |u_i|^2) + \beta_i) + i\gamma u_p^2 u_s^*, \quad (14)$$

where $\beta_{p,s,i}$ are the respective propagation constants for the three waves and

$$P = |u_p|^2 + |u_s|^2 + |u_i|^2 \quad (15)$$

is the total power. These equations were solved and analyzed in detail in Ref. [93], and here we will briefly describe the properties of the solutions in some relevant cases. Other relevant papers solving the general four-wave interaction analytically are [94,95], and the approximate route that we will follow is also done in Refs. [90,96].

First, one can note the existence of conserved quantities to the system [Eqs. (12)–(14)]. The total power P is conserved, as is the power difference between the signal and idler waves, $C = |u_s|^2 - |u_i|^2$, which is called the *Manley–Rowe relation*, after the authors of [11] who derived it for the first time. It essentially says that no signal light can be generated without an equal amount of idler light being generated at the same time. In the next section, we will see that this follows trivially from photon conservation in the quantum mechanical picture.

There is also a third invariant, the Hamiltonian, obtained from the observation that the system [Eqs. (12)–(14)] is a Hamiltonian set of equations, which can be integrated in terms of elliptic functions [93]. The general behavior of the solution is that for an intense pump wave, power is transferred from the pump to the signal and idler waves and then back again in a periodic fashion. The period of oscillation and the amount energy transfer will depend on the initial conditions.

The physical interpretation of the coupled system [Eqs. (12)–(14)] is as follows. The first three terms give rise to phase changes, which have a nonlinear contribution consisting of SPM and XPM (first two terms) and a linear contribution from the

propagation constants $\beta_{p,i,s}$ (third term). These terms cause no power transfer, but the fourth term does. It depends on the phase difference $\Delta\phi = 2\phi_p - \phi_s - \phi_i$ between the three waves, and only if this phase is constant or varies slowly with z can we have a significant power transfer between the pump and signal/idler. This is called *phase matching*. If it varies quickly with distance, the last terms in Eqs. (12)–(14) will average to zero and can be neglected, thus causing no power transfer between frequencies. We will describe the solution to these equations in more detail in the next section.

A simple classical-physics interpretation of the terms like $\sim u_p^2 u_i^*$ in the above equations can be given in terms of the induced refractive index. By writing it like $u_p[u_p u_i^*]$, we view the bracketed factor as an *induced refractive index*, from which the wave u_p scatters. Since u_p and u_i have different frequencies and wavenumbers, the induced refractive index forms a moving grating, with frequency $\omega_p - \omega_i$ and wavenumber $\beta_p - \beta_i$. It will then Doppler-shift the scattered wave to the frequency $\omega_p + \omega_p - \omega_i = \omega_s$. The scattered wave will have a wavenumber according to the Bragg condition $\beta_p + \beta_p - \beta_i$, and the process is phase matched (most efficient) if this wavenumber equals β_s , i.e., if the linear phase mismatch

$$\Delta\beta = 2\beta_p - \beta_s - \beta_i \quad (16)$$

is small, or vanishes. We can further analyze and solve Eqs. (12)–(14) by assuming the pump power is much larger than the signal and idler, which essentially means that we neglect second-order terms in the signal and idler from Eqs. (12)–(14). Then, Eq. (12) becomes decoupled from the other equations and can be solved as $u_p(z) = e_{p0} \exp(i(\beta_p + \gamma P_p)z)$, where e_{p0} is the initial (possibly complex) pump amplitude and $P_p = |e_{p0}|^2$ is the pump power. We then insert this into Eqs. (13) and (14), and substitute $u_{s,i} = e_{s,i} \exp(i(\kappa + \Delta\beta + \beta_{s,i})z)$ to reach a coupled first-order system with constant coefficients as

$$\frac{d}{dz} \begin{pmatrix} e_s \\ e_i^* \end{pmatrix} = i \begin{pmatrix} \kappa & \gamma e_{p0}^2 \\ -\gamma e_{p0}^{*2} & -\kappa \end{pmatrix} \begin{pmatrix} e_s \\ e_i^* \end{pmatrix} = K \begin{pmatrix} e_s \\ e_i^* \end{pmatrix}. \quad (17)$$

Here we have introduced the notation $\kappa = \gamma P_p - \Delta\beta/2$ and the constant matrix K . The solution to these equations can be written in terms of the matrix exponential as

$$\begin{pmatrix} e_s(z) \\ e_i^*(z) \end{pmatrix} = \exp(Kz) \begin{pmatrix} e_s(0) \\ e_i^*(0) \end{pmatrix}. \quad (18)$$

The matrix exponential is defined via its Taylor expansion, and it can be evaluated in closed form as follows: by noting that $K^2 = ((\gamma P_p)^2 - \kappa^2)I = g^2 I$, we conclude that all the even terms in the expansion are proportional to the unity matrix I . Similarly, all the odd terms can be shown to be proportional to K , and the final result is that $\exp(Kz) = I \cosh(gz) + K \sinh(gz)/g$. The solution can be written in terms of the canonical μ and ν coefficients as

$$\begin{pmatrix} e_s(z) \\ e_i^*(z) \end{pmatrix} = \begin{pmatrix} \mu(z) & \nu(z) \\ \nu^*(z) & \mu^*(z) \end{pmatrix} \begin{pmatrix} e_s(0) \\ e_i^*(0) \end{pmatrix}, \quad (19)$$

where z is the fiber length and the coefficients are given by

$$\mu(z) = \cosh(gz) + i\kappa \frac{\sinh(gz)}{g} \quad (20)$$

and

$$\nu(z) = i \frac{\gamma e_{p0}^2}{g} \sinh(gz). \quad (21)$$

Here the parametric gain coefficient $g = \sqrt{(\gamma P_p)^2 - \kappa^2}$, which can be imaginary if $\kappa > \gamma P_p$. Also note that the phase of the pump wave enters via the ν coefficient. The highest gain coefficient (maximum gain) is $g = \gamma P_p$ and occurs for $\kappa = 0$, or

$$2\gamma P_p - \Delta\beta = 0, \quad (22)$$

which generalizes the linear phase matching condition to account for the nonlinear (SPM and XPM) contributions to the propagation constants.

The transfer matrix Eq. (19) of the parametric gain is very general, and the (μ, ν) parametrization is subject to the important condition $|\mu|^2 - |\nu|^2 = 1$, which actually follows from the Manley–Rowe invariance, cf. [3]. We will see that this transfer matrix description underlies nearly all properties of parametric amplifiers.

3.2d. Parametric Amplification: Phase-Insensitive Gain

Let us first consider the case when the initial idler wave is zero, $e_i(0) = 0$. Then, the signal experiences the gain $|\mu|^2$ independently of its phase, and we therefore refer to this situation as PIA. The phase insensitive gain is given by $G_{\text{PIA}} = |\mu|^2$.

For perfect phase matching, as described by Eq. (22), one can show that since $\gamma P_p > 0$, we must have $\Delta\beta > 0$, which implies that the pump should lie in the anomalous dispersion regime. Then, we have $G_{\text{PIA}} = \cosh^2(\gamma P_p z)$. By noting that $\gamma P_p z$ is the nonlinear phase shift, we can conclude that the parametric gain grows exponentially with the nonlinear phase shift at perfect phase matching.

In contrast, when the linear phase mismatch is zero, $\Delta\beta = 0$, we obtain the limit $g \rightarrow 0$ and $\mu = 1 + i\gamma P_p z$ and $\nu = i\gamma e_{p0}^2 z$. This occurs, e.g., when the pump wave is exactly at the zero-dispersion. In this case, $G_{\text{PIA}} = 1 + (\gamma P_p z)^2$, which grows only quadratically with the nonlinear phase shift. However, this is not a generic property, and, for example, dual-pump [69,97] or dual-core [98] amplifiers can have exponential gain also for zero linear mismatch. This is of practical importance since it can be a route to flat and broadband gain.

We may note that the situation without an initial idler wave can be exploited in different ways; if one focuses on the signal wave, one has a parametric amplifier, and if one focuses on the idler wave—which becomes proportional to the conjugate signal—one has a *phase conjugator*, i.e., a device that produces a conjugate signal wave. The idler wave can also be used as a *wavelength converter* that transfers the signal to another wavelength.

3.2e. Phase-Sensitive Amplification

In the above discussion, we saw that PIA arises when the idler wave is zero at the input. In contrast, with both signal and idler present at the input, the output waves described by Eq. (19) are a *coherent superposition* of the two input waves. This may seem counterintuitive at first, since the waves oscillate at different frequencies. However, the ν factor is in fact proportional to u_p^2 , which makes the whole term proportional to $u_p^2 u_i^*$ oscillate with the same frequency as u_s .

The coherent superposition is, just as in interferometry, phase-sensitive, and the signal and idler can interfere constructively and destructively. The phase sensitive gain can be calculated as

$$G_{\text{PSA}} = \frac{|e_s(0)\mu(z) + e_i^*(0)v(z)|^2}{|e_s(0)|^2}. \quad (23)$$

To simplify this expression, we assume the signal and idler input powers are equal, i.e., $|e_s(0)| = |e_i(0)|$, which gives a phase sensitive gain,

$$G_{\text{PSA}}(\phi) = |\mu|^2 + |v|^2 + 2|\mu||v| \cos(\phi), \quad (24)$$

where $\phi = \phi_i + \phi_s + \phi_\mu - \phi_\nu = \phi_i + \phi_s - 2\phi_p + \phi_\mu - \pi/2$ is the phase angle of the complex number $\mu e_s(0)e_i(0)v^*$. Here the $\phi_{p,s,i}$ denotes the initial phase angles for the pump signal and idler waves, ϕ_μ is the phase angle of μ , and we can recall from Eq. (21) that the phase angle of v is $\phi_\nu = \pi/2 + 2\phi_p$. Depending on the relative phase ϕ , we can now realize that this gain is maximum for $\phi = 0$ (constructive interference) and minimum for $\phi = \pi$ (destructive interference), i.e.,

$$G_{\text{PSA-max/min}} = (|\mu| \pm |v|)^2, \quad (25)$$

from which we can see that the product of max and min gain is $G_{\text{PSA-max}}G_{\text{PSA-min}} = (|\mu|^2 - |v|^2)^2 = 1$. This implies that the minimum gain is in fact an induced *attenuation* equal to the inverse maximum gain. The required change of the pump phase for moving between maximum and minimum gain is thus $\pi/2$, and the same holds for the signal and idler phase if they are changed synchronously (as they often are in experiments). This differs from regular interferometry where the corresponding phase change between constructive to destructive interference is π .

To demonstrate, the max/min gains experimentally are a nontrivial task, since one needs to alter the relative phase between two different waves in a controlled way. Independent laser sources, for example, cannot be used since their relative phase wanders randomly. In the early work by Bar-Joseph *et al.* [38], this was done by external modulation of light from a single laser, and in the work by Tang *et al.* [81,82], it was elegantly demonstrated by using a two-step approach: a first parametric amplifier generates the idler from a signal and pump wave with the appropriate phase. In a second step, by inserting a dispersive fiber element before the PSA, the amplification and deamplification were demonstrated as a function of wavelength separation between the signal and idler. By using a commercial waveshaper instrument (that can apply an arbitrary phase and amplitude to a set of wavelengths), this was done in a more controlled way in later experiments by Kakande *et al.* [83], when as high as 30 dB of phase sensitive gain was demonstrated.

Another important observation is that $G_{\text{PSA-max}} = |\mu|^2 + |v|^2 + 2|\mu||v| = 2G - 1 + 2\sqrt{G(G-1)}$, where $G = G_{\text{PIA}} = |\mu|^2$ is the phase insensitive gain. In the limit of high gain, we thus have $G_{\text{PSA-max}} = 4G_{\text{PIA}}$, giving a 6 dB higher gain for PSA compared to PIA for the same pump power. This is just thanks to the coherent superposition of two equal amplitude waves that leads to a 4 times higher power than a single wave would have. This will, as we will see, lead to a 6 dB advantage in SNR for the phase-sensitive case.

3.3. Quantum Mechanical Interpretations and 1/2/4 Mode Operation

The classical-physics picture of FWM as scattering from induced gratings (described in Subsection 3.2c), has a much simpler quantum mechanics interpretation. Within quantum mechanics, a light wave is described as a stream of particles, photons, that must obey certain simple physics conservation laws such as energy and momentum conservation. We need to know that the energy of a photon is given by $E = \hbar\omega$, and the momentum by $\mathbf{p} = \hbar\mathbf{k}$, where ω and \mathbf{k} are the angular frequency and the wave

vector of the photon. The propagation constant is the modulus of the wave vector, i.e., $\beta = |\mathbf{k}|$. The above example with a pump surrounded by the signal and idler waves is then seen as a process in which two pump photons are converted to one signal and one idler photon, while maintaining energy and momentum conservation,

$$2\omega_p = \omega_s + \omega_i \quad 2\mathbf{k}_p = \mathbf{k}_s + \mathbf{k}_i, \quad (26)$$

where we dropped the constant \hbar from the equations. While the vector conservation property of the FWM wave vectors is important to maintain in, e.g., bulk crystals [89], they are all parallel in fibers, so we can simply drop the vector property, and work with propagation constants and thus recover the phase matching condition $2\beta_p = \beta_s + \beta_i$ from the photon momentum conservation. Thus, the Bragg condition used to describe light scattering from diffraction gratings is nothing but photon momentum conservation, and this is also the underlying physics behind applications such as photonic tweezers and radiation pressure and similar laser-based manipulations of particles.

There is, however, another crucial property that the quantum mechanical (photon) model tells us, and that is *photon number conservation*. We see from Eq. (26) that when two pump photons are annihilated, one signal and one idler photon are created. Thus, the signal and idler photons are created in pairs, and therefore the difference in photon number between the signal and idler must be constant. Thus, the photon flux Φ (number of photons per second flowing through the fiber) for signal minus idler must be conserved, i.e.,

$$\Phi_s - \Phi_i = \frac{P_s}{h\nu_s} - \frac{P_i}{h\nu_i} = \text{const}, \quad (27)$$

where $P_{s,i}$ denotes signal idler power. For small differences in signal and idler photon energies (as is often the case in practice), this means that the power difference between the signal and idler is conserved, which we referred to above as the Manley–Rowe condition. The quantum interpretation was pointed out by Weiss [99] around the same time as the Manley and Rowe paper [11], so the condition is sometimes called the Manley–Rowe–Weiss condition. In addition, the photon number conservation will lead to power conservation in the FWM process, i.e., the power lost by the pump is gained by the signal and idler. Since no power or momentum is lost in the process, parametric mixing is referred to as an *elastic scattering* process. In contrast, stimulated Raman and Brillouin scattering are *inelastic*, and lose power and momentum to optical and acoustical phonons (matter waves) in the material.

The single-pump FWM we described above is a special (degenerate) case of a more general (nondegenerate) situation involving two pumps at different frequencies. The corresponding photon energy conservation is then

$$\omega_{p1} + \omega_{p2} = \omega_s + \omega_i, \quad (28)$$

where $\omega_{p1,p2}$ denotes the two pump frequencies. The corresponding linear phase matching condition is $\Delta\beta = \beta_{p1} + \beta_{p2} - \beta_s - \beta_i = 0$, but the nonlinear XPM differs from the single-pump case. For example, the gain coefficient is given by [97]

$$g^2 = 4\gamma^2 P_1 P_2 - \left(\frac{\Delta\beta - \gamma(P_1 + P_2)}{2} \right)^2, \quad (29)$$

where $P_{1,2}$ are the pump powers. This implies that the maximum gain coefficient occurs for $\Delta\beta = \gamma(P_1 + P_2)$ and equals $2\gamma\sqrt{P_1 P_2}$. It also implies that g does not approach zero for zero linear mismatch, $\Delta\beta = 0$, in stark contrast with the single-pump case. This occurs, for example, in a fiber with pumps symmetrically placed

around the zero-dispersion wavelength, where high and flat gain can be obtained as shown in, e.g., [69,70,97].

Often, the various frequency configurations of parametric amplifiers are classified after how many signal frequencies (or modes) that are involved. It is therefore customary to talk about degenerate or nondegenerate pump/signal processes when one or more of the ingoing waves oscillate at the same frequency. Figure 4 shows a number of different FWM processes with one-mode [Fig. 4(a)], two-mode [Fig. 4(b)], and four-mode [Fig. 4(c–f)] interactions. We will discuss them separately below.

One-mode amplifier. The degenerate one-mode process shown in Fig. 4(a) is physically the same as the two-mode process in Fig. 4(b), but the roles of the pump and signal waves have been exchanged. The two cases are described by the same set of Eqs. (12)–(14), but the expected power flow for parametric gain goes in opposite directions. The transfer function for a one-mode parametric amplifier is

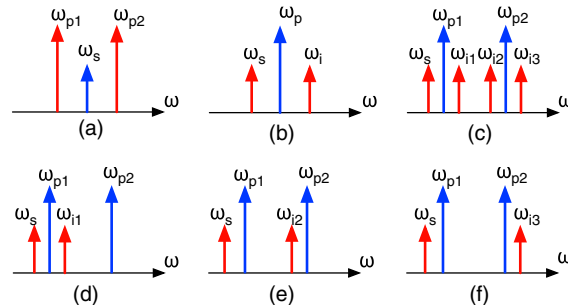
$$e_s(z) = \mu e_s(0) + \nu e_s(0)^*, \quad (30)$$

where, just as for the two-mode amplifier, $|\mu|^2 = G_{PIA} = 1 + |\nu|^2$. In the high-gain limit, where $|\mu| \approx |\nu|$, we find that $e_s(z)$ is the sum of two complex terms with equal amplitude but different phase angles. The phase angle of the first term is $\phi_\mu + \phi_s$, and that of the second term is $\phi_\nu - \phi_s$. When these are equal, i.e., $\phi_s = (\phi_\nu - \phi_\mu)/2$, then we have maximum gain equal to $|\mu| + |\nu|$. When they are π radians out of phase, i.e., $\phi_s = (\phi_\nu - \phi_\mu + \pi)/2$, we have maximum attenuation, $|\mu| - |\nu|$. Thus, one quadrature is amplified, and the other is deamplified by the same amount (in dB units) since $|\mu| + |\nu| = 1/(|\mu| - |\nu|)$.

This type of FOPA was demonstrated, e.g., in connection with optical regeneration, cf. [75,79,100].

Two-mode amplifier. The two-mode amplifier [Figs. 4(b) and 4(d)] has a signal and an idler wave, and it operates in a phase-insensitive mode if the idler is initially zero. It was described in detail in Subsection 3.2c above, and its transfer characteristics are given by the matrix relation Eq. (19). It is also equivalent to the widely studied modulational instability of the NLSE, which describes how the CW solution to the NLSE is unstable when perturbed by a small oscillation [101,102], and will lead to the

Figure 4



Different parametric amplifier configurations with signals/idlers in red and pumps in blue. (a) Degenerate one-mode amplifier. (b) A two-mode amplifier with degenerate pump. (c) A four-mode amplifier with one signal and three idler waves. The following three processes jointly form the four-mode process. (d) The modulational instability process, equivalent to the two-mode shown in (b). (e) The Bragg scattering process. (f) The phase conjugation process.

generation of a pulse train from the CW [103]. In fact, this is exactly the same initial condition as the three waves studied in Subsection 3.2c above, which means that modulational instability and two-mode FWM in optical fibers are equivalent phenomena.

Four-mode amplification. The four-mode interaction shown in Fig. 4(c) arises for two pump waves and actually involves three separate FWM processes, shown in the respective Figures 4(d–f). The four modes are denoted signal and idler1–3, and each of the four waves can obtain gain from each of these three processes.

The first process [Fig. 4(d)] is the modulational instability described above, and it arises around each pump without the other pump taking part in the process.

The second process [Fig. 4(e)] is the Bragg scattering process. This differs from the other two processes in that it does not provide any parametric gain, but rather *power exchange*. It will exchange the signal and idler two waves, similarly to a directional coupler. It has been used for, e.g., wavelength exchange in wavelength division multiplexing (WDM) systems [104,105].

The third process Fig. 4(f) is the phase conjugation process, and it is similar to the modulational instability, with the difference that two pump waves are involved, as described in Eq. (28). Just as for the modulational instability process, the phase conjugation produces a conjugated idler wave from the signal.

It is possible to put all four-mode processes in a transfer matrix formulation, just as the two-mode process, i.e.,

$$\begin{pmatrix} e_s(z) \\ e_{i1}^*(z) \\ e_{i2}(z) \\ e_{i3}^*(z) \end{pmatrix} = \begin{pmatrix} \mu & \nu & \delta & \kappa \\ \dots & \dots & \dots & \dots \\ \dots & \dots & \dots & \dots \\ \dots & \dots & \dots & \dots \end{pmatrix} \begin{pmatrix} e_s(0) \\ e_{i1}^*(0) \\ e_{i2}(0) \\ e_{i3}^*(0) \end{pmatrix} = G \begin{pmatrix} e_s(0) \\ e_{i1}^*(0) \\ e_{i2}(0) \\ e_{i3}^*(0) \end{pmatrix}, \quad (31)$$

where G denotes a 4×4 transfer matrix. The exact form, or a parametrization of this matrix similarly to the μ, ν coefficients in Eq. (19), is an unsolved problem, even if some progress and some studies on the four-mode problem have been made. For example, a generalized Manley–Rowe condition can be formulated in that $|e_s|^2 - |e_{i1}|^2 + |e_{i2}|^2 - |e_{i3}|^2$ is conserved, which will put constraints on G . Some theoretical analysis on the problem is found in the works of McKinstrie [69,71], and a four-mode modulational instability analysis was published in Ref. [106]. A more general theory based on transfer matrix singular value decomposition, so-called Schmidt-mode decomposition, has been published as well [107–109]. Significantly less works on four-mode than two-mode amplifiers have been published, however, and some of the experimental work [110,111] will be discussed in Subsection 5.5f below.

4. NOISE IN PARAMETRIC AMPLIFIERS

4.1. Amplifier Noise Basics

It is a fundamental fact, which follows from basic quantum mechanics [32], that optical amplifiers produce noise. PSAs are sometimes called “noiseless,” because they redistribute the quantum noise among the eigenmodes without adding any excess noise and thus, in theory, do not reduce the SNR of a shot-noise-limited input signal. PIAs on the other hand will always add extra noise and reduce the SNR [30]. For example, a PIA such as the EDFA generates spontaneous emission noise, also called amplified spontaneous emission (ASE) at the output with a power spectral density (PSD) (in units of W/Hz) of [34]

$$S_{\text{sp}} = n_{\text{sp}}(G - 1)h\nu, \quad (32)$$

where G is the amplifier gain, $h\nu$ is the photon energy, and $n_{\text{sp}} \geq 1$ is the spontaneous emission factor, related to the inversion of the amplifier. For a fully inverted amplifier, $n_{\text{sp}} = 1$, and the noise PSD is said to be *quantum-limited* to $(G - 1)h\nu$. It should be noted that this power is emitted in one polarization, and an equal amount is generated in the other polarization, which is usually neglected in theory since it can be filtered away from the signal with a polarizer. However, in measurements of ASE on an optical spectrum analyzer, both polarizations contribute and should be accounted for.

What is relevant in practice is how much the SNR is degraded by the amplifier. Modeling the optical signal amplitude as a signal plus an additive ASE noise leads to, after photodetection and squaring of this field, an electrical photocurrent with three terms, namely (i) the signal power, P_s , (ii) beating between the signal and ASE noise, so-called signal-spontaneous beating, and (iii) beating between the noise and the noise, so called spontaneous-spontaneous noise beating. In most circumstances, the s-sp noise dominates, and it has a variance of [34]

$$\sigma_{s-\text{sp}}^2 = 4R^2 P_s S_{\text{sp}} \Delta f, \quad (33)$$

in units of A^2 , where R is the photodetector responsivity and Δf is the detector bandwidth. This should be compared to the signal that gives an average photocurrent of RP_s . We then define the amplifier NF as the ratio of the SNRs before and after the amplifier,

$$NF = \frac{\text{SNR}_{\text{in}}}{\text{SNR}_{\text{out}}}, \quad (34)$$

which is a measure of how much the SNR (after photodetection) has degraded after the amplifier. It should be noted that this NF definition is based on direct-detected signals for simplicity, and the use of a more strict definition based on field quadratures and homodyne detection is possible but beyond the scope of this work. The different definitions agree for high signal powers when noise–noise interaction can be neglected. To obtain the SNR at the input, we use the fundamental shot noise (stemming from the discreteness of photons and the generated photoelectrons), which has a variance of $\sigma_s^2 = 2eRP_{\text{in}}\Delta f$, where e is the electron charge and P_{in} is the input power to the amplifier. The SNR at the output is affected by both shot noise and ASE noise, so the NF for the PIA such as the EDFA is

$$\text{NF}_{\text{PIA}} = \frac{(RP_{\text{in}})^2 \sigma_{s,\text{out}}^2 + \sigma_{s-\text{sp}}^2}{\sigma_{s,\text{in}}^2 (RG P_{\text{in}})^2} = 2n_{\text{sp}} \frac{G - 1}{G} + \frac{1}{G}, \quad (35)$$

where $\sigma_{s,\text{in/out}}$ denotes the shot noise variances based on the signal power before and after the amplifier. We also need to assume a unit-quantum-efficiency detector with responsivity $R = e/h\nu$ to derive the right-hand side of Eq. (35). The first term in Eq. (35) is the ASE contribution, and the second is the shot noise contribution. For a link with m amplifiers of gain G , the noise variances need to be added by multiplying the first term with m . We can invert the relationship (35) to express n_{sp} ,

$$n_{\text{sp}} = \frac{\text{NF} G - 1}{2(G - 1)}, \quad (36)$$

which is often approximated with $n_{\text{sp}} \approx \text{NF} G / (2(G - 1))$ and used instead of n_{sp} to express the ASE spectral density as

$$S_{\text{sp}} \approx \text{NF} G \frac{h\nu}{2}, \quad (37)$$

from which we can interpret the NF as a measure of how much in excess of G the vacuum fluctuations, which carry half a photon ($h\nu/2$) of energy, are amplified, or, alternatively, a noise PSD amounting to NF half-photons added at the amplifier input.

The above is based on a so-called *semiclassical* analysis of an optical amplifier, where the interaction medium is quantized but the optical field is still classical, and the vacuum fluctuations need to be incorporated as a classical field with a PSD of half a photon, $h\nu/2$. The ASE is then interpreted as amplified vacuum fluctuations (as shown above), and shot noise can be seen as arising from beating between the signal and the vacuum fluctuations in the photodetection process [112].

Similar results can be obtained also by a fully quantized optical field as described in, e.g., [30,32,71]. Such models often recover the NF in the idealized $n_{s,p} = 1$ limit, and give the well-known results for PIAs,

$$\text{NF}_{\text{PIA}} = 2 - \frac{1}{G}. \quad (38)$$

4.2. Noise in the Two-Mode Parametric Amplifier

4.2a. Quantum Noise

In this section, we will perform a NF analysis for the two-mode parametric amplifier. We model the amplifier with the transfer matrix Eq. (19). This discussion follows partly that of [54], App. B, and similar treatments can be found, for example, in Refs. [64,65] for the phase-insensitive FOPA, and [2,87] for the PSAs. At the input, we assume shot-noise-limited fields, i.e., we have $e_s + n_s$ and $e_i + n_i$ as input signal/idler fields to the amplifier, where $|e_{s,i}|^2 = P_{s,i}$ denotes the signal/idler powers and $n_{s,i}$ denotes independent noise fields with a PSD of $h\nu/2$. It is important to account for both noise fields even if no signal/idlers are present. The input SNR is then shot-noise-limited, and

$$\text{SNR}_{\text{in},s} = \frac{(RP_s)^2}{2eRP_s\Delta f} = \frac{RP_s}{2e\Delta f} = \frac{P_s}{2h\nu\Delta f}. \quad (39)$$

The same expression applies for the input idler. Note that this result can be obtained in two ways: (i) We either square the input field directly to yield a photocurrent $i = R(P_s + 2\sqrt{P_s}n_s)$, where the second term is additive noise with a variance given by $R^2 4P_s h\nu/2\Delta f = 2eRP_s\Delta f$. Here the factor of 4 in the detected photocurrent variance comes from the squared factor 2, times 1/2 from the averaging over $\langle \cos^2(\theta) \rangle$, which is the relative phases between signal and noise, times 2 since the optical noise is collected over an optical bandwidth of $2\Delta f$. (ii) Alternatively, we neglect the vacuum fluctuations and postulate the presence of shot noise with variance $\sigma_s^2 = 2eRP_s\Delta f$ when the input signals are detected.

At the output of the two-mode amplifier, we obtain for the signal wave

$$e_s(z) = \mu e_s + \nu e_i^* + \mu n_s + \nu n_i^*, \quad (40)$$

where the last two terms are the PSD of the ASE noise (or amplified vacuum fluctuations). After photodetection, we obtain the signal current

$$i_s = R|\mu e_s + \nu e_i^* + \mu n_s + \nu n_i^*|^2 = R(P_{s,\text{out}} + 2\text{Re}[(\mu e_s + \nu e_i^*)(\mu n_s + \nu n_i^*)^*]), \quad (41)$$

where $P_{s,\text{out}}$ is the optical signal power after the amplifier, the second term is the signal-noise beating, and we neglect the noise-noise beating. The signal gain after the two-mode amplifier is

$$G_s = \frac{P_{s,\text{out}}}{P_s} = \frac{|\mu e_s + \nu e_i^*|^2}{P_s} = \left| \mu \frac{e_s}{|e_s|} + \nu \frac{e_i^*}{|e_s|} \right|^2, \quad (42)$$

as we saw earlier in Eq. (23). The idler gain can be obtained by exchanging the s/i indices. We may note that this gain is signal-phase-independent only when the idler is zero, and then the phase-independent gain is $G_{\text{PIA}} = |\mu|^2$ as noted in Subsection 3.2e. If no idler is present at the input (as for a copier, wavelength converter, or phase conjugator), we define a conversion efficiency, η , instead of an idler gain as

$$\eta = \frac{P_{i,\text{out}}}{P_s} = \frac{|\nu e_s^*|^2}{P_s} = |\nu|^2. \quad (43)$$

The signal-noise beating variance can be obtained as

$$\begin{aligned} \sigma_{s-sp}^2 &= 4R^2 \langle (Re[(\mu e_s + \nu e_i^*)(\mu n_s + \nu n_i^*)^*])^2 \rangle = 2R^2 P_{s,\text{out}} \langle |\mu n_s + \nu n_i^*|^2 \rangle = \\ &= 2R^2 P_{s,\text{out}} (|\mu|^2 + |\nu|^2) \left(\frac{h\nu}{2} \right) (2\Delta f) = 2R^2 P_{s,\text{out}} (|\mu|^2 + |\nu|^2) h\nu \Delta f, \end{aligned} \quad (44)$$

where $\langle \cdot \rangle$ means average. Thus, the SNR at the output becomes

$$\text{SNR}_{\text{out}} = \frac{P_{s,\text{out}}}{2(|\mu|^2 + |\nu|^2) h\nu \Delta f}, \quad (45)$$

and finally the NF is obtained as

$$\text{NF} = \frac{P_s (|\mu|^2 + |\nu|^2)}{|\mu e_s + \nu e_i^*|^2} = \frac{|\mu|^2 + |\nu|^2}{G_{\text{PSA}}} = \frac{2G_{\text{PIA}} - 1}{G_{\text{PSA}}}, \quad (46)$$

where $G_{\text{PIA}} = |\mu|^2 = 1 + |\nu|^2$ is the phase-insensitive gain and G_{PSA} is the phase-sensitive gain, which depends on the complex initial pump, signal, and idler fields as given by Eqs. (23), (24) and (42). We can now investigate this expression in a number of different cases.

- The phase-insensitive case is obtained for $e_i = 0$ for which $G_{\text{PSA}} = G_{\text{PIA}}$ and $\text{NF} = 2 - 1/G_{\text{PIA}}$ as expected.
- The NF for the generated idler in the phase-insensitive case is obtained by replacing G_{PSA} in Eq. (46) with the conversion efficiency, $P_{i,\text{out}}/P_s = |\nu|^2 = G_{\text{PIA}} - 1$, thus obtaining $\text{NF}_i = (2G_{\text{PIA}} - 1)/(G_{\text{PIA}} - 1) = 2 + 1/(G_{\text{PIA}} - 1)$, which goes to infinity as $G_{\text{PIA}} \rightarrow 1$ in contrast to the signal behavior, whose NF goes to zero in the same limit. However, for large gains, it approaches 2 just as the NF of the signal.
- When the signal and idler have equal amplitudes, $G_{\text{PSA}} = |\mu|^2 + |\nu|^2 + 2|\mu||\nu| \cos(\phi)$, where ϕ is the phase angle of the complex number $\mu\nu^* e_s e_i$. We obtain $\text{NF} = 1/(1 + x \cos(\phi))$, where $x = 2|\mu||\nu|/(|\mu|^2 + |\nu|^2) \in [0, 1]$. The NF is then largest, $\text{NF}_{\text{max}} = 1/(1 - x)$, for the phase-sensitive deamplification case $\phi = \pi$, and smallest, $\text{NF}_{\text{min}} = 1/(1 + x)$, for the maximum amplification case $\phi = 0$. The leading behavior for large gain is $x \sim 1 - 1/(8G_{\text{PIA}}^2)$ so that

$NF_{\max} \sim 8G_{\text{PIA}}^2$ and $NF_{\min} \sim 1/2 + 1/(8G_{\text{PIA}}^2)$ in the two cases. The seemingly unphysical $NF < 1$ for the maximum phase sensitive gain will be discussed below.

If the signal and idler are correlated and if the idler phase is conjugate to the signal phase, the phase sensitive gain will be $4G_{\text{PIA}}$. This extra 6 dB of gain is real and clearly observed in experiments, cf. e.g., [86,113]. This will give a 6 dB higher optical SNR (OSNR, defined as the optical signal power divided by the optical noise power within some reference bandwidth, see, e.g., Fig. 16 in Ref. [87]) since the same amplifier noise PSD is generated irrespective of whether the idler is present or not.

It might seem unphysical that the NF approaches 1/2 in the PS case. In fact, a NF less than 1 means the SNR is *improved* after the amplifier. How can the SNR be higher relative to the input? The resolution of this paradox is that we have the same (or actually a conjugate) signal present at a second wavelength, which is not accounted for at the input, and the noises on these two waves are uncorrelated. The coherent superposition will then add the signals coherently and the noise incoherently, thereby improving the SNR by a factor of 2. This is the same as when two independent measurements of the same signal can be averaged to increase the effective SNR by a factor of 2. Therefore, the -3 dB of the NF must be interpreted with some care.

If instead both the signal and idler powers were accounted for at the input, the NF would equal 2 times Eq. (46), and for maximum PS gain, it will then be given by $NF_{\max} \rightarrow 1 + 1/(4G_{\text{PIA}}^2)$ for large G_{PIA} . This then agrees with the 0 dB NF predicted for PSAs by quantum field theory [30–32].

4.2b. Additional Noise Sources

The above section discussed the fundamental quantum mechanical noise sources related to amplified vacuum fluctuations. However, in practice, there are also a number of additional noise sources when FOPAs are realized. These have been described and discussed in, e.g., [66]. We will briefly list them here.

Raman-scattering-induced noise. The strong pump wave will cause spontaneous Raman scattering, and also downconversion of the high-frequency signals in FOPAs. This was described originally in a series of papers by Voss *et al.* [114–116]. This effect is expected to put a limit on the attainable PSA NF to be > 0.4 dB [117]. It will also act asymmetrically depending on which side of the pump the signal is located.

Pump transfer noise. The ultrafast nature of FOPAs leads to a sensitivity in the gain to pump power variations [64,118]. This will act as rapid gain fluctuations with asymmetric statistics [119]. It will be an additive noise source whose expectation value is proportional to the signal power, and therefore it will be more significant for high signal powers in to the FOPA.

Residual ASE. Since the pump is typically amplified with a booster amplifier, the residual ASE from this amplifier might leak through filters and add to the signal. In principle, this can be filtered away, but in practice it can be difficult since the generated booster ASE power may be significant.

In Ref. [66], all these noise sources in addition to the quantum noise were theoretically analyzed and experimentally characterized with good agreement.

4.3. Link Noise Figures and Distributed Amplification

The following section extends the discussion from Section 1 around Fig. 2. In lumped amplifier links, the SNR will fall off linearly with the number of amplifier spans, if we assume a balanced link, where the gain of each amplifier exactly compensates the loss in each span. One can introduce a *link NF* that states how the SNR degrades from the

input. Since the NF is inversely proportional to SNR_{out} , the link NF will increase linearly with the number of amplifiers.

Two viewpoints can be taken: the type A link, where the amplifier precedes the loss, and the type B link, where the loss precedes the amplifier of each span. Figure 2 shows a type B link. For a PIA amplified link, the NF increases with the number of spans m as [120,121]

$$\text{NF}_{\text{PIA},A} = 1 + 2m \left(1 - \frac{1}{G} \right), \quad (47)$$

$$\text{NF}_{\text{PIA},B} = 1 + 2mG \left(1 - \frac{1}{G} \right). \quad (48)$$

In a PSA amplified link, the NF increases as [72,120,121]

$$\text{NF}_{\text{PSA},A} = 1 + m \left(1 - \frac{1}{G} \right), \quad (49)$$

$$\text{NF}_{\text{PSA},B} = 1 + mG \left(1 - \frac{1}{G} \right). \quad (50)$$

These can now be compared to the copier-PSA links, where a complication is the presence of the copier, which acts as a PIA (with a quantum-limited $\text{NF} = 3$ dB), but where the 6 dB gain benefit discussed above reduces the contribution from each span with a factor of 4 relative to the PIA. The copier-PSA link NF is approximately [121]

$$\text{NF}_{C\text{-PSA},A} = \frac{5}{2} + \frac{m}{2}, \quad (51)$$

$$\text{NF}_{C\text{-PSA},B} = \frac{3G}{2} + \frac{mG}{2}. \quad (52)$$

This shows that the copier-PSA link has a 6 dB advantage over the PIA link and a 3 dB advantage over the non-copier-PSA link assuming that the second terms in the expressions dominate, which is the case in a many-span scenario. This comes at the expense of sacrificing spectral efficiency as the data occupy two wavelengths. The 3 dB advantage over the non-copier-PSA link (which equally sacrifices spectral efficiency) is a result of the copier-PSA link carrying twice the power since the idler is generated in the copier and is not part of the system input signal power.

In fact, it is possible to do even better in terms of link NF, by considering *distributed amplification*. This can be understood if one considers a link of total length L with loss $\exp(\alpha L)$ that contains m amplifiers of gain G so that $G = \exp(\alpha L/m)$. Inserting this in Eq. (47) gives $\text{NF}_{\text{PSA},A} = 1 + 2m(1 - \exp(-\alpha L/m))$, and in the limit of many infinitesimal spans, we obtain $\text{NF}_{\text{PSA},A} = 1 + 2m(1 - (1 - \alpha L/m)) = 1 + 2\alpha L$, so that for such a distributed amplifier, the NF grows logarithmically with the link losses. This type of distributed amplification can be used also for a PSA link as suggested by Vasilyev [8]. The benefits of copier-PSA relative to a PSA link remains even in the distributed case, so the ultimate link amplification should employ a distributed copier-PSA scheme.

5. IMPLEMENTATION CONSIDERATIONS

In this chapter, we will discuss practical aspects of the implementations of FOPAs. We first discuss aspects relevant for both phase-insensitive and phase-sensitive operation. Later, we discuss specific aspects related only to phase-sensitive operation. We will also here discuss aspects relevant when using PSAs in optical transmission links.

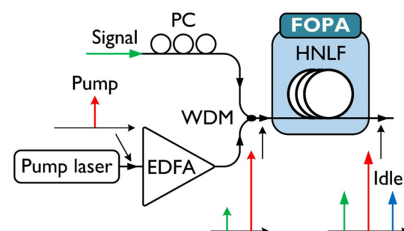
5.1. General Aspects of Parametric Amplifiers

Figure 5 illustrates a possible implementation of a FOPA in a phase-insensitive implementation. In the case of phase-sensitive operation, an idler wave also needs to be present at the input along with the signal. The key components are the pump laser and the nonlinear medium providing the amplification, which dictate all the essential performance characteristics. In many of the reported experiments, the nonlinear medium was a solid core silica fiber being tailored such that the core diameter is very small (typically around 4 μm) leading to a significantly larger nonlinearity compared with SSMF, while at the same time having low group-velocity dispersion (GVD), which is needed to achieve good phase matching and high parametric gain. Such fibers are referred to as HLNLF. There exists, however, a large range of other nonlinear platforms that can serve as the nonlinear gain media. While it is not easy to define a single figure of merit that captures all essential aspects, it is fair to state that from a “black-box” perspective, the HLNLF does provide the best performance to date. If the pump laser is not providing enough power to achieve sufficient gain, its power can be boosted by, e.g., an EDFA as illustrated in the figure. In practice, an optical bandpass filter at the EDFA output is often needed to reduce the amount of ASE. As FWM is a polarization-dependent process, and the parametric gain is as well, which in practice makes this a single-polarization amplifier: A polarization controller (PC) is needed to set the pump and signal waves at the same polarization as they enter then nonlinear medium. Polarization-independent amplification is, however, possible with either a so-called diversity scheme or a so-called vector approach (using two orthogonally polarized pump lasers), further discussed in Subsection 5.5c.

Some other fundamental characteristics specific to FOPAs are summarized here:

- An idler will be generated as a result of the FWM process. If the signal wave in Fig. 5 is modulated with data, the idler will contain a phase conjugated copy of this data. While the presence of the idler is not always desired, it is essential when considering PSA as discussed in Subsections 3.2e and 5.5.
- FOPAs are, in contrast to most other amplifiers, unidirectional, as phase matching is only fulfilled in the forward direction. This can be important as the buildup of backward propagating ASE or other reflected optical power is not possible. This directionality enables very high gain FOPAs. This is in contrast to, e.g., EDFA, where this can cause gain reduction and increase of the NF. In addition, optical

Figure 5



Possible implementation of a fiber-optic parametric amplifier.

isolation may not be necessary as a cavity with gain in both directions is not being formed.

- FOPAs become essentially transparent in the signal band in absence of pump power, while for EDFAs, the absence of pump power results in the erbium fiber having a very large attenuation. This difference may have consequence when considering system reliability.
- Finally, in FOPAs, the fundamental gain mechanism is a result of the anharmonic motion of the bound electrons in the fiber host and is thus a process with very short relaxation time ($\ll 1$ ps). This means that a FOPA can be used for many functions operating at very high speed other than optical amplification, including, for example, add-drop multiplexing, wavelength conversion, optical phase conjugation, pulse compression, ultrafast switching and sampling, and phase regeneration. This will be further discussed in Section 8. However, a related consequence of this is that the noise properties of the pump are very important as excess intensity noise from the pump will be transferred to the signal, thus potentially degrading the amplifier performance. In addition, the pump laser should be operating in a single mode. This is in contrast to EDFAs, having a time constant near 1 ms, effectively averaging any pump noise (and also allowing multimode pumps), while thus not being capable of other high-speed functionalities.

From Subsection 3.2d., we find a remarkably simple expression for the spectral peak gain of a FOPA only being dependent on three parameters. In the case of large gain and ideal phase matching condition, for a PIA, this is approximately $G = \frac{1}{4} \exp(2\gamma PL)$, while for a PSA, it is up to 4 times (6 dB) higher. Here, γ is the nonlinearity coefficient of the HNLFF, typically 10 (W km)^{-1} , P is the pump power (W) and L (km) is the length of the HNLFF. Thus, a simple rule of thumb is that a nonlinear phase shift (γPL) of π radians is needed to reach a PIA gain of about 20 dB (and a PSA gain of 26 dB). Typically, an HNLFF may be 500 m long and the pump power about 1 W in the case of using an HNLFF. As in most FOPA experiments, the pump power is not itself providing enough power to serve as a FOPA pump, but it is often first amplified in an EDFA. Thus, the OSNR at the EDFA output is in practice the main limiting factor in terms of intensity noise. A simple rule of thumb is to maintain a pump OSNR larger than about 50 dB in order not to significantly suffer from this noise transfer; however, this value also depends on the signal power entering the amplifier [64,119]. The quantum limit of the NF of a high-gain FOPA operated in phase-insensitive mode is 3 dB, while if operated in phase-sensitive mode, it is 0 dB.

5.2. Gain Spectrum Characteristics

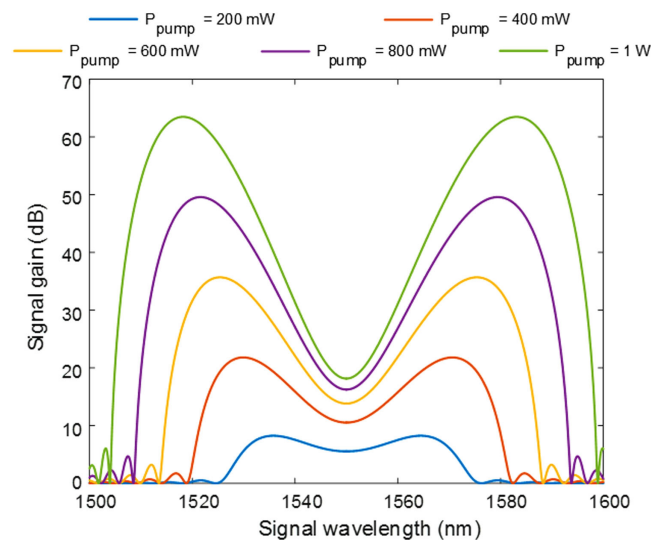
Clearly, the spectral gain characteristic of any amplifier is important. In FOPAs, this depends primarily on the GVD of the HNLFF, which ideally should be very small. The discussion in this section is focusing on the gain of phase-insensitive FOPAs. However, the results essentially apply also to phase-sensitive FOPAs with the main difference that PSA gain will be 6 dB higher (at high gain and with proper phase condition), as discussed in Section 3. Figure 6 shows a calculated gain spectrum with the following assumptions: HNLFF with $L = 500$ m, $\gamma = 16 \text{ (W km)}^{-1}$, a dispersion slope (S) of $0.02 \text{ ps}/(\text{nm}^2 \text{ km})$, and a pump wavelength of 1550 nm, which is 2 nm above the zero-dispersion wavelength (λ_0) of the HNLFF. In this single-pump case, the peak gain grows exponentially with the pump power where perfect phase matching occurs. At wavelengths close to the pump wavelength, the gain grows only quadratically with the pump power. As seen in this example, significant gain can be expected over nearly 100 nm. It should be noted that ASE is here ignored, which can have an impact in

saturating the gain. For proper modeling, particularly when targeting high gain, this aspect should be considered.

In Fig. 7, the gain spectrum of a dual-pump amplifier is shown with otherwise same parameters as in Fig. 6. The pump wavelengths are 1466.5 nm and 1643.6 nm, respectively, i.e., their “center of gravity” is 0.3 nm above λ_0 , carefully chosen to reach good spectral flatness. It is seen that the gain spectrum is much flatter in this case, and the gain grows approximately exponentially with the pump power across a broad spectral range, a result of four perfectly phase matched signal wavelengths. One can also note that the peak gain is the same in Figs. 6 and 7 for any given total pump power. Thus, for a certain peak gain target, the dual-pump case requires only half the power in each pump laser compared with the single-pump case. While the dual-pump case is more challenging to implement, aside from the advantage of a flat gain spectrum, it is easier to deal with the problem of SBS (discussed later) since the power of each pump is 50% lower in this case. It should be noted that, while in Fig. 6 higher-order dispersion, i.e., β_4 is not influencing the shape of the gain spectrum (for reasonable values of β_4) due to the relatively large difference between the pump wavelength and the zero-dispersion wavelength, in Fig. 7, however, β_4 has a large impact on the gain shape. In this case, β_4 was carefully chosen to obtain a broad and flat gain spectrum, resulting in significant gain over about 180 nm.

Figure 8 shows an example of the impact of the nonlinear coefficient and dispersion on the gain spectrum in dual-pumped amplifiers with a total power of 800 mW. The red-colored gain spectrum being approximately 180 nm wide is from Fig. 7, while the blue-colored spectrum corresponds to a case with 10 times larger nonlinearity with the length of the HNLF being correspondingly 10 times shorter than the case in the red spectrum. The nonlinear phase shift and the peak gain are thus the same. However, as seen, the spectral width of the latter is significantly larger (about 350 nm). This illustrates that it is, in principle, beneficial to use a more nonlinear element, while at the same time being shorter. A key challenge is to develop a suitable platform to implement this. Currently used solid core silica HLNLFs cannot be expected to reach such a high nonlinear coefficient. Other much more nonlinear platforms are being

Figure 6

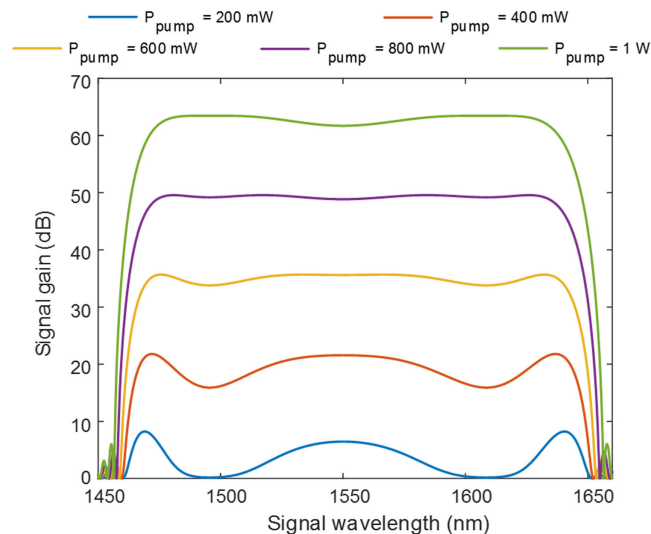


Parametric gain spectrum at various pump powers with a single pump at 1550 nm, which is 2 nm above the wavelength of zero-dispersion in the HNLF, which is 500 m long with $\gamma = 16 \text{ (W km)}^{-1}$ and dispersion slope $S = 0.02 \text{ ps}/(\text{nm}^2 \text{ km})$.

explored, but it is challenging to achieve a large effective length to reach a sufficient nonlinear phase shift due to relatively high waveguide losses.

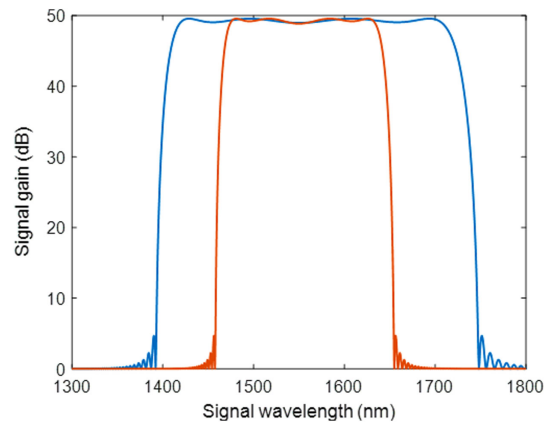
From Figs. 6–8, it is clear that the spectral width of the gain of an HNLFF-based parametric amplifier can be expected to be up to a few 100 nm. However, the above examples are ideal, and, in reality, other factors can degrade the spectral gain performance. These include dispersion variation along the HNLFF [54,90,122] (which was here assumed constant), nonideal higher-order dispersion, SRS (causing a spectral gain tilt), and polarization-mode dispersion (PMD), causing a relative polarization

Figure 7



Parametric gain spectrum at various pump powers with two pumps operating at 1466.5 nm and 1643.6 nm, respectively. The power in each pump is equal, and the power mentioned reflects the total power of the two pumps. The value of the dispersion curvature (β_4) was $2.4 \cdot 10^{-5} \text{ps}^4/\text{km}$. The average pump wavelength was 0.3 nm above λ_0 . Other parameters are same as in Fig. 6.

Figure 8

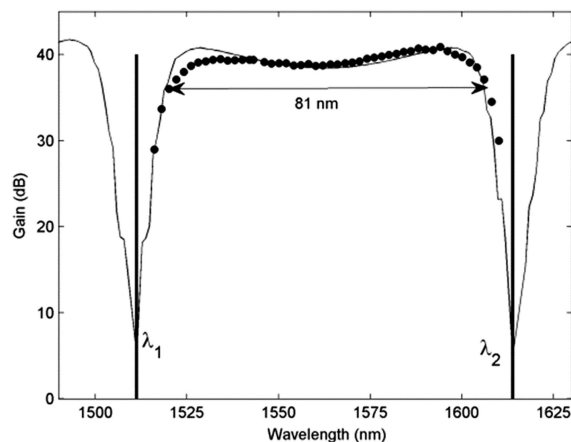


Parametric gain spectra with a 500 m HNLFF having $\gamma = 16 \text{ (W km)}^{-1}$ (red curve) and a 50 m hypothetical HNLFF having $\gamma = 160 \text{ (W km)}^{-1}$ (blue curve). The total pump power was 800 mW. Red curve is from Fig. 7. For the 50 m case, the pump wavelengths were optimized as 1406.5 nm and 1726.2 nm, and their average wavelength was 0.95 nm above λ_0 . Other parameters are the same as in Fig. 7.

rotation of the involved waves thus impacting the gain). The latter problem can essentially be solved by using a polarization-maintaining HLNLF by keeping all waves copolarized [123]. In general, all of the above aspects become increasingly important when targeting a broad spectral gain, but their importance clearly will depend on the nonlinear platform being used, and it is generally also easier to achieve a broad and flat gain spectrum if the target gain value is smaller. Parametric gain over 270 nm has been experimentally observed [61]. Figure 9 shows a measured gain spectrum using two pumps separated by 103 nm resulting in a flat 40 dB gain across 81 nm [124]. The impact of SRS on dual-pumped FOPAs with a pump wavelength separation up to 180 nm was experimentally studied in Ref. [62]. An analysis of broadband and flat two-pump FOPA gain spectra was provided in Ref. [97].

It should be noted that, in many applications, the idlers generated in a FOPA reduce the useful spectral range of the amplifier to 50% of the bandwidth discussed above. One exception to this is the use of FOPA as a gain medium in a wavelength tunable laser [60]. In addition, in PSAs (discussed in Subsection 6.4), the idlers play a key role and need to be present at the input along with the signal. As observed in Fig. 6, the FOPA gain spectrum with a single-pump laser has characteristic peaks at each side of the pump wavelength. As discussed, a much flatter gain spectrum is possible by using two pumps. However, it should be pointed out that it is possible to obtain a broadband and flat gain spectrum with a single pump as well, by either minimizing the net dispersion at the pump wavelength [63] (e.g., by operating the pump very close to the zero-dispersion wavelength of the HNLFF), which comes at the expense of lower spectral peak gain with the same pump power as in the dual-pump case, or by performing QPM [125,126]. The fundamental reason for the two-lobed gain feature in the single-pump case is that perfect phase matching only occurs at two specific signal wavelengths while the phase mismatch at other wavelengths grows as the waves propagate along the fiber. This also becomes more pronounced at higher pump power and gain. An interesting approach to mitigate this is to apply the QPM method by periodically inserting spectrally selective phase correctors only affecting the phase of the pump. This approach attempts to maintain ideal phase matching (relative phase

Figure 9



Measured (symbols) and calculated FOPA gain spectrum in a dual-pump configuration. The pump separation was 103 nm with their average wavelength being near the zero-dispersion of the HNLFF used. The total pump power was 2.1 W, and the length and nonlinearity coefficient of the HNLFF were approximately 350 m and 14 (W km)^{-1} , respectively. Reprinted with permission from [124]. Copyright 2008 Optical Society of America.

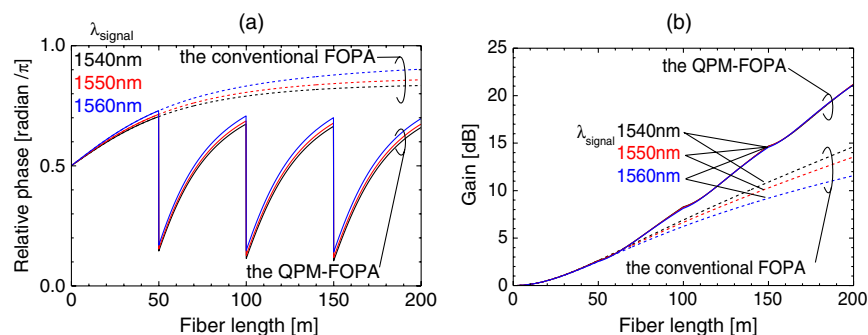
being $\pi/2$) along the HLNLF, by periodically realigning the phases [see Fig. 10(a)]. This results in an accumulated gain that grows nearly exponentially along the full fiber over a wide spectral range, while otherwise the accumulated gain increases at different rates at different wavelengths, as illustrated in Fig. 10(b).

5.3. Dealing with Detrimental Stimulated Brillouin Scattering

When implementing a parametric amplifier in an optical fiber, one undesired phenomenon that needs to be dealt with is SBS. This is a fiber nonlinearity occurring due to the interaction of the input wave and the fiber that manifests itself as the generation of an amplified backward propagating wave once a threshold power of input power has been reached. This prohibits the growth of parametric gain since much of the pump wave is thus being reflected. The input power threshold for this to occur is typically 10 mW in a long SSMF, and decreases with increasing effective length of the fiber. At such powers, no FOPA gain can be expected when using a conventional HLNLF as the nonlinear element. The use of smaller fiber core area (resulting in a larger nonlinear coefficient) or the use of a shorter HLNLF is not helping here. This is because, if we target a certain FOPA gain, the scaling of the SBS threshold will follow along these changes. Thus, if one wants to use a solid core silica fiber as the nonlinear medium on a FOPA, other approaches to avoid SBS have to be pursued. One commonly used approach is to phase modulate the pump with a frequency higher than the spectral bandwidth of SBS (typically up to 100 MHz in optical fibers) such that the SBS threshold is increased (see Ref. [127] and references therein). If several appropriately chosen frequencies are used, the threshold can theoretically be increased 3 times per RF frequency used. A drawback with this approach is that phase modulation can unintentionally convert into intensity modulation (e.g., due to dispersion or optical pump filtering [128]), thus degrading the FOPA performance. Another method is to impose a temperature gradient along the HLNLF such that the spectral peak of the SBS is gradually changing along the fiber [129]. Finally, another approach is to impose a strain along the fiber also causing a shift in the SBS spectral peak (along with some amount of undesired dispersion changes along the fiber) [130]. The result of using the last approach, along with the insertion of optical isolators in between sections of HLNLF, to prevent buildup of SBS is shown in Fig. 11 [85].

The relative SBS threshold increase by using these two approaches was 11 dB (approximately half due to the strain and half due to the isolators). This allowed up to 10 dB of parametric gain without any use of pump phase modulation. Without

Figure 10



(a) Simulated phase matching along an HLNLF with and without periodically inserted pump phase correctors. (b) Corresponding signal gain along the HLNLF. © 2012 IEEE. Reprinted, with permission, from S. Takasaka *et al.*, *Optical Fiber Communication Conference and Exposition (OFC/NFOEC)*, 2012 [126].

this approach, no parametric gain was observed. As also indicated in the figure, with only one pump phase modulation frequency (300 MHz), the gain can further be increased significantly as the SBS threshold is increased another factor of 3 (4.8 dB).

5.4. Saturation Properties and Nonlinear Penalties

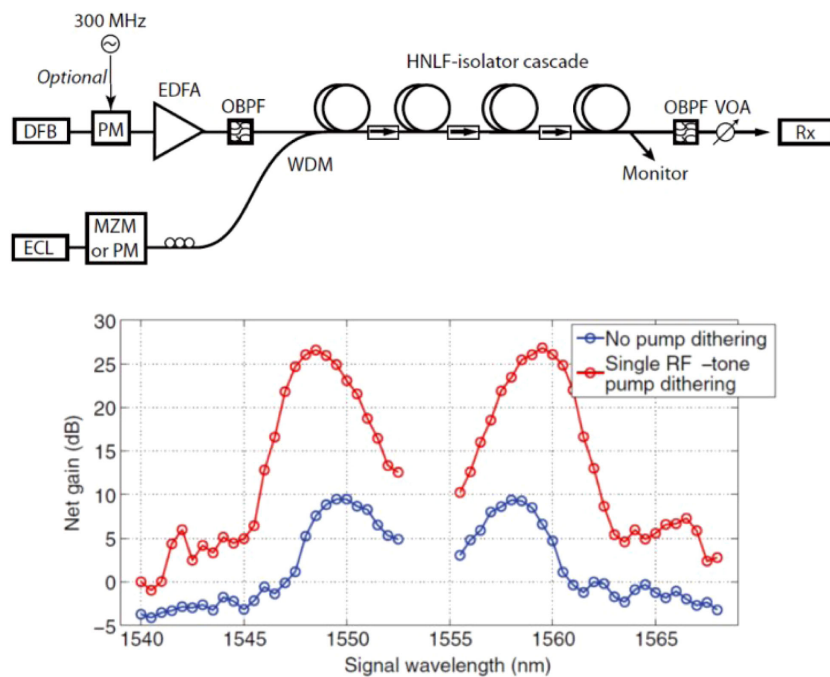
In optical amplifiers, saturation of the gain will take place whenever the amplified signal power reaches a level approaching that of the pump power, and this is certainly the case also with parametric amplifiers, albeit with a number of particular features. Theoretically, for an amplifier with (small-signal) gain G_0 , saturation will occur for an input signal power P_s when $G_0 P_s$ is a significant fraction of the pump power. For phase-insensitive FOPAs, a semiempirical theory can be derived to obtain a simple formula for the gain as function of the input signal power [131],

$$G(P_s) = \frac{G_0}{1 + \frac{2P_s G_0}{P_p}}, \quad (53)$$

where P_p denotes the pump power.

Figure 12 from [132] shows the measured and calculated output signal, idler, and pump powers, respectively, in a FOPA versus input signal power. At low input signal power, the gain is about 27 dB, but it starts to reduce at input powers of about -10 dBm (thus, the sum of output signal and idler powers at that point are about 0.1 W), at which point the pump output power is also starting to reduce with increasing signal power. The pump power depletion continues, and in contrast to other amplifiers, it reaches a sharp minimum at a particular level of input signal power, in this case about 5 dBm. At that point, as much as 99.92% of the pump power was depleted, and as the signal input power is further increased, power from the signal

Figure 11



Top, FOPA with increased SBS threshold using four strained HNLf sections with optical isolators in between, and no phase modulation of the pump. Bottom, measured FOPA gain spectrum. © 2012 IEEE. Reprinted, with permission, from C. Lundström *et al.*, IEEE Photon. Technol. Lett. **25**, 234–237 (2013) [85].

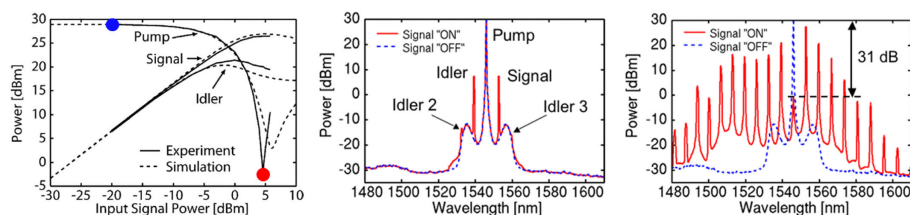
and idler is being transferred back to the pump. This is a direct consequence of the phase matching condition being changed due to SPM in the HLNLF to the extent that a situation of “parametric attenuation” is occurring (see Subsection 3.2e). In a first-order theory, the FOPA will periodically alter between amplification and attenuation as the optical input power is increased, and no power will actually be lost. However, this is too simplistic, as there will be many new idlers generated in this process. This can be seen by comparing the output spectra of the FOPA in the unsaturated case (middle figure in Fig. 12 corresponding to the blue operating point in left figure) and in the maximum pump depletion case (right figure in Fig. 12 corresponding to the red operating point in left figure). In the unsaturated case, only the pump, signal, and one idler are present, while in the other case, where the pump is nearly fully depleted, not only the signal is present at the output, but also tens of new idlers, which are a result of higher-order mixing products. The maximum observed conversion of input pump power to the signal output power was 53% (at an input signal power of 2 mW). This illustrates that the conversion efficiency in FOPAs can be quite large and similar to that in EDFAs. The pump depletion feature has been used to demonstrate a fast switching operation with very low power (less than 0.01 mW) [133], and for time-domain add-drop multiplexing [134].

It should finally be noted that precaution is needed when amplifying multiwavelength signals with parametric amplifiers (e.g., for dense WDM transmission). While cross talk among these wavelengths may be negligible at low power into FOPAs, it will at some power start to cause a penalty [86,135]. Also nonlinear cross talk from FWM between WDM channels might cause signal distortions [136–139]. It was suggested that using shorter fibers and higher pump powers would reduce the problems [136,137]. Stephens *et al.* [138] showed experimentally that a hybrid Raman–FOPA would reduce the problem significantly. In PSAs, the problem is worsened due to the presence of the idlers, and a theoretical analysis of the problem was performed by Chen *et al.* [139].

5.5. Phase-Sensitive Operation of Parametric Amplifiers

When a FOPA is implemented such that not only the pump and signal waves are present at the input, but also an idler wave, it can provide some remarkable features such as squeezing of phase noise [79] and amplification with a quantum-limited NF of 0 dB. A simple explanation of how 0 dB NF can be reached is as follows: the signal and idler waves are mutually coherent and will thus add up coherently while the noise in the waves are entirely uncorrelated, and will add up only in terms of power. Thus, there is some similarity between PSAs and coherent receivers (where a local oscillator and signal are added coherently, while in a PSA, a signal and its conjugate are added

Figure 12



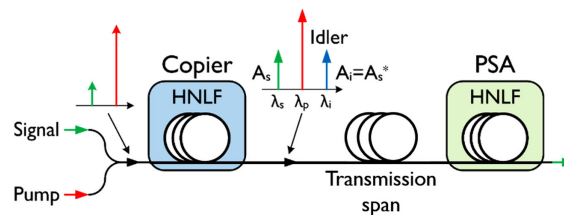
Saturation characteristics of a FOPA. Power evolution versus signal input power (left). Output spectrum with input power being -20 dBm (middle). Output spectrum with input power being 4.6 dBm (right). The input pump power was 1 W, and the fiber length was 750 m. Reprinted with permission from [132]. Copyright 2007 Optical Society of America.

coherently), and one could refer PSAs as a “coherent amplifier” where the output is optical in contrast to a coherent receiver where it is electrical. A parametric two-mode-FOPA-based, single-ended, single-quadrature coherent receiver in which the FOPA served simultaneously as amplifier and mixer was analyzed and compared to a traditional coherent receiver in Ref. [140]. While the needed idler can be generated in different ways, one very simple approach is to use the process of FWM in, e.g., an optical fiber. With a signal and pump with sufficient power entering this fiber, an idler will be generated at the wavelength $2\lambda_p - \lambda_s$ (see Fig. 13). If the signal wave at the input contains information, the idler will contain the same data but will be phase conjugated. Thus, we refer to this element as the copier, and the scheme was originally proposed by Tang *et al.* in Refs. [81,82]. In fact, this is essentially a PIA as discussed in Subsection 5.1 but without the need to provide gain. An important point of using a phase-conjugated idler wave is that the amplification in subsequent PSAs will become modulation format independent—both quadratures will be amplified independently allowing the use of any modulation format, e.g., m-QAM signals. The copier concept is also readily compatible with WDM signal transmission with a separate idler being generated from each of the input signal waves. Since the quantum-limited NF of the copier is 3 dB (at high conversion efficiency), this will generate excess noise. However, it has been shown [87] that with a sufficiently large loss between the copier and a subsequent PSA (as in practice would be the case in many transmission systems), this excess noise becomes insignificant relative to the quantum noise and will not impact the overall system noise performance.

However, since PSAs provide a gain that depends on the relative optical phase among the pump, signal, and idler wave, it is important to ensure that the desired phase relationship is maintained. This can in practice be achieved by implementing an optical phase-locked loop (PLL) controlling the phase of one of the waves [for example with a piezoelectric transducer (PZT) stretcher] to maintain the PSA gain at its maximum. As PSAs are normally polarization-dependent (for polarization-independent implementations, see Subsection 5.5c), the three waves should be copolarized once they enter the PSA.

In optical fiber links, it is possible to use PSAs both as in-line amplifiers and as preamplifiers in receivers as illustrated in Fig. 14. Idler waves containing the same information as the signal waves need to copropagate along the link with the signal. Thus, the spectral occupancy in the optical domain is twice that of conventional systems using, e.g., EDFA in-line amplifiers. However, as pointed out earlier, PSAs can potentially have very large gain bandwidth. It should also be noted that the idlers are not needed at the receiver and can simply be dumped along with the pump at that point (no added benefit can be expected by also detecting the idlers). Thus, the purpose of the idlers is only to participate in the PSA amplification process. There are neither any particular

Figure 13



Copier-based approach for generation of a pump, signal, and idler waves needed for operating a PSA. With sufficient loss between the copier and the PSA, the nonideal NF of the copier will not impact the overall link NF.

requirement on the receivers, e.g., in terms of bandwidth when compared to conventional receivers.

The link NF was described in Subsection 4.3, and it was stated that a PSA-based link will have a 3 dB advantage due to its lower NF. In the copier-PSA case illustrated in Figs. 13 and 14, however, there is a 6 dB link NF advantage over a conventionally amplified link (using ideal amplifiers with 3 dB NF), in the case of propagation over many spans. This advantage can be used to extend the overall link reach by a factor of 4 in the linear case (and sometimes even more in the nonlinear case—see below), and/or increase the span length or the number of bits transmitted per symbol, albeit this comes with the disadvantage of the need to copropagate the idlers resulting in less efficient use of spectrum and in transmitting 2 times the power over the transmission fiber.

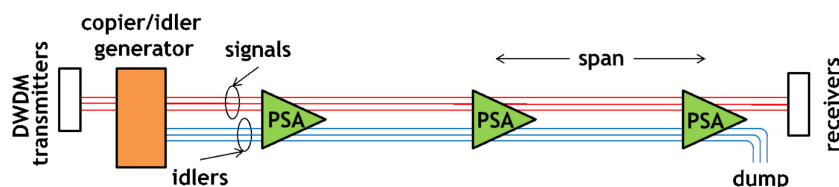
While in most cases it is desired that the signal and idler power are equal as they enter a PSA, as this will provide the best overall NF, they do not need to be equal. One can in such a case define a different NF for the signal and idler (the overall NF can never reach below 0 dB), and this was analyzed in detail in Ref. [141]. In Ref. [142], it was shown that in a situation of unequal signal and idler power or OSNR at the PSA input, the two amplified waves at the output are equalized both in terms of their power and OSNR. As an example, an input idler being 20 dB smaller in power (and OSNR) relative to the signal at the PSA input was observed to have increased its OSNR by 17 dB at the PSA output, while the signal was observed to have reduced its OSNR by 3 dB.

As the spectral gain characteristics of PSAs fundamentally are not different than those in the PIAs discussed earlier, aside from the 6 dB gain increase as described in Subsection 3.2e, we will not discuss this further here. However, broadband PSAs have been demonstrated in Ref. [123], where a single pumped polarization-maintaining HLNF was used to demonstrate more than 10 dB gain across 170 nm with a sub-3-dB NF.

5.5a. Optical Pump Recovery Using Injection Locking

An important aspect when considering PSAs in optical transmission is the need for a high-performance pump wave in each of the in-line PSAs or for PSA preamplified receivers. This can be achieved by propagating the pump wave along with the signal and idler (not shown in Fig. 14), but its power in the transmission fiber needs to be low enough to avoid SBS. In practice, this means the power of the pump wave at the PSA input can be very small. This necessitates an approach to recover the pump wave with sufficiently high SNR and high power to serve as a proper pump for the PSAs. A useful approach for this is to use optical injection locking (OIL) [143]. It has recently been demonstrated that a CW wave can be recovered to provide a high-performance pump for use in PSAs at power levels below -60 dBm [144]. Figure 15 illustrates the concept and some experimental results. As the frequency of the slave laser and the frequency of the incoming wave from the master laser are free-running, it is important

Figure 14



Schematic of a copier-PSA optical fiber transmission link.

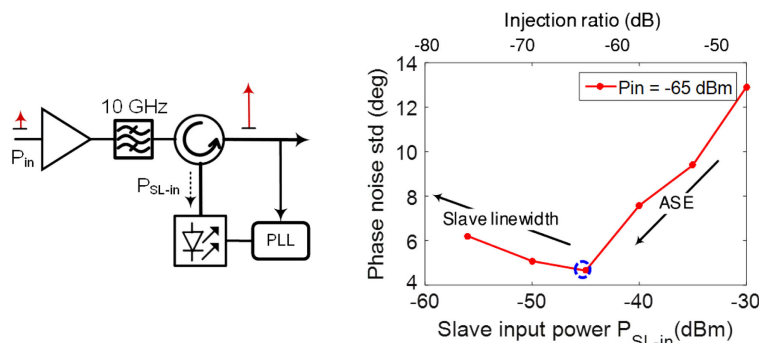
that their relative frequency offset is minimized for stable injection locking, in particular when locking at low powers when the locking bandwidth will be small. For this purpose, an electrical PLL was used to control the slave laser frequency. In addition, the incoming wave was preamplified with an EDFA, which allowed the optimization of the power actually being injected into the slave laser. While the phase noise is reduced with lower power into the slave laser (due to the filtering bandwidth in the OIL process becoming smaller), eventually the impact of the slave laser linewidth becomes important resulting in an optimum injected power [144]. As shown in Fig. 15 (right), phase locking with low phase noise can be achieved at a power into the slave of around -45 dBm, which corresponds to an input power to the EDFA of only -65 dBm. In subsequent measurement in a PSA, the observed penalty compared to a back-to-back scenario without the OIL was only about 0.3 dB.

5.5b. Dispersion Management in PSA Links

In PSA amplified links, the waveform and temporal position of the signal and idler wave should ideally be equal as they enter each PSA. Therefore, dispersion compensation is needed in each span for proper operation of the PSAs, such that the coherent superposition of the waves operates properly. If the dispersion length is much larger than the span length (which can be the case when operating at low symbol rates or if the transmission fiber is dispersion shifted to provide low GVD at the operating wavelength), it may be sufficient to only match the relative propagation delay of the signal and idler waves. If we consider linear wave propagation, it does not matter where the dispersion compensation is made within the span. However, in the nonlinear regime, its placement will play an essential role. In fact, the amount of pre- and postspan transmission dispersion compensation can be optimized for a given case (this depends on many aspects including the symbol rate and modulation format). The reason for this is the PSA capability to mitigate nonlinearities in the transmission fiber. This is possible because both the signal and idler essentially experience the same distortion, which to a relatively large extent can be canceled in the coherent signal plus idler superposition process in PSAs, as discussed in Section 6.

Figure 16 shows a few experimental results on the impact of the amount of dispersion-precompensation in each of the 81 km long SSMF spans of a transmission link [145]. The postcompensation is equal to the span dispersion minus the precompensation. As seen in Fig. 16(a), there is a clear optimum precompensation corresponding to about 15 km of SSMF in the case of PSA that results in a large transmission reach increase compared with no precompensation or with the PIA. In the case of PIA, the impact of precompensation is much smaller. It is interesting to consider the case of

Figure 15



Injection locking principle (left) and measured phase-noise variation versus slave laser input power (right). Reprinted with permission from [144]. Copyright 2018 Optical Society of America.

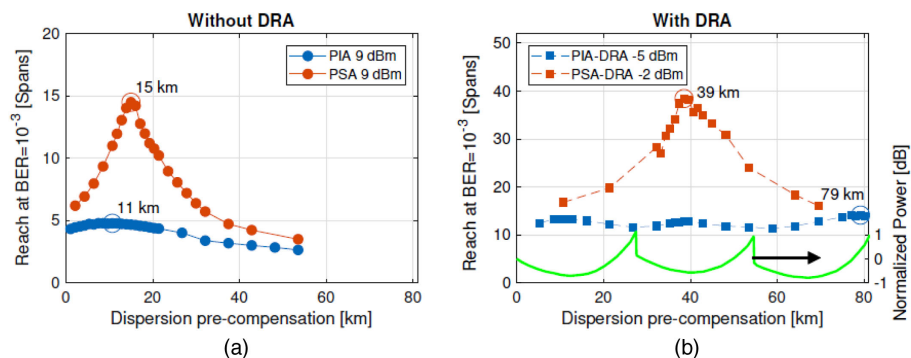
distributed Raman amplification (DRA), which is well known to improve the overall link NF, see, e.g., Eq. (2). However, in principle, it can also improve the PSA-enabled nonlinearity mitigation further. This is because a first-order perturbation analysis suggests that a flat or symmetric span power map in a link could lead to very efficient nonlinearity mitigation [145–147]. Figure 16(b) shows the measured reach in this case where Raman pumps were placed 27 km apart in the 81 km spans. Again, significant impact is observed from the amount of precompensation, and approximately 50% precompensation is found to be optimum in accordance with theory. It should be pointed out that when DRA is used to compensate for span losses, the low noise property of the PSAs have limited impact on the link performance, but it is rather their nonlinearity mitigation capability that is essential.

A further reach improvement can be expected by optimizing the dispersion precompensation in each span independently. In Ref. [148], a two-span optimization in a lumped amplification case resulted in optimal precompensation values of 5% and 35% (or vice versa) for the two spans (in contrast to the 15% in the single-span optimization) with a corresponding 50% further transmission reach increase. This was extended to more spans, and a four-span dispersion map optimized PSA link provided 2.1 times reach improvement over a single-span optimized PSA link, which represents a 4.3 times reach extension compared to a dispersion unmanaged (i.e., all dispersion compensation is performed in the electrical domain after coherent detection) PIA link [149]. Finally, it can be noted that the use of a Volterra equalizer, which is capable of mitigating nonlinearities after signal detection using digital signal processing (DSP), is useful also in the context of PSA amplified links. In Ref. [150], it was shown that such equalization can significantly relax the precise requirement on the dispersion precompensation discussed above.

5.5c. Polarization Management in PSAs

As the FWM process upon which the parametric amplifiers rely on is polarization-dependent, so is the parametric gain. In cases with polarization-independent operation or cases when signals in both polarizations need to be amplified, there are two basic options available. These are illustrated in Fig. 17 from [151]. The first is a so-called diversity scheme in which a nonlinear medium (e.g., an HLNf) is utilized in two directions such that the pump power is split equally among the two paths. As the signal state of polarization (SOP) varies, it will travel partially in each direction

Figure 16



(a) Maximum transmission reach (in terms of number of 81 km spans) for both PSA and PIA implementations versus the amount of dispersion compensation before the transmission span. (b) Maximum reach in the case when the spans are amplified using distributed Raman amplification. Reprinted with permission from [145]. Copyright 2018 Optical Society of America.

with the net (ideal) result that the signal is amplified independently of its SOP. The second approach (right in Fig. 17) is referred to as the “vector approach,” in which two orthogonal pumps are used to essentially independently amplify each SOP of the signal. Approaches similar to these have been demonstrated in several experiments in the case of PIA [152–156]. Some recent examples include the demonstration of a diversity loop implementation with improved SBS suppression capability [157], which was extended to show polarization-insensitive amplification of WDM signals carrying an aggregate data rate of over 2 Tb/s [158]. In Ref. [159], the vector implementation of a FOPA was demonstrated to be capable of polarization-insensitive amplification of WDM signals as well.

The situation is, however, more complicated in the case of PSAs, since we now have to deal with polarization and the optical phase simultaneously. Nevertheless, these schemes can also provide functionalities that conventional PSAs cannot provide, e.g., quadrature demultiplexing [160].

In Ref. [151], an analysis of how to achieve polarization independence was provided. The conclusion was (valid for both vector and diversity amplifiers and in presence of PMD) that polarization-independent PSA operation is only possible with polarization trackers in realistic optical transmission scenarios:

- A nondegenerate PSA with a dual-polarization-modulated signal is possible with one polarization tracker rotating the idler or the signal.
- A no-degenerate PSA with a single-polarization-modulated signal is possible with one polarization tracker rotating both the idler and signal.

5.5d. Capacity Considerations

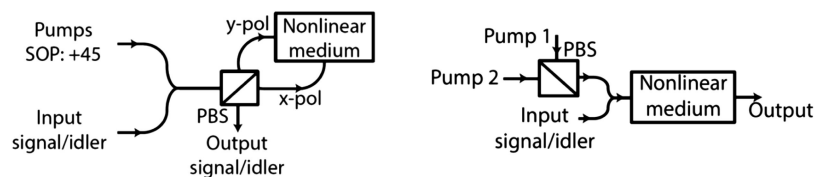
The capacity of a communication channel is given by the famous expression [161],

$$C = B \log_2(1 + \text{SNR}), \quad (54)$$

where B is the channel bandwidth and SNR is the signal-to-noise ratio. In PSAs, we need to transmit the idler along with the signal while it does not contain any additional information. Therefore, at very high SNR, the PSA approach will suffer from a factor of 2 reduction in terms of capacity relative to that of PIA-based systems (e.g., using EDFAs). However, at low SNR, the opposite holds, i.e., the capacity in a PSA-based system is twice that of a conventional one. This can be seen by simply comparing the capacity of a PSA versus a PIA system,

$$\frac{C_{\text{PSA}}}{C_{\text{PIA}}} = \frac{1 \log_2(1 + 4\text{SNR})}{2 \log_2(1 + \text{SNR})}, \quad (55)$$

Figure 17



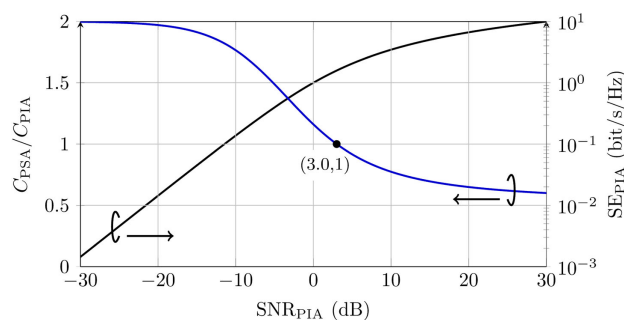
Schematics of two possibilities to implement polarization-independent operation with parametric amplifiers. Left, diversity approach. Right, vector approach. Reprinted with permission from [151]. Copyright 2016 Optical Society of America.

where SNR is the signal-to-noise ratio for the PIA case. The reason for the factor of 4 improvement for the SNR in the case of PSA can be extracted from the discussion in Subsection 4.2a, and can be explained as follows: if we consider the signal or the idler independently, its quantum-limited $NF = 1/2$, while that of a PIA is 2. Of course, the signal and idler need to be present simultaneously at the amplifier input, such that their combined $NF = 1$. However, the presence of the idler is already accounted for in (55) by the factor 2 in the denominator. The SNR advantage can be leveraged, e.g., to extend the transmission system reach as demonstrated in Section 7. At very low SNR, the term $\log_2(1 + \text{SNR}) \approx \text{SNR} / \ln(2)$ and what is outside and inside of the logarithm are thus equally important for the system capacity. Figure 18 illustrates this where it is also indicated that the PSA and PIA system capacities are equal at $\text{SNR}_{\text{PIA}} = 3$ dB, or equivalently at a spectral efficiency of 1.58 bit/s/Hz. An interesting case where this is relevant is in deep-space transmission where the SNR can be very small. It should be pointed out here that the above discussion is only considering a linear system. The capacity for nonlinear optical links is unknown in most cases. However, as is discussed in Section 6, PSAs can significantly mitigate impairments caused by transmission fiber nonlinearities. In addition, it is worth mentioning that there is no need to recover the idler at the receiver meaning that the capacity loss at high SNR only applies in the optical domain and not in the electrical domain, i.e., there is no need for additional received bandwidth relative to a system using PIAs. An experimental study of using a PSA-preamplified receiver with a very low SNR incoming signal was presented in Ref. [162]. This showed a record sensitivity (at $\text{BER} = 10^{-6}$) of only one photon-per-information bit using a QPSK modulation format at 10 Gb/s data rate and 100% forward-error-correction overhead. It should be pointed out that the sensitivity included all the power of the incoming signal and idler, as well as the pump wave.

5.5e. Parametric Amplification in Multimode Fibers

The discussion so far has focused on parametric amplification in a SMF. However, there has also been some recent work on such amplification in multimode fibers [163–166]. This can be of interest in future spatial-division multiplexed (SDM) transmission systems that rely on carrying independent data in each of the modes [167]. The modeling of such a solution is of course more complex than the case of a SMF. As an example, if the target is amplification in four spatial modes, one needs to solve 12 coupled nonlinear equations as there are three different nonlinear processes taking place simultaneously. In addition, the geometry of the fiber has to be carefully optimized. It is of particular interest to consider the case of using only a single laser to provide pump power to all modes while having minimal amount of nonlinear cross talk among the signals in the modes. It is then important to target a situation such that the relative phase velocity difference between any two modes ($\Delta\beta_1$) is large

Figure 18



Comparison of relative capacity of a PSA versus a PIA amplified system. The solid black line is the capacity for a PIA system.

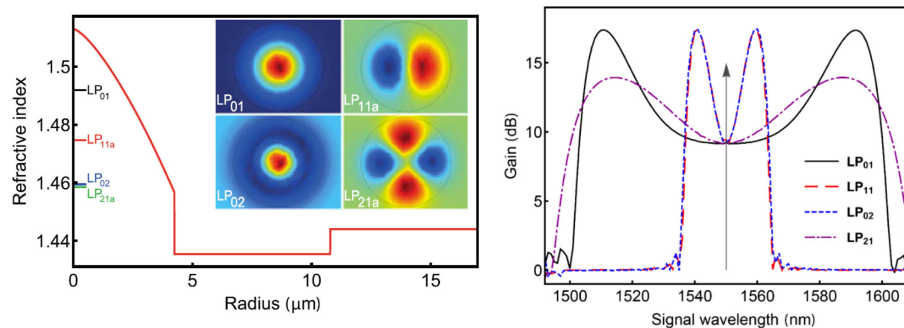
(efficiency of intermodal processes are low), while at the same time, all modes should have a small GVD (β_2) for efficient parametric amplification. Figure 19 shows an attempt to reach this situation in a realistic fiber case [168,169]. The Ge-doped fiber has an index profile that is graded in the core with double cladding surrounding it and supports four linearly polarized modes. As seen in Fig. 19(b), it is possible to amplify all four modes with a gain on at least 10 dB across a spectral range of 30 nm. Note that while the dispersion properties of the fiber were optimized, its nonlinear coefficient was not, and varied between $4.3 - 13.1 \text{ (W km)}^{-1}$ among the modes. In addition, amplification of such a fiber could be used to perform efficient wavelength conversion among the spatial modes.

5.5f. Four-Mode PSAs

As discussed in Subsection 3.3, it is possible to implement a so-called four-mode PSA in which four information carrying waves (one signal and three idlers) are interacting nonlinearly with two pump waves. The process can be described by a 4×4 transfer matrix [69]. Similar to the single-pump two-mode PSA, the dual-pump four-mode PSA is modulation format independent and compatible with WDM supporting many signal channels. Here, the PSA amplification is in theory 12 dB higher than the corresponding PIA gain (in the two-mode PSA, it is 6 dB), which is a result of a coherent superposition of the four information carrying waves giving $4^2 = 16$ times, or 12 dB coherent gain. The overall quantum-limited NF is still 0 dB, while the expected link NF improvement is 9 dB (in contrast to 6 dB for a conventional copier-PSA implementation). Figure 20 shows experimental spectra of an HLNf-based four-mode PSA output in the case of no idlers at the input and with the idlers (each with the same input power as the signal) at the input [110]. The observed signal (-10 dBm input power at 1540 nm) gain in the former case was 9.3 dB while in the second case it was 19.6 dB. The observed gain increase of 10.3 dB was thus relatively close to the expected 12 dB.

While this approach can improve the link NF compared with a two-mode PSA, it is also useful to, e.g., further reduce the impact of SBS given a certain gain target. However, an obvious drawback with this implementation is the loss of spectral efficiency as four waves at different frequencies will need to carry the same information, while also being rather complex to implement [110].

Figure 19



Left, geometry and spatial modes of a fiber dispersion-optimized for parametric amplification. Right, resulting simulated gain spectrum using a single pump with total power of 12 W (optimized among the modes) and fiber length of 150 m. The arrow indicates the pump wavelength. Reprinted with permission from [168,169]. Copyright 2016 and 2017 Optical Society of America.

As will be discussed in Section 6, PSAs have the capability to mitigate nonlinear transmission fiber impairments, and this has also been confirmed experimentally. However, to date, no such studies have been made regarding the particular nonlinearity mitigation capabilities for four-mode PSAs.

It should be mentioned that four-mode PSAs have been used to demonstrate frequency multicasting with significant enhancement of the SNR. In Ref. [111], a spectrally uniform 12 dB OSNR advantage over conventional, phase-insensitive parametric multicasting was demonstrated. The prospects of truly noiseless signal spectral replication with four-mode PSAs is extensively discussed in Ref. [2].

6. TRANSMISSION FIBER NONLINEARITY MITIGATION

It was, somewhat surprisingly, observed in the early experiments of copier-PSA transmission that not only was the PSA superior in the linear but in the nonlinear regime as well [170,171]. The reason for this is the coherent superposition of the signal and idler and the fact that they have accumulated similar, correlated, nonlinear distortions.

The phenomenon can be explained as follows. Consider a complex signal with a constant complex value a subject to additive noise n . We call this noisy signal $x_1 = a + n$. Then we generate the conjugate signal $x_2 = x_1^*$. These signals are shown in Fig. 21(a) for $a = \exp(i\pi/4)$ and an ensemble of 5000 independent noise realizations. We then transmit these signals in a nonlinear fiber so both signals are subject to self-phase (and cross-phase) modulation. We neglect dispersion. This leads to the signals

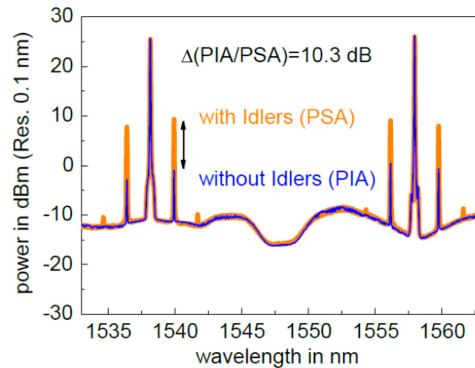
$$y_1 = (a + n) \exp(ip|a + n|^2), \quad (56)$$

$$y_2 = (a + n)^* \exp(ip|a + n|^2), \quad (57)$$

where p is a measure of the nonlinearity, and for weak noise, the nonlinear phase shift would be given by $p|a|^2$. These signals are shown in Fig. 21(b), and in Fig. 21(c) with y_2 conjugated. The conjugate superposition now forms

$$z = \frac{y_1 + y_2^*}{2} = (a + n) \cos(p|a + n|^2), \quad (58)$$

Figure 20



Measured output spectrum of a four-mode PSA without and with the idlers at the input. The observed signal gain with the idlers is 10.3 dB higher than without them, which is due to the coherent superposition of four waves. Reprinted with permission from [110]. Copyright 2012 Optical Society of America.

which turns the phase noise (partly) into amplitude noise and also, importantly, reduces the overall spread of the resulting constellation point. This shows how the transmission of conjugate data followed by coherent superposition can significantly improve the tolerance to nonlinear distortions.

Since this configuration is precisely the one used in a copier-PSA transmission link, the robustness to NL distortions was indeed observed in some of the first transmission experiments of that type [171]. Independently, a similar idea was proposed by Liu *et al.* around the same time [147,172]. The implementation was different in that they used the second polarization to transmit the conjugate data and performed the coherent superposition in DSP in a coherent receiver, rather than optically in a PSA. Also other schemes were proposed based on DSP implementations, e.g., different wavelength channels [173] or different temporal symbols [174], so-called “conjugate data repetition.”

An important unique benefit in the PSA implementation is that the signal is maintained in the optical domain, and the coherent superposition can be distributed and repeated several times in a PSA link. The DSP-based implementations are limited to receiver processing only.

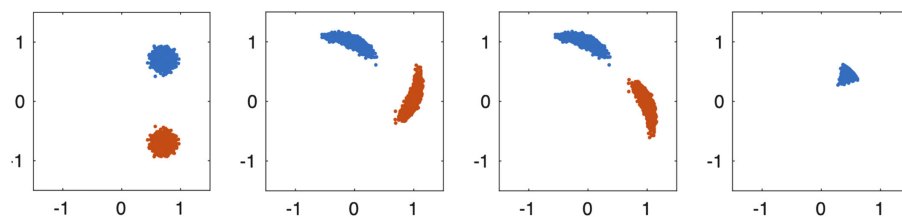
This makes a copier-PSA link extremely tolerant to nonlinear distortions, and nonlinear phase shifts as high as 6 radians (likely the highest ever reported) were found in a 10 Gbaud experiment using QPSK modulation [175]. A reach extension of 5.6 times compared to a PIA-based link was found, where we can note that only 4 times is to be expected from the 6 dB improved SNR, and the rest can be attributed to the nonlinear compensation.

While the theory for this twin wave mitigation neglects dispersion, it can indeed be shown that a large amount of accumulated dispersion will degrade the performance of the scheme used for coherent long-haul transmission. However, for copier-PSA links, the periodic coherent superposition makes it possible to optimize the dispersion. This will be discussed more in the next section.

7. EXPERIMENTAL TRANSMISSION RESULTS USING PHASE-SENSITIVE AMPLIFIERS

In this section, some examples of experimental results relying on PSAs being used in optical communication links will be presented. This is not intended to be a review of experimental results, but rather illustrate key features of using PSAs in real experiments. First, we discuss results using HNLF-based PSAs as in-line amplifiers in long-haul optical fiber transmission systems in which both noise and transmission

Figure 21



Effect of conjugate twin wave transmission. (a) The initial signal (blue) and its conjugate (red). (b) Both signal after propagation subject to SPM and XPM. (c) As in (b) but with the red signal conjugated. (d) The resulting signal after coherent superposition. The simulation is based on 5000 points, with an SNR of 20 dB and a nonlinear phase shift of 0.8 rad.

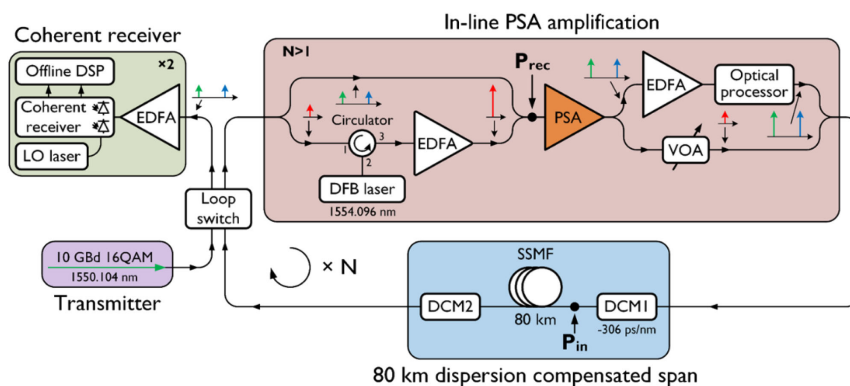
fiber nonlinearities degrade the performance. Then, we also discuss results demonstrated with PSAs based on lithium niobate in which the second-order nonlinearity is used.

7.1. System Results Using Highly Nonlinear Fiber-Based PSAs

As already mentioned, the key benefits of using PSAs as the in-line amplifier are that fiber communication links are the improved link NF and the nonlinearity mitigation. Figure 22 shows a schematic of a setup used with the aim to experimentally quantify these in the case of single channel system [176]. A conventional transmitter (using I-Q modulator encoded with 16-QAM data at 10 Gb/s) and coherent receiver were used. As span-by-span optical dispersion compensation is needed, this was implemented with dispersion compensating modules (DCMs) with the precompensation value set with the aim to optimize the nonlinearity mitigation. The span loss in the experiment was significantly higher than the 80 km span itself (which was 21.5 dB including the SSMF and the two DCMs) due to the other component in the loop resulting in a total loss per span of 34.5 dB. The PSA gain was 21.5 dB, while the additional gain needed to cancel the loop transmission loss was compensated by an EDFA without any significant excess noise contribution. The PSA used was implemented by strained, HNLF, and in-line isolators for SBS suppression as described in Subsection 5.3. Prior to the PSA in each revolution in the loop, the signal and idler were separated from the weak and noisy pump, which was recovered using the optical injection-locking technique described in Subsection 5.5a. In addition, the polarization states were coaligned. After the PSA, the signal and idler power were equalized in an optical processor (WaveShaper), and the signal gain was maximized using a PLL (not shown in the figure) adjusting the relative optical phase of the pump branch prior to the PSA with a PZT. In addition, the pump power was attenuated not to excite SBS in the span transmission fiber. It can be noted that the PSA acted as a “copier” prior to the first transmission in the loop, but as a PSA for all remaining circulations. After the final circulation under consideration in the experiment, nonlinearity mitigation in the last span was carried out by using coherent superposition of the signal and idler after detection in the digital domain, similar to [147].

Figure 23 shows experimental constellation diagrams of the received signal under different conditions for the experiment discussed above. Constellation diagrams after N round trips with in-line PSA or PIA amplification are shown at low (-3 dBm) and

Figure 22



Setup of long-haul transmission of data emulated with circulating loop using PSA as in-line amplifiers. Reprinted with permission from [176]. Copyright 2017 Optical Society of America.

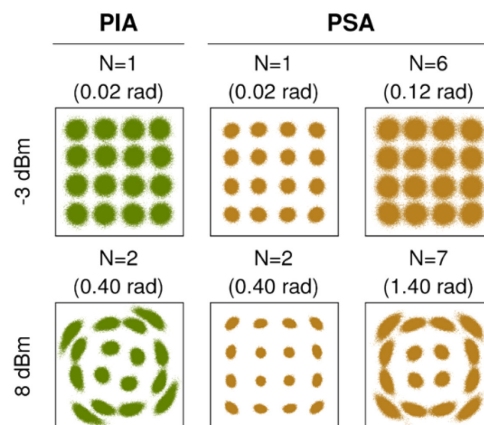
high (+8 dBm) span launch powers. Constellations in the left and right columns correspond to a bit error rate (BER) of 10^{-3} , and the values in parenthesis are calculated accumulated nonlinear phase shifts.

It is clear that the PSA performs significantly better than the PIA in the low power (essentially linear transmission regime), resulting in an extension of the noise-limited reach (BER = 10^{-3}) from about one to six 80 km spans, which is due to the link NF improvement in this case. In the case of high launch power, nonlinear distortion is clearly seen already after 160 km in the case of PIA, while for the PSA, a similar amount of distortion is noted only after 560 km, clearly demonstrating the capability of PSA to compensate SPM-induced distortion in the transmission fiber. When optimizing the launch power in each case for maximum reach (3 dBm in both cases), the maximum reach for the PSA was 1040 km, being about 4 times larger than in the PIA case. Recent experiments have demonstrated a reach improvement of as much as 5.6 times at optimal launch powers with 10 Gbd QPSK data, operating at a total estimated accumulated nonlinear phase shift of 6.2 rad due to SPM in the signal [175]. Also, recently [177] the first experimental demonstration of PSA-based mitigation of XPM in a WDM transmission system was presented.

7.2. System Results Using LiNbO₃-Based PSAs

The second-order nonlinearity, $\chi^{(2)}$ discussed in Subsection 3.2a, can also be utilized to perform phase-sensitive parametric amplification. A suitable platform for this is periodically poled LiNbO₃ (PPLN). These are compact devices, typically a few centimeters long, with a large second-order nonlinearity, while also not suffering from the SBS problems in HNLf as discussed in Subsection 5.3. There exist several configurations to achieve parametric amplification in this platform. A PPLN-based PSA for in-line operation, e.g., in a fiber transmission system, was demonstrated in Refs. [178,179]. As shown in Fig. 24, the setup relied on three PPLN waveguides, as well as on injection locking for carrier recovery and a PLL for stable operation. One of the PPLN waveguides was used for carrier recovery, using a cascade of the SHG process and the DFG process, as indicated in the bottom of the figure. The other two waveguides were used for PSA pump generation (0.3 W at 770 nm, relying on SFG) and for PSA amplification, respectively. This represents a one-mode PSA, which is very suitable for phase regeneration.

Figure 23



10 Gbd, 16-QAM signal constellation diagrams for PIA and PSA in-line amplifier operation in the loop experiment in Fig. 22. The number of round trips is denoted N . Reprinted with permission from [176]. Copyright 2017 Optical Society of America.

The experimental results showed a PSA gain of up to 11 dB, and very clear phase noise regeneration features by studying a 40 Gb/s binary phase modulated signal. In addition, nonlinear phase noise caused by a transmission fiber was successfully mitigated. A long-haul transmission study was later demonstrated in a circulating loop experiment using a PSA with 18 dB gain in a 40 km span over 1000s of km [178].

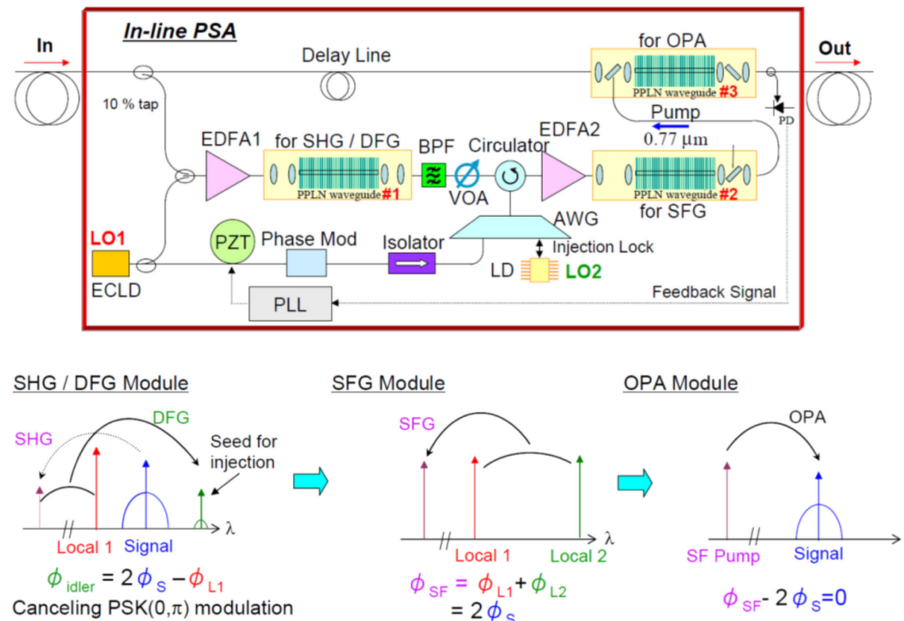
8. OTHER APPLICATIONS OF FIBER-OPTIC PARAMETRIC AMPLIFIERS

Aside from the basic function of amplifying light, both PIA and PSA implementations have several interesting applications beyond those described earlier for optical transmission applications. There are too many such applications suggested and demonstrated in the literature to be listed here, so we just provide some examples. An obvious one is wavelength conversion as idler(s) are generated at new frequencies dictated by the input waves. An impressive example is in Ref. [180] where HLNLF-based FWM of waves at 1300 nm and 1589 nm was used to generate a wave at around 2000 nm. Another wave was similarly generated in another HNLN being tunable over 1912–2155 nm. These waves were subsequently used for FWM in a short silicon waveguide resulting in a conversion range of over 600 nm with an idler being generated at up to 2388 nm. A very different application example is quadrature signal decomposition [160] where a polarization diverse PSA (see Section 5.53) was used to convert a 20 Gbaud, 16-QAM encoded signal to two independent 4-PAM output signals. We should here also highlight that the phase conjugation of signals enabled by the FWM process can itself be used to mitigate both dispersive and nonlinear effects in optical transmission fibers. This topic is beyond the scope of this tutorial, but an overview of the capabilities is provided in Ref. [181]. Below, we discuss in more detail two particular applications, signal regeneration and all-optical sampling.

8.1. Amplitude and Phase Regeneration

As signals for a variety of reasons can be impaired in terms of amplitude and phase, it is of interest to explore all-optical approaches that can regenerate such signals. PSA

Figure 24



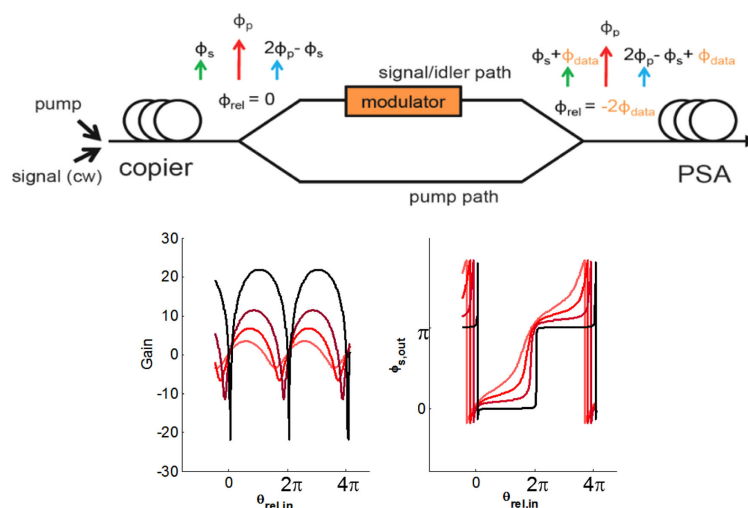
Schematic of a PPLN-based PSA implementation (top) and principle (bottom). Reprinted with permission from [178]. Copyright 2013 Optical Society of America.

has been shown to have such capabilities. An example on how phase regeneration can be implemented is illustrated in Fig. 25 (top). Here a single-pump, two-mode PSA approach with a copier is considered. However, in contrast to the transmission experiments described in Subsection 7.1, the signal and idler are here encoded with identical data (i.e., the idler is not a phase-conjugated copy of the signal). The bottom figure shows the calculated signal gain and output phase as a function of the input phase at different pump power. The result is, when the PSA gain is large enough, the output signal phase can only become a multiple of π , irrespective of the input signal phase, which is the basis for phase regeneration.

Figure 26 from [84] shows an experimental validation of this functionality, illustrating the measured output phase and constellation diagram. Here, instead of varying the pump power (i.e., gain), the relative power difference of the idler and signal was varied. The left figure illustrates the case without idler, i.e., a PIA, and shows an output phase tracking that of the input, as expected. However, as the idler power becomes equal to the signal power in the right set of figures, the output phase can only be 0 or π , and the constellation diagram is squeezed to a single line across the real axis. Under certain operating conditions, it has been found that also amplitude noise can be reduced significantly, which is a consequence of the signal-induced gain saturation of the PSA.

In Ref. [79], a “black-box” one-mode PSA-based all-optical amplitude and phase regenerator was presented. The principle, shown in Fig. 27, is that two pumps are symmetrically located around a single, degenerated signal/idler wave. Amplitude and phase noise was emulated by adding RF tones to the signal wave in the experiment. The key aspect to obtain a “black-box” operation is the use of injection locking in order to generate two phase-stable pumps. In a first HNLF stage, an idler was generated by FWM of a small fraction of the signal and a local pump, which did not contain any data since the idler phase is equal to twice the signal phase (being encoded with a BPSK signal) minus the pump phase. The idler was subsequently fed into a slave laser for injection locking, resulting in a high SNR pump wave for the subsequent PSA regenerator stage. It may be noted that in this experiment, the “black-box” NF was dictated by the EDFA at the system input, and can thus only reach 3 dB at best.

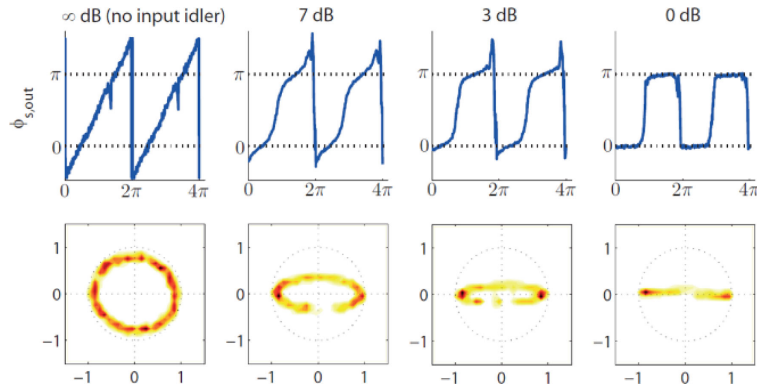
Figure 25



Top, principle of optical phase regeneration in a two-mode PSA. Bottom, calculated gain and output signal phase at increasing pump powers.

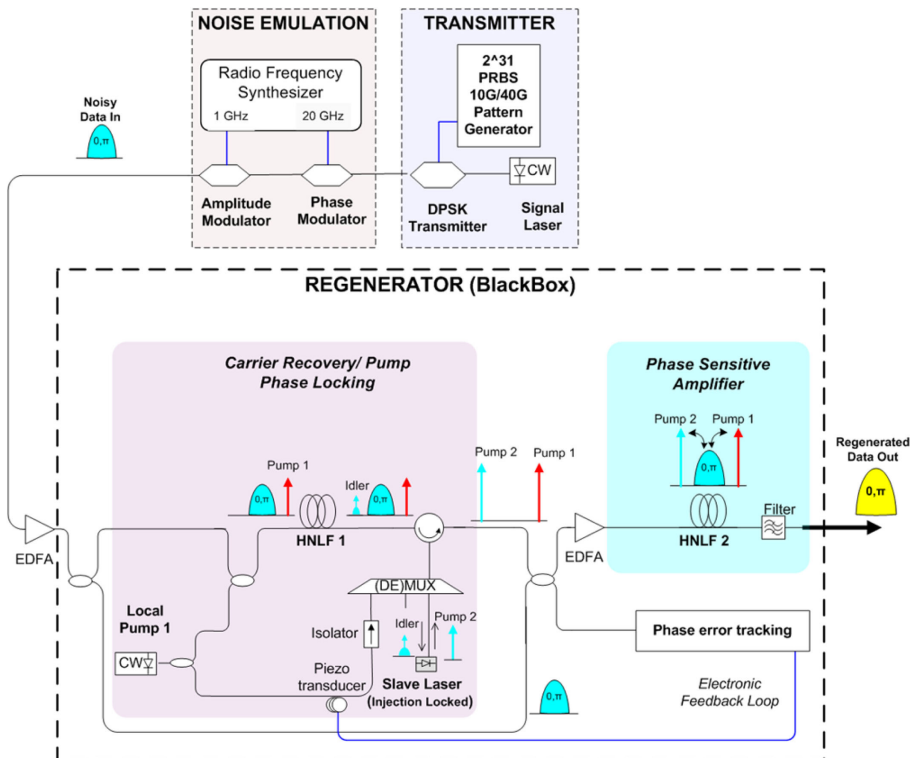
Figure 28 shows an example of the phase noise regeneration capability. It shows the elimination of ± 80 deg of peak differential phase distortion. In addition, it was shown that both amplitude and phase noise could be substantially reduced with a corresponding reduction of the BER. While this demonstration relied on a binary phase modulation format, this work has later been significantly extended, showing the compatibility of phase-regeneration with multiple wavelength channels [182], and to QPSK modulation format [183]. Although the amplitude regeneration in the

Figure 26



Experimental results of two-mode PSA-based phase regeneration. Top, output phase versus input phase. Bottom, corresponding constellation diagrams. The idler power is increasing from left to right, where it is equal to the signal power. Reprinted with permission from [84]. Copyright 2011 Optical Society of America.

Figure 27



Schematic of a “black-box” all-optical phase regenerator based on a one-mode PSA. Reprinted with permission from Macmillan Publishers Ltd: R. Slavik *et al.*, Nat. Photonics **4**, 690–695 (2010) [79]. Copyright 2010.

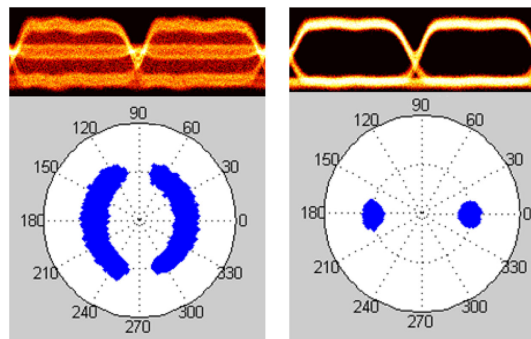
scheme above relied on gain saturation, which only works with a single wavelength channel, more advanced schemes have been proposed [184] that combine PSA-based phase regeneration with multichannel-compatible amplitude regeneration [185] for multichannel regeneration of advanced modulation formats.

8.2. All-Optical Sampling

A parametric amplifier can be used as an optical waveform sampling device with very high bandwidth due to its very fast response time. The basic principle [186] is shown in Fig. 29 (top). Instead of using a CW pump, here a pulsed pump is used. Whenever the pump is present, an idler will be generated that has a power proportional to the input signal. The typical parametric gain is 0–10 dB. For equivalent-time sampling oscilloscope operation, the repetition rate of the pump can be arbitrarily low, but requires the signal to be repetitive. The idler can thus be filtered out and captured with a slow detector for waveform or eye diagram reconstruction. The signal waveform is then built up by adding up all the stroboscopic snapshots of the signal. In contrast to electronic sampling, in this case, there are no concerns with impedance-mismatch-induced waveform distortion. In addition, since the measurement bandwidth is dictated by the pump pulse duration, it can be very high. In Fig. 29 (bottom left), an example waveform of a part of a $2^7 - 1$ pseudo-random sequence of data pulses at 640 Gb/s is shown, illustrating the high bandwidth capability. The approach was made independent of the signal polarization state by inserting a short section of polarization-maintaining fiber in front of the HNLF and aligning the pump to 45 deg between the principal axes, resulting in temporally displaced sampling of the two polarizations, which are detected jointly in the slow detector [187,188].

The principle above can readily be extended to the characterization of complex modulation formats by replacing the detector in Fig. 29 (top) with a coherent receiver. An example of the capture of a 10 Gbd QPSK signal including the detailed transitions is also shown in the figure (bottom right). The approach can also be modified to a real-time signal capture by using several parallel HNLF to capture the waveform with high sampling rate to circumvent a possible electronic bandwidth/sampling rate bottleneck. In Ref. [189], four HNLFs were used to equidistantly sample a 40 Gb/data in real time with an aggregate rate of 100 Gsamples/s, which, of course, can be scaled further to higher rates.

Figure 28

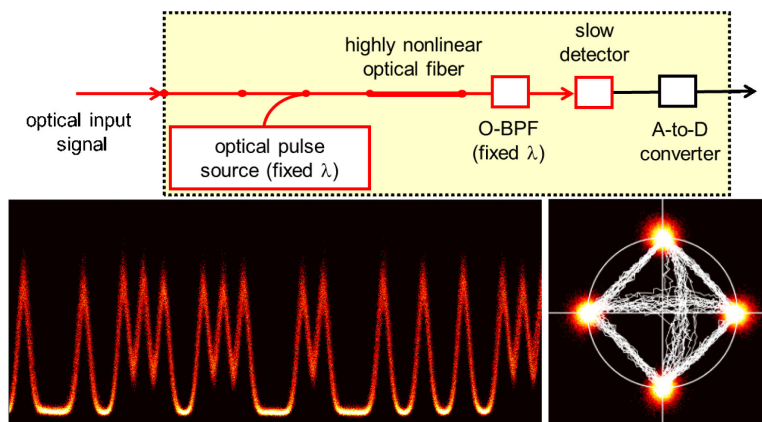


Experimental results of phase regeneration in a one-mode PSA. Reprinted with permission from Macmillan Publishers Ltd.: Slavík *et al.*, Nat. Photonics 4, 690–695 (2010) [79]. Copyright 2010.

9. FUTURE OUTLOOK INCLUDING OTHER NONLINEAR PLATFORMS

While the fundamental properties of parametric amplifiers are well understood and many experimental demonstrations have been made as discussed in this tutorial paper, there are still several challenges remaining to be solved in order for them to be implemented in a broad range of applications. The key merits of HNLFs as a nonlinear platform for parametric amplification are its low dispersion and very low loss, of the order of 0.5 dB/km, which makes it possible to reach a large gain with a few 100 m of fiber. As discussed earlier, a nonlinear phase shift of $\gamma PL = 3$ radians will result in a small-signal PIA gain of about 20 dB assuming perfect phase matching and no loss. However, HNLFs suffer from SBS and from SRS, which set practical limits to the possible NF, as well as from PMD. Signal-polarization-independent operation is desired in many applications and is in practice very difficult to achieve in a conventional HNLFs, in particular for phase-sensitive operations. Here, both phase and polarization need to be carefully controlled over a sufficiently broad spectral range. One possibility would be to consider polarization-maintaining HNLFs, since the impact of PMD will then be negligible. There are, however, other nonlinear platforms that can serve as platforms for parametric amplifiers, including the PPLN waveguides discussed earlier. An important aspect to first consider when studying these platforms is the intended operating wavelength range for a given application keeping in mind that, in principle, the parametric amplification approach described here can be translated to any other wavelength range given a suitable nonlinear platform. Other aspects to consider include not only the target gain and bandwidth, but also the output signal power, as some platform may suffer more than others from nonlinear two- or three-photon absorption, which may prohibit high enough power operation. Fundamentally, parametric amplifiers can be very power efficient with a suitable very high nonlinearity platform, which would require less pump power for a given gain target. It should be pointed out that the “black-box” NF includes the insertion loss into the amplifying medium, which thus needs to be very small to take full advantage of the noise performance of PSAs. Here, we will not review the many potential candidate platforms that have been investigated, Si, SiN, AlGaAs, Hydrex, holey microstrand fibers with $\gamma > 1000 \text{ (W km)}^{-1}$ [190,191], but simply state that the main target criteria may be summarized as nonlinear phase shift of at least 3 rad with small and anomalous

Figure 29



Top, all-optical sampling based pulsed-pump PIA operation. Bottom, examples shown are a pulsed data sequence at 640 Gb/s (left) and a QPSK signal captured by using a coherent receiver to detect the idler (right). Reprinted with permission from [187,188]. Copyright 2007 Wiley-VCH Verlag GmbH & Co. and 2008 Optical Society of America.

dispersion in the waveguide to support the target operating bandwidth, and operation at sufficiently high output signal power for a given application. Therefore, we believe there are interesting prospects to develop compact parametric amplifiers that promise large optical bandwidth, polarization-diversity, very low PMD, a NF approaching 0 dB, negligible SBS, and a high bandwidth PLL for excellent phase control (small device latency).

10. CONCLUSION

In this tutorial, we have described the fundamental principles, theory, and applications of optical parametric amplifiers. We have discussed their spectral gain characteristics and the distinctions between phase-insensitive and phase-sensitive operation. The implementations considered here mostly rely on the use of a nonlinear platform using HNLFs in FOPAs, but there are certainly other promising candidates as well. While most applications discussed related to optical communications, it is likely that other application areas, such as spectroscopy or quantum photonics, can benefit from parametric amplification and processing. A key aspect here is that the response time of FOPAs is very fast, implying many possible functionalities aside from pure amplification, such as phase regeneration discussed here. This, on the other hand, places stringent requirement on the pump laser in order not to suffer from performance degradation. Perhaps the most intriguing aspects of PSAs is their quantum-limited NF of 0 dB, i.e., amplification without adding excess noise (with 1 dB being experimentally demonstrated) and the fact that, in principle, it can be scaled to any wavelength for a large variety of potential applications.

FUNDING

Vetenskapsrådet (VR-2015-00535); Knut och Alice Wallenbergs Stiftelse; European Research Council (ERC-2018-PoC 813236).

ACKNOWLEDGMENT

The authors wish to acknowledge the contributions from C. Lundström, S. Olsson, J. Hansryd, M. Westlund, H. Sunnerud, M. Sköld, P. Kylemark, T. Torounidis, R. Kakarla, K. Vijayan, H. Eliasson, A. Lorences-Riesgo, E. Astra, B. Corcoran, A. Kumpera, R. Malik, Z. Tong, E. Nazemosadat, B. Foo, and J. Schröder. We wish to acknowledge a large number of helpful comments, suggestions for improvements, identification of typos and errors, and suggestions for additional references by the two anonymous reviewers. We also wish to acknowledge Sumitomo Electric Industries and OFS Denmark for supplying HNLFs used in several of our experiments.

REFERENCES

1. R. J. Mears, L. Reekie, I. M. Jauncey, and D. N. Payne, "Low-noise erbium-doped fibre amplifier operating at 1.54 μm ," *Electron. Lett.* **23**, 1026–1028 (1987).
2. Z. Tong and S. Radic, "Low-noise optical amplification and signal processing in parametric devices," *Adv. Opt. Photon.* **5**, 318–384 (2013).
3. M. Karlsson, "Transmission systems with low noise phase-sensitive parametric amplifiers," *J. Lightwave Technol.* **34**, 1411–1423 (2015).
4. M. E. Marhic, *Fiber Optical Parametric Amplifiers, Oscillators and Related Devices* (Cambridge University, 2008).

5. M. E. Marhic, P. A. Andrekson, P. Petropoulos, S. Radic, C. Peucheret, and M. Jazayerifar, "Fiber optical parametric amplifiers in optical communication systems," *Laser Photon. Rev.* **9**, 50–74 (2015).
6. T. Akiyama, M. Ekawa, M. Sugawara, K. Kawaguchi, H. Sudo, A. Kuramata, H. Ebe, and Y. Arakawa, "An ultrawide-band semiconductor optical amplifier having an extremely high penalty-free output power of 23 dBm achieved with quantum dots," *IEEE Photon. Technol. Lett.* **17**, 1614–1616 (2005).
7. J. Bromage, "Raman amplification for fiber communications systems," *J. Lightwave Technol.* **22**, 79–93 (2004).
8. M. Vasilyev, "Distributed phase-sensitive amplification," *Opt. Express* **13**, 7563–7571 (2005).
9. A. Cullen, "A travelling-wave parametric amplifier," *Nature* **181**, 332 (1958).
10. S. Wirkus, R. Rand, and A. Ruina, "How to pump a swing," *College Math. J.* **29**, 266–275 (1998).
11. J. M. Manley and H. E. Rowe, "Some general properties of nonlinear elements—Part I. General energy relations," *Proc. IRE* **44**, 904–913 (1956).
12. T. H. Maiman, "Stimulated optical radiation in ruby," *Nature* **187**, 493–494 (1960).
13. P. A. Franken, A. E. Hill, C. W. Peters, and G. Weinreich, "Generation of optical harmonics," *Phys. Rev. Lett.* **7**, 118–119 (1961).
14. J. A. Armstrong, N. Bloembergen, J. Ducuing, and P. S. Pershan, "Interactions between light waves in a nonlinear dielectric," *Phys. Rev.* **127**, 1918–1939 (1962).
15. S. Akhmanov and R. Khokhlov, "Concerning one possibility of amplification of light waves," *Sov. Phys. JETP* **16**, 252–254 (1963).
16. P. Maker, R. Terhune, and C. Savage, "Intensity-dependent changes in the refractive index of liquids," *Phys. Rev. Lett.* **12**, 507–509 (1964).
17. P. D. Maker and R. W. Terhune, "Study of optical effects due to an induced polarization third order in the electric field strength," *Phys. Rev.* **137**, A801–A818 (1965).
18. R. H. Stolen, J. E. Bjorkholm, and A. Ashkin, "Phase-matched three-wave mixing in silica fiber optical waveguides," *Appl. Phys. Lett.* **24**, 308–310 (1974).
19. K. O. Hill, D. C. Johnson, B. S. Kawasaki, and R. I. MacDonald, "CW three wave mixing in single mode optical fibers," *J. Appl. Phys.* **49**, 5098–5106 (1978).
20. K. Washio, K. Inoue, and T. Tanigawa, "Efficient generation of near-I.R. stimulated light scattering in optical fibres pumped in low-dispersion region at 1.3 μm ," *Electron. Lett.* **16**, 331–333 (1980).
21. K. Washio, K. Inoue, and S. Kishida, "Efficient large-frequency-shifted three-wave mixing in low dispersion wavelength region in single-mode optical fibre," *Electron. Lett.* **16**, 658–660 (1980).
22. J. P. Pocholle, J. Raffy, M. Papuchon, and E. Desurvire, "Raman and four photon mixing amplification in single mode fibers," *Opt. Eng.* **24**, 244600 (1985).
23. C. J. Koester and E. Snitzer, "Amplification in a fiber laser," *Appl. Opt.* **3**, 1182–1186 (1964).
24. E. Snitzer and R. Woodcock, " Yb^{3+} - Er^{3+} glass laser," *Appl. Phys. Lett.* **6**, 45–46 (1965).
25. R. H. Stolen and E. P. Ippen, "Raman gain in glass optical waveguides," *Appl. Phys. Lett.* **22**, 276–278 (1973).
26. R. H. Stolen, "Phase-matched-stimulated four-photon mixing in silica-fiber waveguides," *IEEE J. Quantum Electron.* **11**, 100–103 (1975).
27. E. Ippen and R. Stolen, "Stimulated Brillouin scattering in optical fibers," *Appl. Phys. Lett.* **21**, 539–541 (1972).

28. E. Desurvire, J. R. Simpson, and P. Becker, "High-gain erbium-doped traveling-wave fiber amplifier," *Opt. Lett.* **12**, 888–890 (1987).
29. N. S. Bergano, "Wavelength division multiplexing in long-haul transoceanic transmission systems," *J. Lightwave Technol.* **23**, 4125–4139 (2005).
30. C. M. Caves, "Quantum limits on noise in linear amplifiers," *Phys. Rev. D* **26**, 1817–1839 (1982).
31. Y. Yamamoto and T. Mukai, "Fundamentals of optical amplifiers," *Opt. Quantum Electron.* **21**, S1–S14 (1989).
32. Y. Yamamoto and H. Haus, "Preparation, measurement and information capacity of optical quantum states," *Rev. Mod. Phys.* **58**, 1001–1020 (1986).
33. J. Gordon, "Quantum effects in communications systems," *Proc. IRE* **50**, 1898–1908 (1962).
34. N. A. Olsson, "Lightwave systems with optical amplifiers," *J. Lightwave Technol.* **7**, 1071–1082 (1989).
35. H. Takahashi, "Information theory of quantum mechanical channels," in *Advances in Communication Systems*, A. V. Balakrishnan, ed. (Academic, 1965), pp. 277–310.
36. H. P. Yuen, "Two-photon coherent states of the radiation field," *Phys. Rev. A* **13**, 2226–2243 (1976).
37. R. E. Slusher, L. W. Hollberg, B. Yurke, J. C. Mertz, and J. F. Valley, "Observation of squeezed states generated by four-wave mixing in an optical cavity," *Phys. Rev. Lett.* **55**, 2409–2412 (1985).
38. I. Bar-Joseph, A. A. Friesem, R. G. Waarts, and H. H. Yaffe, "Parametric interaction of a modulated wave in a single-mode fiber," *Opt. Lett.* **11**, 534–536 (1986).
39. M. D. Levenson, R. M. Shelby, and S. H. Perlmutter, "Squeezing of classical noise by nondegenerate four-wave mixing in an optical fiber," *Opt. Lett.* **10**, 514–516 (1985).
40. M. Kitagawa and Y. Yamamoto, "Number-phase minimum-uncertainty state with reduced number uncertainty in a Kerr nonlinear interferometer," *Phys. Rev. A* **34**, 3974–3988 (1986).
41. M. Shirasaki and H. A. Haus, "Squeezing of pulses in a nonlinear interferometer," *J. Opt. Soc. Am. B* **7**, 30–34 (1990).
42. K. Bergman and H. Haus, "Squeezing in fibers with optical pulses," *Opt. Lett.* **16**, 663–665 (1991).
43. M. E. Marhic, C. H. Hsia, and J. M. Jeong, "Optical amplification in a nonlinear fibre interferometer," *Electron. Lett.* **27**, 210–211 (1991).
44. J. A. Levenson, P. Grangier, I. Abram, and T. Rivera, "Reduction of quantum noise in optical parametric amplification," *J. Opt. Soc. Am. B* **10**, 2233–2238 (1993).
45. A. Takada and W. Imajuku, "Amplitude noise suppression using a high gain phase sensitive amplifier as a limiting amplifier," *Electron. Lett.* **32**, 677–679 (1996).
46. W. Imajuku and A. Takada, "In-line phase-sensitive amplifier with optical-PLL-controlled internal pump light source," *Electron. Lett.* **33**, 2155–2156 (1997).
47. W. Imajuku and A. Takada, "Error-free operation of in-line phase-sensitive amplifier," *Electron. Lett.* **34**, 1673–1674 (1998).
48. W. Imajuku and A. Takada, "Gain characteristics of coherent optical amplifiers using a Mach-Zehnder interferometer with Kerr media," *IEEE J. Quantum Electron.* **35**, 1657–1665 (1999).
49. W. Imajuku and A. Takada, "In-line optical phase-sensitive amplifier with pump light source controlled by optical phase-lock loop," *J. Lightwave Technol.* **17**, 637–646 (1999).

50. D. Levandovsky, M. Vasilyev, and P. Kumar, "Amplitude squeezing of light by means of a phase-sensitive fiber parametric amplifier," *Opt. Lett.* **24**, 984–986 (1999).
51. D. Levandovsky, M. Vasilyev, and P. Kumar, "Near-noiseless amplification of light by a phase-sensitive fibre amplifier," *Pramana J. Phys.* **56**, 281–285 (2001).
52. W. Imajuku, A. Takada, and Y. Yamabayashi, "Low-noise amplification under the 3 dB noise figure in high-gain phase-sensitive fibre amplifier," *Electron. Lett.* **35**, 1954–1955 (1999).
53. W. Imajuku, A. Takada, and Y. Yamabayashi, "Inline coherent optical amplifier with noise figure lower than 3 dB quantum limit," *Electron. Lett.* **36**, 63–64 (2000).
54. M. Karlsson, "Four-wave mixing in fibers with randomly varying zero-dispersion wavelength," *J. Opt. Soc. Am. B* **15**, 2269–2275 (1998).
55. M. Hirano, T. Nakanishi, T. Okuno, and M. Onishi, "Silica-based highly nonlinear fibers and their application," *IEEE J. Sel. Top. Quantum Electron.* **15**, 103–113 (2009).
56. J. Hansryd and P. A. Andrekson, "Broad-band continuous-wave-pumped fiber optical parametric amplifier with 49-dB gain and wavelength-conversion efficiency," *IEEE Photonics Technol. Lett.* **13**, 194–196 (2001).
57. J. Hansryd, P. A. Andrekson, M. Westlund, J. Li, and P.-O. Hedekvist, "Fiber-based optical parametric amplifiers and their applications," *IEEE J. Sel. Top. Quantum Electron.* **8**, 506–520 (2002).
58. W. Gambling, H. Matsumura, and C. Ragdale, "Mode dispersion, material dispersion and profile dispersion in graded-index single-mode fibres," *IEE J. Microwave Opt. Acoust.* **3**, 239–246 (1979).
59. T. Torounidis, P. A. Andrekson, and B.-E. Olsson, "Fiber-optical parametric amplifier with 70-dB gain," *IEEE Photonics Technol. Lett.* **18**, 1194–1196 (2006).
60. T. Torounidis and P. A. Andrekson, "Broadband single-pumped fiber-optic parametric amplifiers," *IEEE Photonics Technol. Lett.* **19**, 650–652 (2007).
61. M. Jamshidifar, A. Vedadi, and M. E. Marhic, "Continuous-wave one-pump fiber optical parametric amplifier with 270 nm gain bandwidth," in *European Conference and Exhibition on Optical Communication (ECOC)* (2009).
62. J. M. C. Boggio, S. Moro, E. Myslivets, J. R. Windmiller, N. Alic, and S. Radic, "155-nm continuous-wave two-pump parametric amplification," *IEEE Photonics Technol. Lett.* **21**, 612–614 (2009).
63. V. Gordienko, M. F. C. Stephens, A. E. El-Taher, and N. J. Doran, "Ultra-flat wideband single-pump Raman-enhanced parametric amplification," *Opt. Express* **25**, 4810–4818 (2017).
64. P. Kylemark, P. O. Hedekvist, H. Sunnerud, M. Karlsson, and P. A. Andrekson, "Noise characteristics of fiber optical parametric amplifiers," *J. Lightwave Technol.* **22**, 409–416 (2004).
65. P. Kylemark, P. O. Hedekvist, H. Sunnerud, M. Karlsson, and P. A. Andrekson, "Correction to 'noise characteristics of fiber optical parametric amplifiers'," *J. Lightwave Technol.* **23**, 2192 (2005).
66. Z. Tong, A. Bogris, M. Karlsson, and P. A. Andrekson, "Full characterization of the signal and idler noise figure spectra in single-pumped fiber optical parametric amplifiers," *Opt. Express* **18**, 2884–2893 (2010).
67. M. E. Marhic, N. Kagi, T.-K. Chiang, and L. G. Kazovsky, "Broadband fiber optical parametric amplifiers," *Opt. Lett.* **21**, 573–575 (1996).
68. M. E. Marhic, K. K.-Y. Wong, and L. G. Kazovsky, "Wide-band tuning of the gain spectra of one-pump fiber optical parametric amplifiers," *IEEE J. Sel. Top. Quantum Electron.* **10**, 1133–1141 (2004).

69. C. J. McKinstrie, S. Radic, and A. R. Chraplyvy, "Parametric amplifiers driven by two pump waves," *IEEE J. Sel. Top. Quantum Electron.* **8**, 538–547 (2002).
70. S. Radic and C. J. McKinstrie, "Two-pump fiber parametric amplifiers," *Opt. Fiber Technol.* **9**, 7–23 (2003).
71. C. J. McKinstrie, S. Radic, and M. G. Raymer, "Quantum noise properties of parametric amplifiers driven by two pump waves," *Opt. Express* **12**, 5037–5066 (2004).
72. C. J. McKinstrie, M. Yu, M. G. Raymer, and S. Radic, "Quantum noise properties of parametric processes," *Opt. Express* **13**, 4986–5012 (2005).
73. C. J. McKinstrie, M. G. Raymer, S. Radic, and M. Vasilyev, "Quantum mechanics of phase-sensitive amplification in a fiber," *Opt. Commun.* **257**, 146–163 (2006).
74. C. J. McKinstrie and S. Radic, "Phase-sensitive amplification in a fiber," *Opt. Express* **12**, 4973–4979 (2004).
75. K. Croussore, C. Kim, and G. Li, "All-optical regeneration of differential phase-shift keying signals based on phase-sensitive amplification," *Opt. Lett.* **29**, 2357–2359 (2004).
76. K. Croussore, I. Kim, Y. Han, C. Kim, G. Li, and S. Radic, "Demonstration of phase-regeneration of DPSK signals based on phase-sensitive amplification," *Opt. Express* **13**, 3945–3950 (2005).
77. K. Croussore, I. Kim, C. Kim, Y. Han, and G. Li, "Phase-and-amplitude regeneration of differential phase-shift keyed signals using a phase-sensitive amplifier," *Opt. Express* **14**, 2085–2094 (2006).
78. K. Croussore and G. Li, "Phase and amplitude regeneration of differential phase-shift keyed signals using phase-sensitive amplification," *IEEE J. Sel. Top. Quantum Electron.* **14**, 648–658 (2008).
79. R. Slavík, F. Parmigiani, J. Kakande, C. Lundström, M. Sjödin, P. A. Andrekson, R. Weerasuriya, S. Sygletos, A. D. Ellis, L. Grüner-Nielsen, D. Jakobsen, S. Herstrøm, R. Phelan, J. O’Gorman, A. Bogris, D. Syvridis, S. Dasgupta, P. Petropoulos, and D. J. Richardson, "All-optical phase and amplitude regenerator for next-generation telecommunications systems," *Nat. Photonics* **4**, 690–695 (2010).
80. R. Slavík, A. Bogris, F. Parmigiani, J. Kakande, M. Westlund, M. Sköld, L. Grüner-Nielsen, R. Phelan, D. Syvridis, P. Petropoulos, and D. J. Richardson, "Coherent all-optical phase and amplitude regenerator of binary phase-encoded signals," *IEEE J. Sel. Top. Quantum Electron.* **18**, 859–869 (2012).
81. R. Tang, P. Devgan, J. Lasri, V. Grigoryan, and P. Kumar, "Experimental investigation of a frequency-nondegenerate phase-sensitive optical parametric amplifier," in *Optical Fiber Communication Conference (OFC)* (2005).
82. R. Tang, J. Lasri, P. S. Devgan, V. Grigoryan, P. Kumar, and M. Vasilyev, "Gain characteristics of a frequency nondegenerate phase-sensitive fiber-optic parametric amplifier with phase self-stabilized input," *Opt. Express* **13**, 10483–10493 (2005).
83. J. Kakande, C. Lundström, P. A. Andrekson, Z. Tong, M. Karlsson, P. Petropoulos, F. Parmigiani, and D. J. Richardson, "Detailed characterization of a fiber-optic parametric amplifier in phase-sensitive and phase-insensitive operation," *Opt. Express* **18**, 4130–4137 (2010).
84. C. Lundström, Z. Tong, M. Karlsson, and P. A. Andrekson, "Phase-to-phase and phase-to-amplitude transfer characteristics of a nondegenerate-idler phase-sensitive amplifier," *Opt. Lett.* **36**, 4356–4358 (2011).
85. C. Lundström, R. Malik, L. Grüner-Nielsen, B. Corcoran, S. L. I. Olsson, M. Karlsson, and P. A. Andrekson, "Fiber optic parametric amplifier with 10-dB net gain without pump dithering," *IEEE Photon. Technol. Lett.* **25**, 234–237 (2013).

86. Z. Tong, C. Lundström, P. A. Andrekson, C. J. McKinstrie, M. Karlsson, D. J. Blessing, E. Tipsuwannakul, B. J. Puttnam, H. Toda, and L. Grüner-Nielsen, “Towards ultrasensitive optical links enabled by low-noise phase-sensitive amplifiers,” *Nat. Photonics* **5**, 430–436 (2011).
87. Z. Tong, C. Lundström, P. A. Andrekson, M. Karlsson, and A. Bogris, “Ultralow noise, broadband phase-sensitive optical amplifiers, and their applications,” *IEEE J. Sel. Top. Quantum Electron.* **18**, 1016–1032 (2012).
88. M. Berry, “Pumping a swing revisited: minimal model for parametric resonance via matrix products,” *Eur. J. Phys.* **39**, 055007 (2018).
89. Y.-R. Shen, *Principles of Nonlinear Optics* (Wiley-Interscience, 1984).
90. G. P. Agrawal, *Nonlinear Fiber Optics*, 5th ed. (Academic, 2012).
91. J. H. Marburger, “Self-focusing: theory,” *Prog. Quantum Electron.* **4**, 35–110 (1975).
92. A. Hasegawa and F. Tappert, “Transmission of stationary nonlinear optical pulses in dispersive dielectric fibers. I. Anomalous dispersion,” *Appl. Phys. Lett.* **23**, 142–144 (1973).
93. G. Cappellini and S. Trillo, “Third-order three-wave mixing in single-mode fibers: exact solutions and spatial instability effects,” *J. Opt. Soc. Am. B* **8**, 824–838 (1991).
94. Y. Chen, “Four-wave mixing in optical fibers: exact solution,” *J. Opt. Soc. Am. B* **6**, 1986–1993 (1989).
95. M. E. Marhic, “Polarization independence and phase-sensitive parametric amplification,” *J. Opt. Soc. Am. B* **28**, 2685–2689 (2011).
96. R. H. Stolen and J. E. Bjorkholm, “Parametric amplification and frequency conversion in optical fibers,” *IEEE J. Quantum Electron.* **18**, 1062–1072 (1982).
97. M. E. Marhic, Y. Park, F. S. Yang, and L. G. Kazovsky, “Broadband fiber-optical parametric amplifiers and wavelength converters with low-ripple Chebyshev gain spectra,” *Opt. Lett.* **21**, 1354–1356 (1996).
98. V. Ribeiro, M. Karlsson, and P. Andrekson, “Parametric amplification with a dual-core fiber,” *Opt. Express* **25**, 6234–6243 (2017).
99. M. T. Weiss, “Quantum derivation of energy relations analogous to those for nonlinear reactances,” *Proc. IRE* **45**, 1012–1013 (1957).
100. J. Kakande, C. Lundström, P. A. Andrekson, Z. Tong, M. Karlsson, P. Petropoulos, F. Parmigiani, and D. J. Richardson, “Multilevel quantization of optical phase in a novel coherent parametric mixer architecture,” *Nat. Photonics* **5**, 748–752 (2011).
101. A. Hasegawa and W. Brinkman, “Tunable coherent IR and FIR sources utilizing modulational instability,” *IEEE J. Quantum Electron.* **16**, 694–697 (1980).
102. K. Tai, A. Hasegawa, and A. Tomita, “Observation of modulational instability in optical fibers,” *Phys. Rev. Lett.* **56**, 135–138 (1986).
103. A. Hasegawa, “Generation of a train of soliton pulses by induced modulational instability in optical fibers,” *Opt. Lett.* **9**, 288–290 (1984).
104. R. W. Fung, H. K. Cheung, and K. K. Wong, “Widely tunable wavelength exchange in anomalous-dispersion regime,” *IEEE Photon. Technol. Lett.* **19**, 1846–1848 (2007).
105. K. Uesaka, K. K.-Y. Wong, M. E. Marhic, and L. G. Kazovsky, “Wavelength exchange in a highly nonlinear dispersion-shifted fiber: theory and experiments,” *IEEE J. Sel. Top. Quantum Electron.* **8**, 560–568 (2002).
106. M. Yu, C. J. McKinstrie, and G. P. Agrawal, “Instability due to cross-phase modulation in the normal-dispersion regime,” *Phys. Rev. E* **48**, 2178–2186 (1993).
107. C. J. McKinstrie and M. Karlsson, “Schmidt decompositions of parametric processes I: Basic theory and simple examples,” *Opt. Express* **21**, 1374–1394 (2013).

108. C. J. McKinstrie, J. R. Ott, and M. Karlsson, "Schmidt decompositions of parametric processes II: Vector four-wave mixing," *Opt. Express* **21**, 11009–11020 (2013).
109. C. J. McKinstrie, "Schmidt decompositions of parametric processes III: Simultaneous amplification and conversion," *Opt. Express* **23**, 16949–16966 (2015).
110. T. Richter, B. Corcoran, S. L. Olsson, C. Lundström, M. Karlsson, C. Schubert, and P. A. Andrekson, "Experimental characterization of a phase-sensitive four-mode fiber-optic parametric amplifier," in *European Conference and Exhibition on Optical Communication (ECOC)* (Optical Society of America, 2012), paper Th.1.F.1.
111. Z. Tong, A. O. Wiberg, E. Myslivets, B. P. Kuo, N. Alic, and S. Radic, "Broadband parametric multicasting via four-mode phase-sensitive interaction," *Opt. Express* **20**, 19363–19373 (2012).
112. E. Berglind and L. Gillner, "Optical quantum noise treated with classical electrical network theory," *IEEE J. Quantum Electron.* **30**, 846–853 (1994).
113. Z. Tong, C. Lundström, E. Tipsuwannakul, M. Karlsson, and P. A. Andrekson, "Phase-sensitive amplified DWDM DQPSK signals using free-running lasers with 6-dB link SNR improvement over EDFA-based systems," in *European Conference and Exhibition on Optical Communication (ECOC)* (2010).
114. P. L. Voss, R. Tang, and P. Kumar, "Measurement of the photon statistics and the noise figure of a fiber-optic parametric amplifier," *Opt. Lett.* **28**, 549–551 (2003).
115. R. Tang, P. L. Voss, J. Lasri, P. Devgan, and P. Kumar, "Noise-figure limit of fiber-optical parametric amplifiers and wavelength converters: experimental investigation," *Opt. Lett.* **29**, 2372–2374 (2004).
116. P. L. Voss and P. Kumar, "Raman-noise-induced noise-figure limit for parametric amplifiers," *Opt. Lett.* **29**, 445–447 (2004).
117. P. L. Voss, K. G. Köprülü, and P. Kumar, "Raman-noise-induced quantum limits for nondegenerate phase-sensitive amplification and quadrature squeezing," *J. Opt. Soc. Am. B* **23**, 598–610 (2006).
118. A. Durécu-Legrand, C. Simonneau, D. Bayart, A. Mussot, T. Sylvestre, E. Lantz, and H. Maillotte, "Impact of pump OSNR on noise figure for fiber-optical parametric amplifiers," *IEEE Photon. Technol. Lett.* **17**, 1178–1180 (2005).
119. P. Kylemark, M. Karlsson, T. Torounidis, and P. A. Andrekson, "Noise statistics in fiber optical parametric amplifiers," *J. Lightwave Technol.* **25**, 612–620 (2007).
120. R. Loudon, "Theory of noise accumulation in linear optical-amplifier chains," *IEEE J. Quantum Electron.* **21**, 766–773 (1985).
121. Z. Tong, C. J. McKinstrie, C. Lundström, M. Karlsson, and P. A. Andrekson, "Noise performance of optical fiber transmission links that use non-degenerate cascaded phase-sensitive amplifiers," *Opt. Express* **18**, 15426–15439 (2010).
122. M. Farahmand and M. de Sterke, "Parametric amplification in presence of dispersion fluctuations," *Opt. Express* **12**, 136–142 (2004).
123. R. Malik, A. Kumpera, M. Karlsson, and P. A. Andrekson, "Demonstration of ultra wideband phase-sensitive fiber optical parametric amplifier," *IEEE Photon. Technol. Lett.* **28**, 175–177 (2016).
124. J. M. C. Boggio, C. Lundström, J. Yang, H. Sunnerud, and P. A. Andrekson, "Double-pumped FOPA with 40 dB flat gain over 81 nm bandwidth," in *European Conference and Exhibition on Optical Communication (ECOC)* (2008).

125. J. Kim, O. Boyraz, J. H. Lim, and M. N. Islam, "Gain enhancement in cascaded fiber parametric amplifier with quasi-phase matching: theory and experiment," *J. Lightwave Technol.* **19**, 247–251 (2001).
126. S. Takasaka, Y. Mimura, M. Takahashi, R. Sugizaki, and H. Ogoshi, "Flat and broad amplification by quasi-phase-matched fiber optical parametric amplifier," in *Optical Fiber Communication Conference and Exposition (OFC/NFOEC)* (IEEE, 2012).
127. J. B. Coles, B.-P. Kuo, N. Alic, S. Moro, C.-S. Bres, J. C. Boggio, P. Andrekson, M. Karlsson, and S. Radic, "Bandwidth-efficient phase modulation techniques for stimulated Brillouin scattering suppression in fiber optic parametric amplifiers," *Opt. Express* **18**, 18138–18150 (2010).
128. M. Stephens, A. Redyuk, S. Sygletos, I. Phillips, P. Harper, K. Blow, and N. Doran, "The impact of pump phase-modulation and filtering on WDM signals in a fibre optical parametric amplifier," in *Optical Fiber Communication Conference* (Optical Society of America, 2015), paper W2A.43.
129. J. Hansryd, F. Dross, M. Westlund, P. A. Andrekson, and S. N. Knudsen, "Increase of the SBS threshold in a short highly nonlinear fiber by applying a temperature distribution," *J. Lightwave Technol.* **19**, 1691–1697 (2001).
130. J. M. C. Boggio, S. Moro, E. Myslivets, J. R. Windmiller, N. Alic, and S. Radic, "Experimental and numerical investigation of the SBS-threshold increase in an optical fiber by applying strain distributions," *J. Lightwave Technol.* **23**, 3808–3814 (2005).
131. P. Kylemark, H. Sunnerud, M. Karlsson, and P. A. Andrekson, "Semi-analytic saturation theory of fiber optical parametric amplifiers," *J. Lightwave Technol.* **24**, 3471 (2006).
132. S. Oda, H. Sunnerud, and P. A. Andrekson, "High efficiency and high output power fiber-optic parametric amplifier," *Opt. Lett.* **32**, 1776–1778 (2007).
133. P. A. Andrekson, H. Sunnerud, S. Oda, T. Nishitani, and J. Yang, "Ultrafast, atto-joule switch using fiber-optic parametric amplifier operated in saturation," *Opt. Express* **16**, 10956–10961 (2008).
134. H. Sunnerud, S. Oda, J. Yang, T. Nishitani, and P. A. Andrekson, "Optical add-drop multiplexer based on fiber optical parametric amplification," in *33rd European Conference and Exhibition of Optical Communication* (VDE, 2007).
135. T. Torounidis, H. Sunnerud, P. O. Hedekvist, and P. A. Andrekson, "Amplification of WDM signals in fiber-based optical parametric amplifiers," *IEEE Photon. Technol. Lett.* **15**, 1061–1063 (2003).
136. J. L. Blows, "Design strategy for controlling four-wave mixing-induced crosstalk between channels in a fibre optical parametric amplifier," *Opt. Commun.* **236**, 115–122 (2004).
137. M. Jamshidifar, A. Vedadi, and M. E. Marhic, "Reduction of four-wave-mixing crosstalk in a short fiber-optical parametric amplifier," *IEEE Photon. Technol. Lett.* **21**, 1244–1246 (2009).
138. M. F. C. Stephens, I. D. Phillips, P. Rosa, P. Harper, and N. J. Doran, "Improved WDM performance of a fibre optical parametric amplifier using Raman-assisted pumping," *Opt. Express* **23**, 902–911 (2015).
139. Z. Chen, X. Guo, X. Fu, C. Shu, and Z. Li, "Investigation of four-wave-mixing crosstalk in phase-sensitive fiber optical parametric amplifier," *J. Lightwave Technol.* **36**, 5113–5120 (2018).
140. A. Kumpera, R. Malik, A. Lorences-Riesgo, and P. A. Andrekson, "Parametric coherent receiver," *Opt. Express* **23**, 12952–12964 (2015).
141. Z. Tong, C. Lundström, M. Karlsson, M. Vasilyev, and P. A. Andrekson, "Noise performance of a frequency nondegenerate phase-sensitive amplifier with unequalized inputs," *Opt. Lett.* **36**, 722–724 (2011).

142. R. Malik, A. Kumpera, S. Olsson, P. Andrekson, and M. Karlsson, "Optical signal to noise ratio improvement through unbalanced noise beating in phase-sensitive parametric amplifiers," *Opt. Express* **22**, 10477–10486 (2014).
143. Z. Ahmed, H. Liu, D. Novak, Y. Ogawa, M. Pelusi, and D. Kim, "Locking characteristics of a passively mode-locked monolithic DBR laser stabilized by optical injection," *IEEE Photon. Technol. Lett.* **8**, 37–39 (1996).
144. R. Kakarla, J. Schröder, and P. A. Andrekson, "Optical injection locking at sub nano-watt powers," *Opt. Lett.* **43**, 5769–5772 (2018).
145. H. Eliasson, K. Vijayan, B. Foo, S. L. Olsson, E. Astra, M. Karlsson, and P. A. Andrekson, "Phase-sensitive amplifier link with distributed Raman amplification," *Opt. Express* **26**, 19854–19863 (2018).
146. H. Eliasson, S. L. I. Olsson, M. Karlsson, and P. A. Andrekson, "Mitigation of nonlinear distortion in hybrid Raman/phase-sensitive amplifier links," *Opt. Express* **24**, 888–900 (2016).
147. X. Liu, A. R. Chraplyvy, P. J. Winzer, R. W. Tkach, and S. Chandrasekhar, "Phase-conjugated twin waves for communication beyond the Kerr nonlinearity limit," *Nat. Photonics* **7**, 560–568 (2013).
148. E. Astra, S. L. Olsson, H. Eliasson, and P. A. Andrekson, "Dispersion management for nonlinearity mitigation in two-span 28 GBaud QPSK phase-sensitive amplifier links," *Opt. Express* **25**, 13163–13173 (2017).
149. E. Astra, H. Eliasson, T. Ruuben, and P. A. Andrekson, "Improved mitigation of self-phase modulation induced impairments in 28 GBaud phase-sensitive amplified links," *Opt. Express* **27**, 4304–4316 (2019).
150. B. Foo, M. Karlsson, K. Vijayan, M. Mazur, and P. A. Andrekson, "Analysis of nonlinearity mitigation using phase-sensitive optical parametric amplifiers," *Opt. Express* **27**, 31926–31941 (2019).
151. A. Lorences-Riesgo, P. A. Andrekson, and M. Karlsson, "Polarization-independent phase-sensitive amplification," *J. Lightwave Technol.* **34**, 3171–3180 (2016).
152. T. Hasegawa, K. Inoue, and K. Oda, "Polarization independent frequency conversion by fiber four-wave mixing with a polarization diversity technique," *IEEE Photon. Technol. Lett.* **5**, 947–949 (1993).
153. P. O. Hedekvist, M. Karlsson, and P. Andrekson, "Polarization dependence and efficiency in a fiber four-wave mixing phase conjugator with orthogonal pump waves," *IEEE Photon. Technol. Lett.* **8**, 776–778 (1996).
154. G. Kalogerakis, M. E. Marhic, and L. G. Kazovsky, "Polarization-independent two-pump fiber optical parametric amplifier with polarization diversity technique," in *Optical Fiber Communication Conference* (Optical Society of America, 2006), paper OWT4.
155. K. K. Y. Wong, M. E. Marhic, K. Uesaka, and L. G. Kazovsky, "Polarization-independent two-pump fiber optical parametric amplifier," *IEEE Photon. Technol. Lett.* **14**, 911–913 (2002).
156. T. Richter, R. Elschner, A. Gandhe, K. Petermann, and C. Schubert, "Parametric amplification and wavelength conversion of single- and dual-polarization DQPSK signals," *IEEE J. Sel. Top. Quantum Electron.* **18**, 988–995 (2011).
157. S. Takasaka and R. Sugizaki, "Polarization insensitive fiber optical parametric amplifier using a SBS suppressed diversity loop," in *Optical Fiber Communications Conference and Exhibition (OFC)* (2016), pp. 1–3.
158. M. F. C. Stephens, V. Gordienko, and N. J. Doran, "20 dB net-gain polarization-insensitive fiber optical parametric amplifier with >2 THz bandwidth," *Opt. Express* **25**, 10597–10609 (2017).
159. H. Hu, R. Jopson, A. Gnauck, M. Dinu, S. Chandrasekhar, C. Xie, and S. Randel, "Parametric amplification, wavelength conversion, and phase conjugation

- of a 2.048-Tbit/s WDM PDM 16-QAM signal,” *J. Lightwave Technol.* **33**, 1286–1291 (2015).
160. A. Lorences-Riesgo, T. Eriksson, M. Mazur, P. Andrekson, and M. Karlsson, “Quadrature decomposition of a 20 Gbaud 16-QAM signal into 2x4-PAM signals,” in *42nd European Conference on Optical Communication ECOC* (VDE, 2016).
161. C. E. Shannon, “Communication in the presence of noise,” *Proc. IRE* **37**, 10–21 (1949).
162. R. Kakarla, J. Schröder, and P. A. Andrekson, “Record-sensitivity Gb/s receiver for free-space applications based on phase-sensitive amplification,” in *Conference on Lasers and Electro-Optics (CLEO)* (IEEE, 2019).
163. R.-J. Essiambre, M. A. Mestre, R. Ryf, A. H. Gnauck, R. W. Tkach, A. R. Chraplyvy, Y. Sun, X. Jiang, and R. Lingle, “Experimental investigation of inter-modal four-wave mixing in few-mode fibers,” *IEEE Photon. Technol. Lett.* **25**, 539–542 (2013).
164. N. Zhao, B. Huang, R. Amezcua-Correa, X. Li, and G. Li, “Few-mode fiber optical parametric amplifier,” in *Optical Fiber Communication Conference* (Optical Society of America, 2013), paper OTu2D–5.
165. M. Guasoni, “Generalized modulational instability in multimode fibers: wideband multimode parametric amplification,” *Phys. Rev. A* **92**, 033849 (2015).
166. S. M. M. Friis, I. Begleris, Y. Jung, K. Rottwitt, P. Petropoulos, D. Richardson, P. Horak, and F. Parmigiani, “Inter-modal four-wave mixing study in a two-mode fiber,” *Opt. Express* **24**, 30338–30349 (2016).
167. D. J. Richardson, J. M. Fini, and L. E. Nelson, “Space-division multiplexing in optical fibres,” *Nature* **7**, 354–362 (2013).
168. E. Nazemosadat, A. Lorences-Riesgo, M. Karlsson, and P. A. Andrekson, “Highly nonlinear few-mode fiber for optical parametric amplification,” in *42nd European Conference on Optical Communication (ECOC)* (VDE, 2016).
169. E. Nazemosadat, A. Lorences-Riesgo, M. Karlsson, and P. A. Andrekson, “Design of highly nonlinear few-mode fiber for C-band optical parametric amplification,” *J. Lightwave Technol.* **35**, 2810–2817 (2017).
170. B. Corcoran, R. Malik, S. L. I. Olsson, C. Lundström, M. Karlsson, and P. A. Andrekson, “Noise beating in hybrid phase-sensitive amplifier systems,” *Opt. Express* **22**, 5762–5771 (2014).
171. S. L. I. Olsson, C. Lundström, M. Karlsson, and P. A. Andrekson, “Long-haul (3465 km) transmission of a 10 GBd QPSK signal with low noise phase-sensitive in-line amplification,” in *European Conference and Exhibition on Optical Communication (ECOC)* (2014).
172. X. Liu, S. Chandrasekhar, P. J. Winzer, R. W. Tkach, and A. R. Chraplyvy, “Fiber-nonlinearity-tolerant superchannel transmission via nonlinear noise squeezing and generalized phase-conjugated twin waves,” *J. Lightwave Technol.* **32**, 766–775 (2014).
173. Y. Tian, Y.-K. Huang, S. Zhang, P. R. Prucnal, and T. Wang, “Demonstration of digital phase-sensitive boosting to extend signal reach for long-haul WDM systems using optical phase-conjugated copy,” *Opt. Express* **21**, 5099–5106 (2013).
174. H. Eliasson, P. Johannisson, M. Karlsson, and P. A. Andrekson, “Mitigation of nonlinearities using conjugate data repetition,” *Opt. Express* **23**, 2392–2402 (2015).
175. S. L. Olsson, H. Eliasson, E. Astra, M. Karlsson, and P. A. Andrekson, “Long-haul optical transmission link using low-noise phase-sensitive amplifiers,” *Nat. Commun.* **9**, 2513 (2018).

176. S. L. Olsson, M. Karlsson, and P. A. Andrekson, "Long-haul optical transmission of 16-QAM signal with in-line phase-sensitive amplifiers," in *European Conference on Optical Communication (ECOC)* (IEEE, 2017).
177. K. Vijayan, B. Foo, M. Karlsson, and P. A. Andrekson, "Cross-phase modulation mitigation in phase-sensitive amplifier links," *IEEE Photon. Technol. Lett.* **31**, 1733–1736 (2019).
178. T. Umeki, M. Asobe, and H. Takenouchi, "In-line phase sensitive amplifier based on PPLN waveguides," *Opt. Express* **21**, 12077–12084 (2013).
179. T. Umeki, T. Kazama, O. Tadanaga, K. Enbutsu, M. Asobe, Y. Miyamoto, and H. Takenouchi, "PDM signal amplification using PPLN-based polarization-independent phase-sensitive amplifier," *J. Lightwave Technol.* **33**, 1326–1332 (2015).
180. S. Zlatanovic, J. S. Park, S. Moro, J. M. C. Boggio, I. B. Divliansky, N. Alic, S. Mookherjea, and S. Radic, "Mid-infrared wavelength conversion in silicon waveguides using ultracompact telecom-band-derived pump source," *Nat. Photonics* **4**, 561 (2010).
181. A. D. Ellis, M. Tan, M. A. Iqbal, M. A. Z. Al-Khateeb, V. Gordienko, G. S. Mondaca, S. Fabbri, M. F. C. Stephens, M. E. McCarthy, A. Perentos, I. D. Phillips, D. Lavery, G. Liga, R. Maher, P. Harper, N. Doran, S. K. Turitsyn, and S. Sygletos, and P. Bayvel, "4 Tb/s transmission reach enhancement using 10×400 Gb/s super-channels and polarization insensitive dual band optical phase conjugation," *J. Lightwave Technol.* **34**, 1717–1723 (2016).
182. F. Parmigiani, K. Bottrill, R. Slavik, D. Richardson, and P. Petropoulos, "Multi-channel phase regenerator based on polarization-assisted phase-sensitive amplification," *IEEE Photon. Technol. Lett.* **28**, 845–848 (2016).
183. K. Bottrill, G. Hesketh, L. Jones, F. Parmigiani, D. Richardson, and P. Petropoulos, "Full quadrature regeneration of QPSK signals using sequential phase sensitive amplification and parametric saturation," *Opt. Express* **25**, 696–705 (2017).
184. L. Li and M. Vasilyev, "All-optical 2R regenerator of 16-QAM signals," *Proc. SPIE* **9009**, 46–51 (2014).
185. L. Li, P. G. Patki, Y. B. Kwon, V. Stelmakh, B. D. Campbell, M. Annamalai, T. I. Lakoba, and M. Vasilyev, "All-optical regenerator of multi-channel signals," *Nat. Commun.* **8**, 1–11 (2017).
186. P. A. Andrekson, "Picosecond optical sampling using four-wave mixing in fibre," *Electron. Lett.* **27**, 1440–1441 (1991).
187. P. A. Andrekson and M. Westlund, "Nonlinear optical fiber based high resolution all-optical waveform sampling," *Laser Photon. Rev.* **1**, 231–248 (2007).
188. M. Westlund, M. Sköld, and P. A. Andrekson, "All-optical phase-sensitive waveform sampling at 40 GSymbol/s," in *Optical Fiber Communication Conference* (Optical Society of America, 2008), paper PDP12.
189. M. Sköld, M. Westlund, H. Sunnerud, and P. A. Andrekson, "100 GSample/s optical real-time sampling system with Nyquist-limited bandwidth," in *33rd European Conference and Exhibition of Optical Communication-Post-Deadline Papers* (VDE, 2007).
190. X. Liu, R. M. Osgood, Jr., Y. A. Vlasov, and W. M. Green, "Mid-infrared optical parametric amplifier using silicon nanophotonic waveguides," *Nat. Photonics* **4**, 557–560 (2010).
191. K. Ooi, D. Ng, T. Wang, A. Chee, S. Ng, Q. Wang, L. Ang, A. Agarwal, L. Kimerling, and D. Tan, "Pushing the limits of CMOS optical parametric amplifiers with USRN:Si₇N₃ above the two-photon absorption edge," *Nat. Commun.* **8**, 13878 (2017).



Peter Andrekson received his Ph.D. from Chalmers University of Technology, Sweden, in 1988. After about three years with AT&T Bell Laboratories, Murray Hill, NJ, he returned to Chalmers, where he is now a Full Professor of photonics. He was Director of Research at Cenix Inc. in Allentown, PA, USA, during 2000–2003 and with the newly established Center for Optical Technologies at Lehigh University, Bethlehem, PA, during 2003–2004. His research interests include many aspects of fiber communications such as optical amplifiers, nonlinear pulse propagation, all-optical functionalities, and high spectral efficiency transmission. He was the cofounder of the optical test and measurement company Picosolve Inc., now part of EXFO. He is the author of over 500 scientific publications and conference papers in the area of optical communications, including four tutorials at the Optical Fiber Communication Conference (OFC), and holds nine patents. Andrekson has held visiting positions at Osaka University and Technical University of Technology in Tallinn, is serving or has served on several technical program committees (e.g., chair of ECOC 2017), and has also twice served as an expert for the evaluation of the Nobel Prize in Physics. He was also member of the executive board of Chalmers University during 2009–2016. He held an ERC Advanced Grant for work on phase-sensitive optical amplifiers (2012–2017) and is currently a distinguished professor by the Swedish Research Council (VR). Andrekson is the director of the Fibre Optic Communications Research Centre (FORCE) at Chalmers, and a Fellow of OSA, IEEE, and the Royal Swedish Academy of Engineering Sciences (IVA).



Magnus Karlsson received his Ph.D. in 1994 from Chalmers University of Technology, Gothenburg, Sweden. Since 1995, he has been with the Photonics Laboratory at Chalmers, first as Assistant Professor and since 2003 as Professor in photonics. He has been visiting researcher at Australian National University and University of California San Diego. He has authored or coauthored over 400 scientific journal and conference contributions in the areas of nonlinear optics and fiber-optic transmission. He cofounded the Chalmers Fiber-Optic Communication Research Center, FORCE, in 2010. He serves and has served in the technical program committees for the Optical Fiber Communication Conference (OFC), the European Conference of Optical Communication (ECOC), Conference on Lasers and Electro-Optics (CLEO), and Asia Conference on Photonics (ACP) and is also active in the committees for the Global Communications Conference (GlobeCom), and International Conference on Communications (ICC). He has been member and chairman of the IEEE Photonics Society Young Investigator Award jury. He is a former Associate and current Deputy Editor for *Optics Express* and an Associate Editor for *Journal of Lightwave Technology*. He contributed to the 100-GET and EO-Net projects that were both awarded the CELTIC excellence award. He supervised students receiving the best student paper awards at GlobeCom 2011, ECOC 2012, and ECOC 2019. He is senior member of IEEE, and Fellow of The Optical Society.